

2012-06-15

# Investigation of Inclusion Complexation between Ferrocene Derivatives and Cucurbiturils

Wei Li

*University of Miami*, w.li4@umiami.edu

Follow this and additional works at: [https://scholarlyrepository.miami.edu/oa\\_dissertations](https://scholarlyrepository.miami.edu/oa_dissertations)

---

## Recommended Citation

Li, Wei, "Investigation of Inclusion Complexation between Ferrocene Derivatives and Cucurbiturils" (2012). *Open Access Dissertations*. 806.

[https://scholarlyrepository.miami.edu/oa\\_dissertations/806](https://scholarlyrepository.miami.edu/oa_dissertations/806)

This Open access is brought to you for free and open access by the Electronic Theses and Dissertations at Scholarly Repository. It has been accepted for inclusion in Open Access Dissertations by an authorized administrator of Scholarly Repository. For more information, please contact [repository.library@miami.edu](mailto:repository.library@miami.edu).

UNIVERSITY OF MIAMI

INVESTIGATION OF INCLUSION COMPLEXATION BETWEEN FERROCENE  
DERIVATIVES AND CUCURBITURILS

By

Wei Li

A DISSERTATION

Submitted to the Faculty  
of the University of Miami  
in partial fulfillment of the requirements for  
the degree of Doctor of Philosophy

Coral Gables, Florida

June 2012

©2012  
Wei Li  
All Rights Reserved

UNIVERSITY OF MIAMI

A dissertation submitted in partial fulfillment of  
the requirements for the degree of  
Doctor of Philosophy

INVESTIGATION OF INCLUSION COMPLEXATION BETWEEN FERROCENE  
DERIVATIVES AND CUCURBITURILS

Wei Li

Approved:

\_\_\_\_\_  
Angel E. Kaifer, Ph.D.  
Professor of Chemistry

\_\_\_\_\_  
Dean of the Graduate School

\_\_\_\_\_  
V. Ramamurthy, Ph.D.  
Professor of Chemistry

\_\_\_\_\_  
Rajeev Prabhakar Ph.D.  
Professor of Chemistry

\_\_\_\_\_  
Lyle Isaacs, Ph.D.  
Professor of Chemistry  
Department of Chemistry & Biochemistry  
University of Maryland

LI, WEI

(Ph.D., Chemistry)

Investigation of Inclusion Complexation  
between Ferrocene Derivatives and Cucurbiturils

(June 2012)

Abstract of a dissertation at the University of Miami.

Dissertation supervised by Professor Angel E. Kaifer

No. of pages in text. (136)

This dissertation investigates the inclusion complexation behavior of various ferrocene derivatives with the receptors: cucurbit[7]uril (CB7) or cucurbit[8]uril (CB8). The author describes three studies on different research emphasis carried out by a wide range of techniques including electrochemistry (cyclic voltammetry, square-wave voltammetry), NMR spectroscopy, electrospray ionization mass spectroscopy (ESI-MS) and UV-Vis spectroscopy.

Chapter 1 is a brief introduction on the evolution of cucurbituril chemistry and describes the extensive research on the applications of members of the cucurbituril family. For instance, the exceptionally high binding affinities of CB7 with certain guests have drawn much attention and led to the design of synthetic guests, which could reach the extraordinarily high binding affinity of ca.  $10^{15} \text{ M}^{-1}$ . Also, the modification of cucurbituril molecules has afforded the opportunity to immobilize the biomolecules by taking advantage of their unique and robust binding affinities. The potential applications and further development of

cucurbiturils are unlimited and exciting in fields from material science to medical devices.

Chapter 2 describes the design and synthesis of a series of ferrocene derivatives featuring a linker between the two cyclopentadienyl rings (cyclic ferrocene guests). The linker controls the conformation of the ferrocene group and substantially limits it from free rotation. ESI-MS, electrochemical and NMR spectroscopic methods were used to investigate the formation of the inclusion complexes between the CB7 host and this series of cyclic ferrocene guests. The results show clearly that the ferrocene group is included inside the CB7 cavity with fairly strong binding affinities ranging from  $10^8$ - $10^{10}$  M<sup>-1</sup>. Due to the bulky macrocyclic linker, which is mostly kept outside the CB7 in the complexes, it is concluded that the resulting complexes adopt a so-called closed conformation.

Chapter 3 describes the interactions between a series of bi-armed ferrocene guests and CB7 (or CB8). The varying degree of methylation on the substituent strongly affects the association kinetics as well as the overall main binding site. Further investigation in the interactions of some model guests and CB7 (or CB8) was carried out to explain the complexation behavior of this series of ferrocene guests with CB7 (or CB8). It has been proved that this series of ferrocene guests can form very stable inclusion complexes with CB7 symmetrically, that is, the ferrocene group resides inside the CB7 cavity, with each of the side arms protruding through each of the CB7 portals. However, the binding stoichiometry varies with CB8 depending on the degree of methylation of the substituents.

Chapter 4 introduces a model ferrocene-CB7 system, in which the pKa of the ferrocene guest shifts 2.6 pH units upon CB7-inclusion-complexation. A four-state thermodynamic model was firstly established between the complexation and protonation processes in order to determine the pKa shifts. The decrease in the stability of the inclusion complex was observed upon deprotonation of the ferrocene guest and further oxidation. A schematic thermodynamic cube is completed for the binding interactions between various forms of this ferrocene guests and CB7 resulting from redox and acid/base properties. This work demonstrates the possibility that simple chemical transformations under relatively mild conditions could substantially decrease the binding affinity of the highly stable complexes formed between cationic ferrocene guest and CB7 host.

## TABLE OF CONTENTS

	Page
LIST OF FIGURES.....	vi
LIST OF SCHEMES .....	xiii
LIST OF TABLES .....	xiv
<b>CHAPTER 1</b>	<b>1</b>
<b>INTRODUCTION</b>	
1.1 A short story of the cucurbit[n]uril (CBn) family .....	1
1.2 The synthesis and functionalization of CBn (n=5-8,10) .....	14
1.2.1 Preparation of CB members.....	14
1.2.2 Functionalization of cucurbiturils .....	15
1.3 Summary and out look .....	17
<b>CHAPTER 2</b>	<b>18</b>
<b>INCLUSION COMPLEXATION BETWEEN CYCLIC FERROCENE DERIVATIVES AND CUCURBIT[7]URIL (CB7)</b>	
2.1 Background .....	18
2.2 Forces driving the binding of cyclic ferrocene guests and CB7 .....	20
2.3 <sup>1</sup> H NMR spectroscopic experiments to investigate the complexation behavior of cyclic ferrocene guests <b>1-4</b> and CB7.....	22
2.4 Electrochemistry of free guests <b>1-4</b> and their CB7 complexes .....	29
2.4.1 Cyclic voltammetry on conventional glassy carbon electrode .....	30
2.4.2 Cyclic voltammetry on Pt disk ultramicroelectrode (UME) for determination of diffusion coefficient (D <sub>o</sub> ) of the free guest <b>1-4</b> and their CB7 complexes .....	33
2.4.2.1 The radius calibration by ferrocenemethanol .....	34
2.4.2.2 Measurement of D <sub>o</sub> for guests <b>1-4</b> .....	35
2.5 Electrospray ionization mass spectrometry for the complexation confirmation.....	36
2.6 <sup>1</sup> H NMR competition experiments for determination of the association equilibrium constants .....	40
2.7 Calculated structures of guests <b>1-4</b> .....	42
2.8 Interaction between guest <b>5</b> with CB7 and Ag <sup>+</sup> .....	46
2.9 Experimental .....	53
2.9.1 Synthesis of guest <b>1</b> .....	53



2.9.2 Synthesis of guest <b>2</b> .....	54
2.9.3 Synthesis of guest <b>3</b> .....	55
2.9.4 Synthesis of guest <b>4</b> .....	56
2.9.5 Synthesis of guest <b>5</b> .....	57
2.10 Conclusion .....	59

## CHAPTER 3

60

### COMPLEXATION OF A SERIES OF BI-ARMED FERROCENE GUESTS WITH CUCURBIT[7]URIL (CB7) AND CUCURBIT[8]URIL (CB8)

3.1 Background .....	60
3.2 Series of bi-armed ferrocene guests .....	62
3.3 Studies on the complexation behavior between bi-armed ferrocene guests and CB7 host .....	63
3.3.1 Interaction between DFc-CH and CB7 .....	65
3.3.2 Interaction between DFc-M-CH and CB7 .....	68
3.3.3 Interaction between DFc-2M-CH and CB7 .....	72
3.4 Study of the complexation kinetics of DFc-2M-CH and CB7 .....	73
3.4.1 Determination of the reaction rate constant <i>k</i> for complexation of DFc-2M-CH with CB7 .....	73
3.4.2 Analysis of the complexation of DFc-2M-CH with two equivalents of CB7 .....	78
3.5 Interaction between the bi-armed ferrocene guests and CB8 .....	82
3.5.1 Study on complexation with CB8 by <sup>1</sup> H NMR spectroscopy .....	82
3.5.2 Study on complexation with CB8 by square-wave voltammetry .....	86
3.5.3 Complexation between bi-armed ferrocene guests with CB8 by ESI-MS .....	89
3.6 Determination of association equilibrium constant <i>K</i> of model compounds .....	91
3.6.1 Determination of association equilibrium constants for the complexes of the model molecules and CB hosts by UV-Vis competition experiments .....	92
3.6.2 Discussion on the complexation behavior of bi-armed ferrocene guests with CB hosts (CB7 and CB8) .....	97
3.6.3 Determination of the <i>K</i> values of complexes DFc-CH•CB7, DFc-M-CH•CB7 and DFc-2M-CH•CB7 by <sup>1</sup> H NMR competition experiments ...	98
3.7 Experimental .....	100
3.7.1 Synthesis of DFc-CH .....	101
3.7.2 Synthesis of DFc-M-CH .....	102
3.7.3 Synthesis of DFc-2M-CH .....	103
3.7.4 Synthesis of 3M-CH .....	103
3.7.5 Synthesis of DFc-3M .....	104
3.8 Conclusion .....	105

**CHAPTER 4** **106**

**CUCURBIT[7]URIL COMPLEXATION-INDUCED pKa SHIFT OF N-METHYLAMINOMEHTYLFERROCENE (MFc)**

4.1 Background .....	106
4.2 Thermodynamic “four-state model” of protonation and complexation of MFc and CB7 .....	109
4.3 Determination of association equilibrium constants by <sup>1</sup> H NMR competition experiment .....	110
4.4 Determination of the pKas of free cationic MFcH <sup>+</sup> and complex MFcH <sup>+</sup> •CB7 by cyclic voltammetry .....	115
4.5 Determination of the pKas of free cationic MFcH <sup>+</sup> and complex MFcH <sup>+</sup> •CB7 using <sup>1</sup> H NMR spectroscopy .....	119
4.6 Thermodynamics .....	122
4.6.1 Prediction of CB7-complexation-induced pKa shift of MFcH <sup>+</sup> by the thermodynamic “four-state model” .....	122
4.6.2 Thermodynamic cube .....	124
4.7 Experimental .....	127
4.7.1 Synthesis of MFc .....	128
4.7.2 pH adjustment and measurement .....	128
4.7.3 Confirmation of CB7-inclusion complex by ESI-MS .....	129
4.8 Conclusion .....	130

**REFERENCES** **131**

## LIST OF FIGURES

	Page
<b>Figure 1.1.1</b> Preparation of CB <sub>n</sub> from condensation reactions between glycoluril and formaldehyde under acidic conditions	2
<b>Figure 1.1.2</b> X-ray crystal structures of CB <sub>[n]</sub> (n=5-8). Color codes: carbon gray; nitrogen, blue; oxygen, red	4
<b>Figure 1.1.3</b> Some examples of ferrocenyl and adamantanyl guests for CB7	5
<b>Figure 1.1.4</b> X-ray crystal structure of the complex of CB7 and 1,1'-bis(trimethylammoniomethyl) ferrocene	6
<b>Figure 1.1.5</b> Guest molecules based on a bicyclo[2,2,2]octane core	7
<b>Figure 1.1.6</b> Some fluorescent dyes for CB7	7
<b>Figure 1.1.7</b> Carbocation guests for CB7	8
<b>Figure 1.1.8</b> Some Nitroxides and TEMPO guests for CB7	9
<b>Figure 1.1.9</b> Ferrocene guests containing methylammonium residue and TEMPO residue with variable degree of methylation	9
<b>Figure 1.1.10</b> X-ray crystal structures of the CB8-inclusion complexes of 1,4-butylienedipyridinium (left) and 1,10-decylienedipyridinium (right)	10
<b>Figure 1.1.11</b> Some guests for 2:1 CB8-inclusion complexation	11
<b>Figure 2.1</b> Molecular structures of cyclic ferrocene guests <b>1-5</b>	20
<b>Figure 2.2</b> Neutral and cationic ferrocene guests for CB7 with high binding affinity	21
<b>Figure 2.3.1</b> <sup>1</sup> H NMR spectra of 1 mM <b>1</b> <sup>2+</sup> (a) in the absence and in the presence of (b) 0.25, (c) 0.5, (d) 0.75, (e) 1.0 and (f) 1.25 equiv. of CB7 in D <sub>2</sub> O (pH ~4)	24
<b>Figure 2.3.2</b> Optimized conformation of <b>1</b> <sup>2+</sup> •CB7 complex (B3LYP/sto3g*)	25
<b>Figure 2.3.3</b> <sup>1</sup> H NMR spectra of 1 mM <b>2</b> <sup>2+</sup> (a) in the absence and in the presence of (b) 0.25, (c) 0.5, (d) 0.75, (e) 1.0 and (f) 1.25 equiv. of CB7 in D <sub>2</sub> O (pH ~4)	25

<b>Figure 2.3.4</b> $^1\text{H}$ NMR spectra of 1 mM $3^{4+}$ (a) in the absence and in the presence of (b) 0.25, (c) 0.5, (d) 0.75, (e) 1.0 and (f) 1.25 equiv. of CB7 in $\text{D}_2\text{O}$ (pH $\sim$ 4)	27
<b>Figure 2.3.5</b> $^1\text{H}$ NMR spectra of 1 mM $4^{2+}$ (a) in the absence and in the presence of (b) 0.25, (c) 0.5, (d) 0.75, (e) 1.0, (f) 1.2 and (g) 1.5 equiv. of CB7 in $\text{D}_2\text{O}$ (pH $\sim$ 4)	27
<b>Figure 2.4.1</b> Cyclic voltammetry of 1 mM $1^{2+}$ with 0 (black), 0.5 (brown) and 1.0 (red) equiv. of CB7 in 0.1 M NaCl / $\text{H}_2\text{O}$ solution (pH $\sim$ 4) at 25 $^\circ\text{C}$ . Scan rate: 100 mV/s	31
<b>Figure 2.4.2</b> Cyclic voltammetry of 1 mM $2^{2+}$ with 0 (black), 0.5 (brown) and 1.0 (red) equiv. of CB7 in 0.1M NaCl / $\text{H}_2\text{O}$ solution (pH $\sim$ 4) at 25 $^\circ\text{C}$ . Scan rate: 100 mV/s	32
<b>Figure 2.4.3</b> Cyclic voltammetry of 1mM $3^{4+}$ with 0 (black), 0.5 (brown) and 1.0 (red) equiv. of CB7 in 0.1M NaCl / $\text{H}_2\text{O}$ solution (pH $\sim$ 4) at 25 $^\circ\text{C}$ . Scan rate: 100mV/s	32
<b>Figure 2.4.4</b> Cyclic voltammetry of 1mM $4^{2+}$ with 0 (black), 0.5 (brown) and 1.0 (red) equiv. of CB7 in 0.1M NaCl / $\text{H}_2\text{O}$ solution (pH $\sim$ 4) at 25 $^\circ\text{C}$ . Scan rate: 100mV/s	32
<b>Figure 2.4.5</b> Cyclic voltammetry on UME of (a) 1 mM and (b) 2 mM of Fc-OH in 0.1 M NaCl/ $\text{H}_2\text{O}$ solution at 25 $^\circ\text{C}$ . Scan rate: 20 mV/s	35
<b>Figure 2.4.6</b> Cyclic voltammetry on UME of 1 mM (a) $1^{2+}$ , (b) $2^{2+}$ , (c) $3^{4+}$ and (d) $4^{2+}$ in the absence (black) and presence of 1 equiv. of CB7 (red) in 0.1M NaCl / $\text{H}_2\text{O}$ solution (pH $\sim$ 4) at 25 $^\circ\text{C}$ . Scan rate: 20 mV/s	36
<b>Figure 2.5</b> Experimental and theoretical simulation of high-resolution ESI-TOF mass spectra of guest (a) <b>1</b> (b) <b>2</b> (c) <b>3</b> and (d) <b>4</b> with 1 equiv. of CB7 carrying two positive charges in the complexes in water solution (pH $\sim$ 4)	38
<b>Figure 2.6.1</b> Reference guest cobaltocenium ( $\text{Cob}^+$ )	40
<b>Figure 2.7</b> Energy-minimized structures of guest <b>1-3</b> in deprotonated conformation (a, c, e) and protonated conformation (b, d, f) and guest <b>4</b> (g) in top and size view	44
<b>Figure 2.8.1</b> Molecular structure of guest <b>5</b> with a bulky linker	47
<b>Figure 2.8.2</b> $^1\text{H}$ NMR spectra of guest <b>5</b> at pH range from 2-11	48

<b>Figure 2.8.3</b> $^1\text{H}$ NMR spectra of 1 mM guest $5^{2+}$ (a) in the absence and in the presence of (b) 0.25, (c) 0.5, (d) 1.0 and (e) 1.25 equiv. of CB7 in $\text{D}_2\text{O}$ (pH ~4)	49
<b>Figure 2.8.4</b> $^1\text{H}$ NMR spectra of 1 mM guest $5^{2+}$ (a) in the absence and in the presence of (b) 0.25, (c) 0.5 and (d) 1.0 equiv. of $\text{Ag}^+$ and then addition of <1 (e) and >1 equiv. of CB7 in $\text{D}_2\text{O}$ (pH ~4)	49
<b>Figure 2.8.5</b> $^1\text{H}$ NMR spectra of 1 mM guest <b>5</b> in the (a) absence and presence of (b) 0.37, (c) 0.75, and (d) 1.0 equiv. of $\text{Ag}^+$ in $\text{D}_2\text{O}$ (pH ~8)	50
<b>Figure 2.8.6</b> $^1\text{H}$ NMR spectra of 1 mM guest <b>5</b> (a) in the absence and in the presence of (b) 0.25, (c) 0.5 and (d) 1.0 equiv. of CB7 and then addition of (e) 1 equiv. of $\text{Ag}^+$ in $\text{D}_2\text{O}$ (pH ~8)	51
<b>Figure 2.8.7</b> Cyclic voltammetry of 1 mM guest $5^{2+}$ with 0 (black), 0.25 (red), 0.5 (brown), 1.0 (green) and 1.25 (blue) equiv. of CB7 in 1M $\text{NaNO}_3$ / $\text{H}_2\text{O}$ solution (pH ~4) at 25 °C. Scan rate: 100mV/s	52
<b>Figure 2.8.8</b> Cyclic voltammetry of 1 mM guest <b>5</b> with 0 (black), 0.5 (brown) and 1.0 (red) equiv. of $\text{Ag}^+$ in 0.1M $\text{NaNO}_3$ / $\text{H}_2\text{O}$ solution (pH ~8) at 25 °C. Scan rate:100 mV/s	52
<b>Figure 3.2</b> Molecular structures of a series of bi-armed ferrocene guests: DFc-CH, DFc-M-CH and DFc-2M-CH	63
<b>Figure 3.3.1.1</b> $^1\text{H}$ NMR spectra of 1 mM DFc-CH in the (a) absence and presence of (b) 0.25, (c) 0.5, (d) 1.0 and (e) 1.25 equiv. of CB7 in $\text{D}_2\text{O}$ (pD 4.5)	66
<b>Figure 3.3.1.2</b> Cyclic voltammetry of 1 mM DFc-CH with 0 (black), 0.5 (brown) and 1.0 (red) equiv. of CB7 in 0.1 M $\text{NaCl}$ / $\text{H}_2\text{O}$ solution (pH ~4) at 25 °C. Scan rate: 100 mV/s	67
<b>Figure 3.3.1.3</b> Experimental and theoretical simulation of high-resolution ESI-TOF mass spectra of the bi-armed guest DFc-CH with 1 equiv. of CB7 The complex is diprotonated in water solution (pH ~4)	68
<b>Figure 3.3.2.1</b> $^1\text{H}$ NMR spectra of 1 mM DFc-M-CH in the (a) absence and presence of (b) 0.25, (c) 0.5, (d) 1.0 and (e) 1.25 equiv. of CB7 in $\text{D}_2\text{O}$ (pD 4.5)	70
<b>Figure 3.3.2.2</b> Cyclic voltammetry of 1 mM DFc-M-CH with 0 (black), 0.5 (brown) and 1.0 (red) equiv. of CB7 in 0.1 M $\text{NaCl}$ / $\text{H}_2\text{O}$ solution (pH ~4) at 25 °C. Scan rate: 100 mV/s	71

<b>Figure 3.3.2.3</b> Experimental and theoretical simulation of high-resolution ESI-TOF mass spectra of the bi-armed guest DFc-M-CH with 1 equiv. of CB7. The complex is diprotonated in water solution (pH ~4)	71
<b>Figure 3.3.3</b> Cyclic voltammetry of 1 mM DFc-2M-CH with 0 (black), 0.25 (red), 0.5 (brown), 0.75 (green), 1.0 (purple) and 1.25 (blue) equiv. of CB7 in 0.1 M NaCl /H <sub>2</sub> O solution (pH ~4) at 25 °C. Scan rate: 100 mV/s, recorded right after the addition of CB7	73
<b>Figure 3.4.1.1</b> Characteristic kinetics plot of complexation of DFc-2M-CH with 1euqiv. of CB7 at 25 °C	76
<b>Figure 3.4.1.2</b> <sup>1</sup> H NMR spectra of 1 mM of DFc-2M-CH in the absence (a) and presence of 1 equiv. of CB7 recorded at (b) 0, (c) 30, (d) 50, (e) 60, (f) 80, (g) 110 and (h) 130 mins at 25 °C	77
<b>Figure 3.4.1.3</b> Experimental and theoretical simulation of high-resolution ESI-TOF mass spectra of the bi-armed guest DFc-2M-CH with 1 equiv. of CB7. The complex is diprotonated in water solution (pH ~4)	77
<b>Figure 3.4.2.1</b> <sup>1</sup> H NMR spectra of DFc-2M-CH in the (a) absence and presence of 1 equiv. of CB7 (black) after (b) 0 min, (c) 30 min, (d) 5h, (e) 1 day and then addition of 1 equiv. of CB7 (red) after (f) 0 min, (g) 10h and (h) 1day at 25 °C	79
<b>Figure 3.4.2.2</b> <sup>1</sup> H NMR spectra of DFc-2M-CH in the (a) absence and presence of 2 equiv. of CB7 after (b) 0 min, (c) 30 min, (d) 3h, (e) 1 day at 25 °C	80
<b>Figure 3.4.2.3</b> Cyclic voltammetry of 1 mM DFc-2M-CH in the absence (black) and the presence of 0.5 (red), 1.0 (brown) and 2.0 (green) equiv. of CB7 in 0.1 M NaCl/H <sub>2</sub> O solution recorded at equilibrium 25 °C. Scan rate: 100mV/s	81
<b>Figure 3.5.1.1</b> <sup>1</sup> H NMR spectra of 0.1 mM DFc-CH in the (a) absence and presence of (b) 0.5, (c) 1.0, (d) 1.5 and (e) 2.0 equiv. of CB8 in D <sub>2</sub> O (pD 4.5)	83
<b>Figure 3.5.1.2</b> <sup>1</sup> H NMR spectra of 0.1 mM DFc-M-CH in the (a) absence and presence of (b) 0.3, (c) 0.6, (d) 1.0, (e) 1.5 and (f) 2.0 equiv. of CB8 in D <sub>2</sub> O (pD 4.5)	84
<b>Figure 3.5.1.3</b> <sup>1</sup> H NMR spectra of 0.1mM DFc-2M-CH (a) in the absence and in the presence of (b) 0.44, (c) 0.88, (d) 1.0, (e) 1.76, (f) 2.65 and (g) 3.52 equiv. of CB8 in D <sub>2</sub> O (pD 4.5)	86

<b>Figure 3.5.2.1</b> Square Wave Voltammetry of 0.1 mM Fc-CH in the absence (black) and the presence of 1 (brown) and 2 (red) equivalent of CB8 in 50 mM NaCl/H <sub>2</sub> O pH 4 at 25 °C. Scan rate: 60 mV/s	87
<b>Figure 3.5.2.2</b> Square Wave Voltammetry of 0.1 mM Fc-M-CH in the absence (black) and the presence of 1 (brown) and 2 (red) equivalent of CB8 in 50 mM NaCl/H <sub>2</sub> O pH 4 at 25 °C. Scan rate: 60 mV/s	88
<b>Figure 3.5.2.3</b> Square Wave Voltammetry of 0.1 mM Fc-2M-CH in the absence (black) and the presence of 1 (brown) and 2 (red) equivalent of CB8 in 50 mM NaCl/H <sub>2</sub> O pH 4 at 25 °C. Scan rate: 60 mV/s	89
<b>Figure 3.5.3.1</b> Experimental and theoretical simulation of high-resolution ESI-TOF mass spectra of the complex DFc-CH•CB8. The complex is diprotonated in water solution (pH ~4)	90
<b>Figure 3.5.3.2</b> Experimental and theoretical simulation of high-resolution ESI-TOF mass spectra of the complex DFc-M-CH•CB8. The complex is diprotonated in water solution (pH ~4)	90
<b>Figure 3.5.3.3</b> Experimental and theoretical simulation of high-resolution ESI-TOF mass spectra of the complex DFc-2M-CH•CB8. The complex carries two positive charges in water solution (pH ~4)	91
<b>Figure 3.6.1</b> Molecular structures of the model molecules	92
<b>Figure 3.6.1.1</b> Cobaltocenium as the reference guest in the binding competition experiments	93
<b>Figure 3.6.1.2</b> Plot of absorbance values of 14.9 μM Cob <sup>+</sup> in the presence of 200 μM NH <sub>3</sub> -CH and increasing CB7 concentrations (0-60 μM) in 50 mM CH <sub>3</sub> COONa/H <sub>2</sub> O solution at 25 °C. Dots are experimental points and the line represents the best fit to the competitive 1:1 binding model	94
<b>Figure 3.6.1.3</b> Plot of absorbance values of 15 μM Cob <sup>+</sup> in the presence of 20 μM 3M-CH and increasing CB7 concentrations (0-30 μM) in 50 mM CH <sub>3</sub> COONa/H <sub>2</sub> O solution at 25 °C. Dots are experimental points and the line represents the best fit to the competitive 1:1 binding model	94
<b>Figure 3.6.1.4</b> Plot of absorbance values of 14.9 μM Cob <sup>+</sup> in the presence of 220 μM NH <sub>3</sub> -CH and increasing CB8 concentrations (0-60 μM) in 50 mM CH <sub>3</sub> COONa /H <sub>2</sub> O solution at 25 °C. Dots are experimental points and the line represents the best fit to the competitive 1:1 binding model	95

<b>Figure 3.6.1.5</b> Plot of absorbance values of 21.3 $\mu\text{M}$ $\text{Cob}^+$ in the presence of 16.2 $\mu\text{M}$ 3M-CH and increasing CB8 concentrations (0-35 $\mu\text{M}$ ) in 50 mM $\text{CH}_3\text{COONa}/\text{H}_2\text{O}$ solution at 25 $^\circ\text{C}$ . Dots are experimental points and the line represents the best fit to the competitive 1:1 binding model	95
<b>Figure 3.6.1.6</b> Plot of absorbance values of 15 $\mu\text{M}$ $\text{Cob}^+$ in the presence of 20 $\mu\text{M}$ DFc-3M and increasing CB8 concentrations (0- 5 $\mu\text{M}$ ) in 50 mM $\text{CH}_3\text{COONa}/\text{H}_2\text{O}$ solution at 25 $^\circ\text{C}$ . Dots are experimental points and the line represents the best fit to the competitive 1:1 binding model	95
<b>Figure 3.6.3.1</b> $^1\text{H}$ NMR spectra of (a) 0.5 mM Ad-Py in the presence of 0.5 mM CB7 and then addition of 0.5 mM DFc-2M-CH at (b) 0 h, (c) 4 h, (d) 8 h, (e) 32 h and (f) 0.5 mM free DFc-2M-CH in 50 mM $\text{CH}_3\text{COONa}/\text{H}_2\text{O}$ at 25 $^\circ\text{C}$ (pD 4.5)	99
<b>Figure 3.6.3.2</b> Potential energy diagram of the complexation of DFc-2M-CH and Ad-Py with CB7	100
<b>Figure 4.1.1</b> pH titration by monitoring the UV absorption band of TBZ ( $\lambda_{\text{mon}}=318$ nm, 15 mm, in water) in the absence (open circles) and presence of 2.5 mM CB7 (filled circles). The pertinent protonation equilibrium is shown on the right	107
<b>Figure 4.1.2</b> Molecular structure of N-Methylaminomethyl ferrocene (MFc)	108
<b>Figure 4.3.1</b> Reference guests 1-(1-adamantyl)-pyridinium bromide (Ad-Py) (left) and cobaltocenium hexafluorophosphate ( $\text{Cob}^+$ )	112
<b>Figure 4.3.2</b> $^1\text{H}$ NMR spectrum of a sample containing 0.5 mM MFcH <sup>+</sup> , 0.5 mM Ad-Py and 0.5 mM CB7 in 50 mM $\text{CD}_3\text{COONa}/\text{D}_2\text{O}$ solution (pH ~4) at 25 $^\circ\text{C}$	113
<b>Figure 4.3.3</b> $^1\text{H}$ NMR spectrum of a sample containing 0.5 mM MFc, 0.5 mM Ad-Py and 0.5 mM CB7 in 50 mM $\text{CD}_3\text{COONa}/\text{D}_2\text{O}$ solution (pH ~12) at 25 $^\circ\text{C}$	115
<b>Figure 4.3.1</b> Cyclic voltammetry on glassy carbon electrodes of 1 mM (a) free MFc and (b) complex MFc•CB7 in 0.1 M NaCl/ $\text{H}_2\text{O}$ solution of pH values range of 4-12 at 25 $^\circ\text{C}$ . Scan rate: 100mV/s	117



- Figure 4.3.2** Plot of the  $E_{1/2}$  values v.s. pH values of 1 mM (a) free MFc and (b) complex MFc•CB7 for determination of the  $pK_{a(\text{free})}$  and  $pK_{a(\text{complex})}$  at 25 °C. The red dotted square in a is the pH range where two pairs of redox peaks were observed 118
- Figure 4.4.3** Cyclic voltammetric behaviors of 1 mM MFc in the absence (black) and the presence of 0.5 (red) and 1.0 (green) of equiv. of CB7 in 0.1 M NaCl/H<sub>2</sub>O solution of pH values of (a) 5, (b) 9 and (c) 12 at 25 °C. Scan rate: 100mV/s 119
- Figure 4.4.1** (a) <sup>1</sup>H NMR spectra of 1 mM free MFc in 0.1 M NaCl/D<sub>2</sub>O solutions of increasing pD range of 4-12. Plots of chemical shifts of protons on (b) –CH<sub>3</sub> and (c) –CH<sub>2</sub>- versus the pD values of solutions 121
- Figure 4.5.2** (a) <sup>1</sup>H NMR spectra of 1 mM free MFc in 0.1 M NaCl/D<sub>2</sub>O solutions of increasing pD range of 4-12. Plots of chemical shifts of protons on (b) –CH<sub>3</sub> and (c) –CH<sub>2</sub>- versus the pD values of solutions 122
- Figure 4.7.3** Experimental and theoretical simulation of high-resolution ESI-TOF mass spectra of the complex MFcH<sup>+</sup>•CB7+Na<sup>+</sup> in water solution (pH ~4) 129

## LIST OF SCHEMES

	Page
<b>Scheme 1.1.1</b> The formation of ternary complex of CB8 and two tetrathiafulvalene cation radicals	12
<b>Scheme 1.1.2</b> CB8- induced protein dimerization by formation of the hetero-ternary complex between $\pi$ -donor dihydroxynaphthalene unit and $\pi$ -acceptor viologen unit with CB8	13
<b>Scheme 1.2.1</b> General purification of the CB <sub>n</sub> mixtures	15
<b>Scheme 1.2.2</b> The procedure of CB6 monofunctionalization with guest assistance and further modification	16
<b>Scheme 2.1</b> Demonstration of open and closed conformation of the ferrocene-CB7 inclusion complex	19
<b>Scheme 2.9</b> Synthetic procedure of guest <b>5</b>	57
<b>Scheme 3.4.1</b> The association and dissociation of DFc-2M-CH and CB7	74
<b>Scheme 4.2</b> Thermodynamic “four-state model” of protonation of MFc and complexation with CB7	110
<b>Scheme 4.6.2.1</b> Thermodynamic “four-state model” of redox of MFc and complexation with CB7	126
<b>Scheme 4.6.2.2</b> Schematic thermodynamic cube of CB7 and various forms of guest MFc	126

## LIST OF TABLES

	Page
<b>Table 2.3</b> Chemical shifts ( $\delta$ ) of protons of interest on the free guests 1-4 (data in black) and their CB7 inclusion complexes (data in red) in ppm in D <sub>2</sub> O (pH ~4)	28
<b>Table 2.4.1</b> Cyclic voltammetric data of compounds <b>1-4</b> in 0.1M NaCl/H <sub>2</sub> O solution (pH ~4) at 25 °C	33
<b>Table 2.4.2</b> Diffusion coefficient values of free guests <b>1-4</b> and their CB7 complexes in 0.1M NaCl /H <sub>2</sub> O solution (pH ~4) at 25 °C. Scan rate: 20 mV/s	36
<b>Table 2.6</b> Association equilibrium constant $K_{Fc}$ of guests <b>1-4</b> in 50 mM sodium acetate (pH 4) at 25 °C	42
<b>Table 3.6.1</b> Association equilibrium constant $K$ values of complexes of model molecules with CB7 and CB8 in 50 mM CH <sub>3</sub> COONa /H <sub>2</sub> O solution (pH4) at 25 °C	96
<b>Table 3.6.2</b> Estimated free energy values of the complexes between fully methylated bi-armed ferrocene guest (DFc-2M-CH) and CB7 (or CB8) at 25 °C	97
<b>Table 4.6.2.1</b> The equilibrium constants values as labeled in <b>Scheme 4.6.2.2</b> , the values in red are determined directly from <sup>1</sup> H NMR and electrochemical experiments and the values in black are obtained through the thermodynamic circles cube in <b>Scheme 4.6.2.2</b>	127
<b>Table 4.6.2.2</b> The half-wave potentials obtained from cyclic voltammetric experiments	127

## CHAPTER 1

### Introduction

#### 1.1 A Short Story of the Cucurbit[n]uril (CBn) Family

Avidin, a tetrameric biotin-binding protein, can bind to biotin with extremely high association equilibrium constant (K) up to  $10^{15} \text{ M}^{-1}$ . This makes biotin-avidin complex one of the strongest non-covalent interaction pairs in nature.<sup>1,2</sup> Because of the high degree of binding affinity and binding specificity of avidin-biotin system, it has been established as a powerful tool in biological sciences such as probes and affinity matrices in numerous projects.<sup>3</sup> Later on, the development of new methods in biotinylation antibodies and other biomolecules allows the avidin-biotin system to be widely used in many applications from research to medical devices and pharmaceuticals.<sup>4</sup> However, this natural robust binding pair suffers some downsides, for example, the avidin-biotin complex could not be easily dissociated unless operated in elevated temperatures, which will cause the denaturation of the proteins. Also, the interaction between avidin and biotin may be interrupted undesirably by bio-systems.<sup>5</sup> Therefore, design and development of synthetic molecular systems that could exhibit ultra-high binding affinity and high binding selectivity are very attractive and important for understanding non-covalent interactions and further more for the practical applications.<sup>6</sup>

Cucurbit[n]urils (CBn) are synthetic macrocycles by condensation reactions between glycoluril and formaldehyde under acidic conditions. They feature a pumpkin-like shape with two identical carbonyl-rimed portals and a

hydrophobic cavity. (**Figure 1.1.1**) The parent cucurbit[n]urils were synthesized unknowingly by German chemist Robert Behrend and his coworkers more than a century ago.<sup>7</sup> However, the detailed recognition of the white solid products had never been reported until 1980s. Mock and coworkers initially investigated the structure of these white powdery solids and found the cyclic hexamer (CB6) and named these solids as “cucurbit[n]urils”.<sup>8</sup>

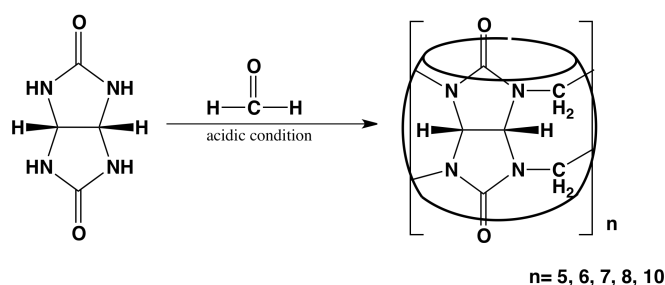


**Figure 1.1.1** Preparation of CB<sub>n</sub> from condensation reactions between glycoluril and formaldehyde under acidic conditions

The recognition of the CB6 structure immediately led to comprehensive investigations of the host-guest inclusion complexation with particularly high binding affinity and numerous guests have been identified.<sup>9</sup> The CB6 (host) generally binds organic ammonium cations (guest). For example, 1,6-hexane- and 1,5-pentanediammonium have the equilibrium association constant (K) values of  $2.9 \times 10^8$  and  $1.5 \times 10^8 \text{ M}^{-1}$  with CB6 in 50 mM NaCl solution, respectively.<sup>10</sup> The positively charged form of spermine displays a highly strong interaction with a K value of  $5.4 \times 10^{10} \text{ M}^{-1}$  in 0.20 M LiCl and  $3.3 \times 10^9 \text{ M}^{-1}$  in 50 mM NaCl. It has been noted that 1,4-butanediammonium is the shortest 1, $\omega$ -alkanediammonium dications that could still relatively strongly bind to CB6 (K=

$2.0 \times 10^7 \text{ M}^{-1}$ ). As the distance between the two positively charged amine groups decreases to have only three methylene groups in between (1,3-propanediammonium), the binding affinity to CB6 dramatically drops to a K value of  $3.3 \times 10^2 \text{ M}^{-1}$  in 50 mM NaCl. According to Kim and Inoue,<sup>11</sup> 1,3-propanediammonium no longer forms the inclusion complex with CB6, instead, it interacts with the portals of the CB6 cavity. The interaction between neutral guests and CB6 has also investigated by several groups. Nau and coworkers recently reported the interaction of some hydrocarbons with CB6 with binding affinities over  $3 \times 10^3 \text{ M}^{-1}$ . Particularly, in 1.0 mM HCl solution, the association equilibrium constants of propane, butane and cyclopentane reach up to  $1.5 \times 10^5$ ,  $2.8 \times 10^5$  and  $1.3 \times 10^6 \text{ M}^{-1}$ , respectively.<sup>12</sup> However, the relatively small cavity of CB6 still limits the research on the binding behavior of CB6 as host, although it can form relatively strong inclusion complexes with 1, $\omega$ - diammonium guests.

Starting in year of 2000, homologues of different sizes, ranging from cucurbit[5]uril to cucurbit[10]uril (CBn, n=5-8 and 10), were subsequently isolated and characterized thanks to the exciting work of Kimoon Kim, Lyle Issacs and Anthony Day.<sup>13</sup> Some members in the cucurbituril family show larger cavities than CB6. **Figure 1.1.2** from Kim's review paper<sup>14</sup> depicts both the side and top views of X-ray structures of some cucurbituril members (CBn, n=5,6,7,8), clearly showing an increasing trend of the cavity outer diameters as well as the cavity volumes. For instance, the outer diameter of cucurbit[7]uril (CB7) and cucurbit[8]uril (CB8) are 16.0 Å and 17.5 Å, respectively, which results in a cavity volume of  $279 \text{ Å}^3$  for CB7 and  $479 \text{ Å}^3$  for CB8.

The enlarged sizes of the CB<sub>n</sub> greatly expand the range of guests that could be potentially included inside the cucurbituril cavities with efficient binding affinities. Thus, the investigation of the interactions of CB<sub>n</sub> with their guests has attracted tremendous interest, that is, the synthetic host–guest pairs, for fundamental chemistry research and eventually the practical applications in many areas, such as nanotechnology,<sup>15</sup> material science<sup>16</sup> and medical devices.<sup>17</sup>

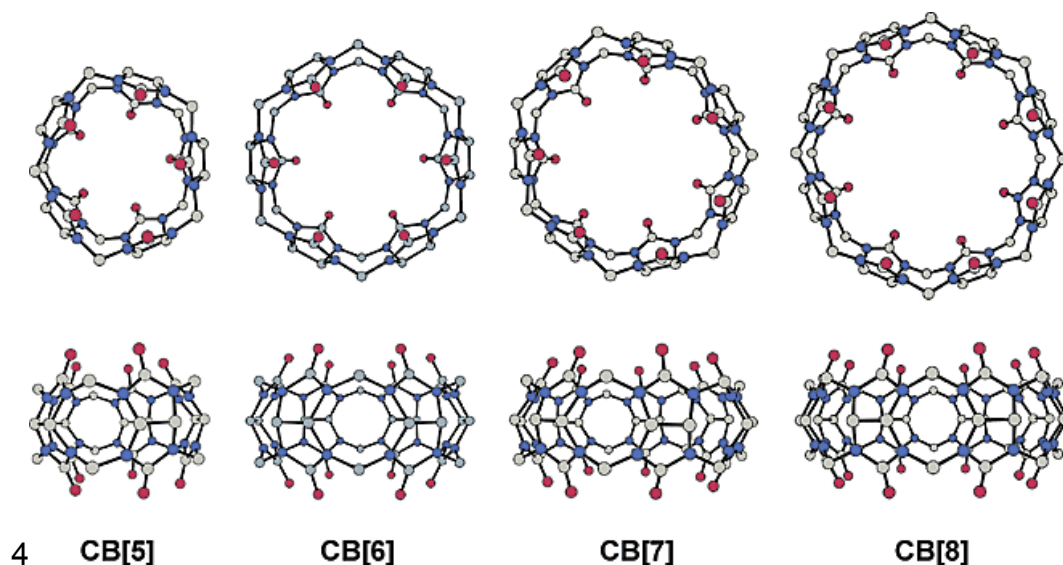


**Figure 1.1.2** X-ray crystal structures of CB[*n*] (*n*=5-8). Color codes: carbon, gray; nitrogen, blue; oxygen, red.<sup>14</sup>

Among all the members in the cucurbituril family, CB7 has drawn much attention in host-guest systems. Unlike CB6 and CB8, which show with poor solubility (0.018 mM and <0.1 mM, respectively),<sup>13d</sup> CB7 possesses a high level aqueous solubility (20-30 mM) in neutral H<sub>2</sub>O. Also, it exhibits a good ability to complex a variety of guest molecules with high binding affinities. Accordingly, it has been used extensively in supramolecular chemistry. In contrast to other

synthetic hosts, such as  $\beta$ -cyclodextrin, whose association equilibrium constants rarely get over  $10^5 \text{ M}^{-1}$ , CB7 commonly displays binding affinities to its guests between  $10^7 \text{ M}^{-1}$  and  $10^{13} \text{ M}^{-1}$ . For example, with the ferrocenemethyl- and adamantyl- containing guests (see some examples in **Figure 1.1.3**), exceptionally high K values ( $\sim 10^{12} \text{ M}^{-1}$ ) in aqueous media have been determined.<sup>18</sup>

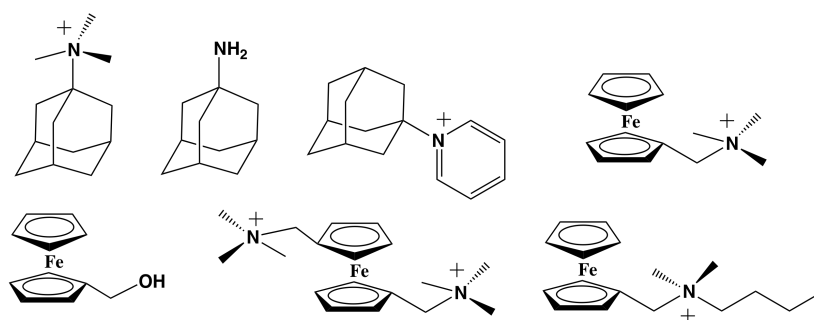


**Figure 1.1.3** Some examples of ferrocenyl and adamantyl guests for CB7

In 2007, a synthetic ferrocene derivative, 1,1'-bis(trimethylaminomethyl)ferrocene, was reported to display an extraordinarily strong interaction with CB7 with a K value as high as  $10^{15} \text{ M}^{-1}$  in pure water, which is competitive to that of natural avidin-biotin pair.<sup>19</sup> The X-ray crystal structure of this complex shows clearly that ferrocene moiety is sitting completely inside the CB7 cavity and each of the trimethylammoniomethyl substituents protrudes through one of the CB7 portals symmetrically. The positive charges of nitrogen atoms electrostatically interact with the rim of carbonyl oxygens, boosting an extraordinarily strong binding affinity (see **Figure 1.1.4** from reference 19).



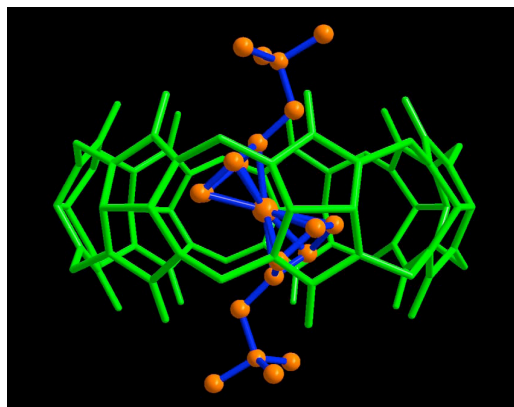


**Figure 1.1.4** X-ray crystal structure of the complex of CB7 and 1,1'-bis(trimethylammoniomethyl) ferrocene<sup>19</sup>

Very recently, inspired by the ferrocene-based guests, Kim, Inoue and Gilson reported a series of designed guests based on a bicyclo[2.2.2]octane core.<sup>20</sup> These three guests (**Figure 1.1.5**) display CB7 affinities strikingly similar to those previously observed for the ferrocene series of CB7 guests, ranging from  $10^9 \text{ M}^{-1}$  for neutral guests to  $10^{15} \text{ M}^{-1}$  for dicationic guests. The binding free energies of these three bicyclo[2,2,2]octane-based guests with CB7 in aqueous media are exceptionally high for such small host-guest system, ranging from -13.4 to -20.6 kcal/mol. These high binding affinities are commensurate with those of ferrocenyl guests with CB7 reported previously.<sup>21</sup> The neutral guest **1** in **Figure 1.1.5** has a binding free energy around -13 kcal/mol, similar to the observed neutral ferrocene guest. The addition of two ammonium groups close to the portals induces ion-dipole interactions, resulting in an increase in the binding affinity by about 7 kcal/mol. The computed conformation of guest **3** in the **Figure 1.1.5** complexed with CB7 indicates the similar positioning as the dicationic

ferrocene guest mentioned above, that is, the CB7 threads through the long chain and resides onto the bicyclo[2,2,2]octane core, with the positively charged ammonium groups interacting with the rim of carbonyl oxygens on the portals of the CB7 cavity through ion-dipole interactions.

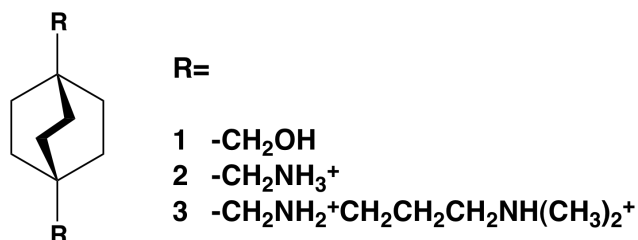


**Figure 1.1.5** Guest molecules based on a bicyclo[2,2,2]octane core <sup>20</sup>

CB7 has also been reported to form complexes with photoactive dyes,<sup>21</sup> such as some examples in **Figure 1.1.6**, which have been extensively used as probes in model biological systems, based on the changes in the photochemical properties upon complexation with biomolecules.<sup>22</sup> The CB7-complexation of these dyes will induce similar changes in the properties of the dyes, such as fluorescent properties and pKa. The binding affinities usually range from 10<sup>5</sup> to 10<sup>7</sup> M<sup>-1</sup>.

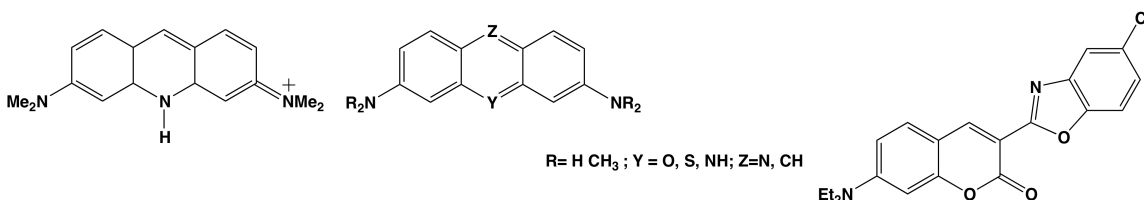


**Figure 1.1.6** Some fluorescent dyes for CB7 <sup>21</sup>

CB7 can interact with carbocations as well. For instance, diphenylmethane, triphenylmethane<sup>23</sup> and triphenylpyrylium<sup>24</sup> carbocations have been found to form complexes with CB7 with binding affinities  $2.0 \times 10^4$ ,  $1.7 \times 10^4$  and  $7.5 \times 10^5$ , respectively (**Figure 1.1.7**).

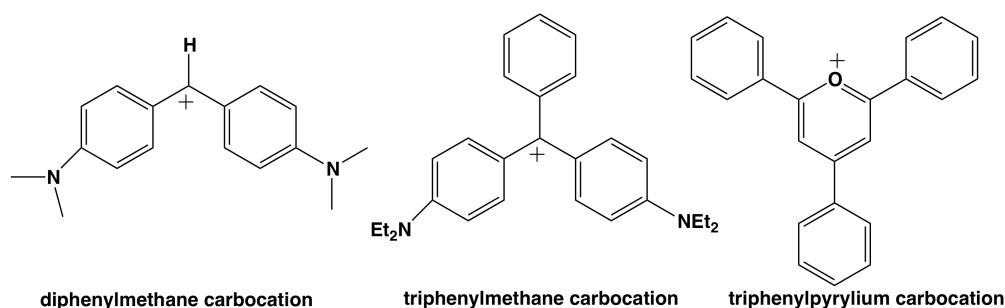


**Figure 1.1.7** Carbocation guests for CB7

The CB7-encapsulation of nitroxides and 2,2,6,6-tetramethyl piperidine-N-oxyl (TEMPO) and their derivatives has been reported.<sup>25</sup> (**Figure 1.1.8**) Very recently, our group has investigated the binding interactions between a series of ferrocene guests containing a methylammonium residue and a TEMPO group at the end of the substituent, where the ammonium nitrogen is connected to a variable number of methyl groups (**Figure 1.1.9**).<sup>26</sup> The interactions were monitored by electron paramagnetic resonance (EPR) spectroscopy and the change in the nitrogen hyperfine splitting on the TEMPO can be observed upon complexation. Not surprisingly, due to the high binding affinity between the ferrocene group and CB7, this series of ferrocene guests containing TEMPO residue all form very stable inclusion complexes with CB7, in which the main

binding site is the ferrocene residue. However, the binding site of the CB8 complexes of this series of guests is highly dependent on the degree of methylation.

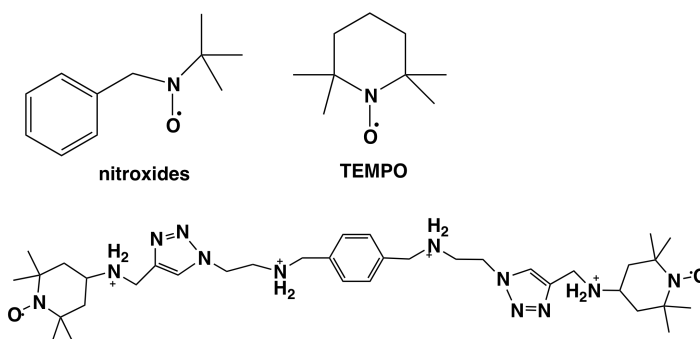


**Figure 1.1.8** Some Nitroxides and TEMPO guests for CB7 <sup>25</sup>

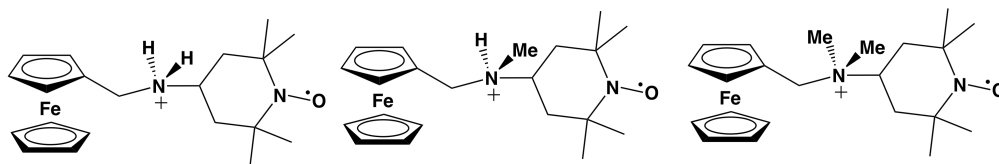


**Figure 1.1.9** Ferrocene guests containing methylammonium residue and TEMPO residue with variable degree of methylation <sup>26</sup>

CB7-control of J- and H-aggregates and disruption of other non-covalent interactions has also been reported. Gadde and coworkers in our group found that CB7 could be used to disrupt the formation of J-aggregates of pseudoisocyanine dye by forming a stable inclusion complex and removing the free dye from the solution. Similarly, the H-aggregate formed with the pinacyanol dye can be controlled by CB7 complexation.<sup>27</sup> The absorption bands of the J-aggregates at 575 nm and H-aggregates at 473 nm vanished upon CB7-complexation.

Similarly to CB7, CB8 also displays very strong binding affinities towards hydrophobic guests, especially those with positive charges. For instance, some adamantyl guests can form 1:1 CB8-inclusion complexes with binding affinities ranging from  $10^8$  to  $10^{11} \text{ M}^{-1}$ .<sup>18a</sup> The long alkylammonium chains containing 8-16 methylene groups have been found to curl inside the CB8 cavity, affording a U-shaped conformation. Kim and coworkers have proposed “The complexation is dominantly or almost exclusively enthalpy-driven, owing to the increased Van Der Waals contact between the folded aliphatic chain and the inner wall of the host cavity.”<sup>28</sup> The binding affinities in this series were found to be  $1.0\text{-}4.8 \times 10^6 \text{ M}^{-1}$  along  $\text{C}_8\text{-C}_{16}$ . This curling behavior inside the CB8 cavity upon complexation is also observed in the cases of 1,12-dodecanediammonium cation,<sup>29</sup> 1,4-butyldiene- and 1,10-decyldienedipyridinium cations.<sup>30</sup> Clearly shown in **Figure 1.1.10** as an example, these dicationic chains adopt a U-shaped confirmation inside the CB8.

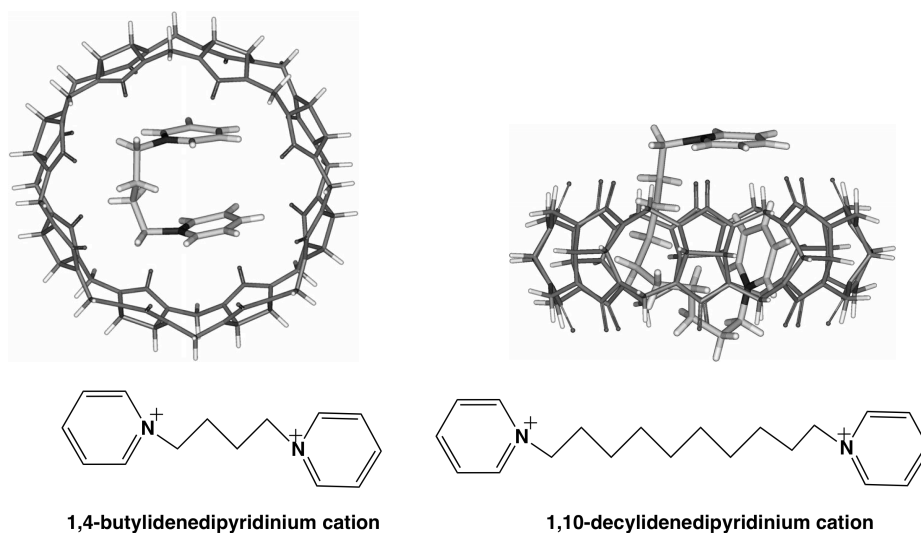


**Figure 1.1.10** X-ray crystal structures of the CB8-inclusion complexes of 1,4-butyldienedipyridinium (left) and 1,10-decyldienedipyridinium (right)<sup>30</sup>

As previously mentioned,<sup>26</sup> our group reported that CB8 could encapsulate the TEMPO residue depending on the degree of the methylation of the nitrogen atom on the ammonium group (see **Figure 1.1.9** for detail). In the fully methylated ferrocene-TEMPO guest results in the main binding site switches to the TEMPO, which is in strong contrast to the case of CB7.

Besides the findings of the 1:1 inclusion complexation between CB8 and various kinds of guests, CB8 is widely investigated for its excitingly unique ability to include two guests in its cavity. Several guests have been reported to form the 2:1 guest-host inclusion complexes with CB8. For example, the guests shown in **Figure 1.1.11** can undergo double encapsulation in the CB8 cavity.<sup>13b,31</sup> In these cases, the two identical encapsulated guests are usually parallel to each other to form homodimers and interact by  $\pi$ - $\pi$  stacking interactions. Kim and coworkers found that CB8 could effectively bind two viologen cation radicals upon the reduction of the guest<sup>32</sup> or two tetrathiafulvalene cation radicals (see **Scheme 1.1.1**).<sup>33</sup>

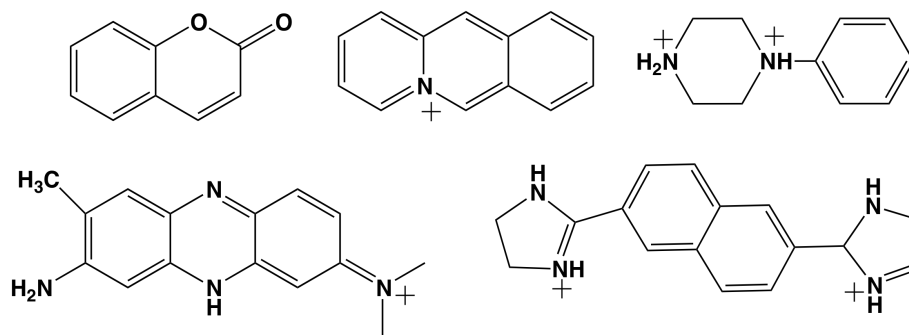
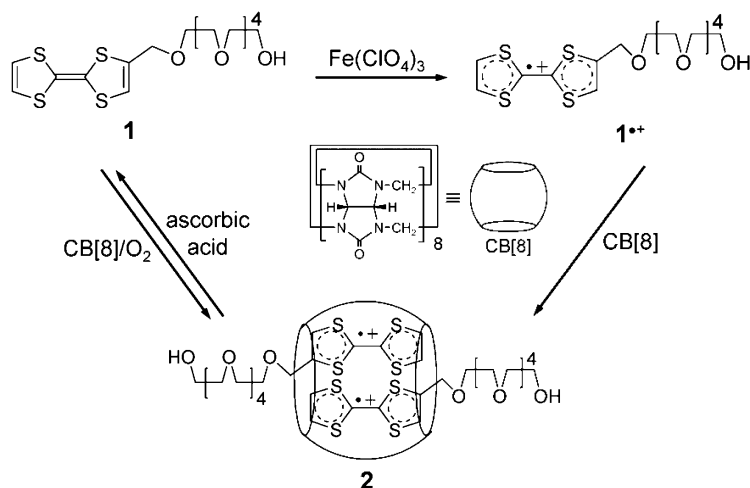


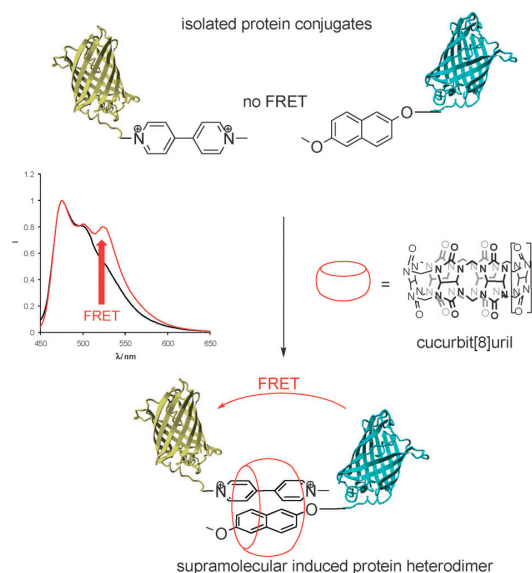
**Figure 1.1.11** Some guests for 2:1 CB8-inclusion complexation



**Scheme. 1.1.1** The formation of ternary complex of CB8 and two tetrathiafulvalene cation radicals<sup>13</sup>

CB8 can also engulf two different guests to form hetero-ternary complexes. The favorable interactions between both guests would further stabilize the whole ternary complex. Our group has found that the dicationic guest 2,7-dimethyldiazaphenanthrenium forms a fluorescent 1:1 inclusion complex with CB8, which can effectively bind to indole derivatives, such as serotonin and tryptophan.<sup>34</sup> Our group also found a similar inclusion complex of 2,7-dimethyldiazapyrenium and CB8 with a  $K$  value of  $8.9 \times 10^5 \text{ M}^{-1}$ , which can act as host to bind the second guest containing aromatic  $\pi$ -donor residues, such as catechol and dopamine.<sup>35</sup> Kim and coworkers reported the formation of stable ternary CB8 complexes, where an aromatic electron rich guest and an aromatic electron deficient guest share the CB8 cavity, undergoing charge transfer interactions to form a stable complex inside the cavity, such as 2,6-dihydroxynaphthalene and methylviologen.<sup>36</sup> The unique ability of CB8 to contain

$\pi$  donor-acceptor charge transfer complexes or homodimers of cation radicals has inspired the design of biomolecular conjugates<sup>37</sup> (**Scheme 1.1.2**) as well as systems for dendrimer self-assembly under redox control.<sup>38</sup> Urbach and coworkers unveiled the amino acid-recognition properties of the stable viologen-CB8 inclusion complex, which acts as a receptor to bind aromatic amino acids, such as tryptophan, tyrosine and phenylalanine as well as singly charged tryptophan derivatives and tryptophan containing peptides.<sup>39</sup>



**Scheme 1.1.2** CB8- induced protein dimerization by formation of the hetero-ternary complex between  $\pi$ -donor dihydroxynaphthalene unit and  $\pi$ -acceptor viologen unit with CB8<sup>37</sup>

Cucurbit[10]uril (CB10) has been studied since 2005, when Isaacs and coworkers reported their successful isolation of CB10 from the CB5•CB10 complex.<sup>13e</sup> They also reported the formation of the ternary complex between CB10, calix[4]arene derivative and some adamantyl guests.<sup>13e</sup> Due to the

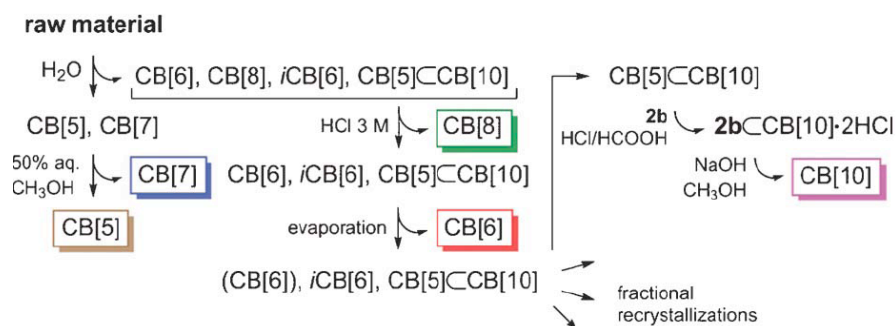


spacious cavity, CB10 is found to be a suitable molecular container for cationic porphyrins to form inclusion complexes. Moreover, these complexes could further form ternary complexes in aqueous media with a variety of aromatic amines, which interact with porphyrin rings through  $\pi$ - $\pi$  stacking.<sup>40</sup> The conformation of the CB10 complexes with some selected guests and the complexation driving forces have also been studied.<sup>41</sup>

## 1.2 The Synthesis and Functionalization of CBn (n=5-8,10)

### 1.2.1 Preparation of the CB members

Generally, CBn mixtures are obtained by reacting glycoluril and formaldehyde in concentrated hydrochloric or sulfuric acid solution at 80-100 °C, following by evaporation and consecutive precipitations in water and methanol. The major product is CB6 in this mixture. Each CB member may be separated based on the different solubility in water, water/methanol and HCl solutions (see detail in **Scheme 1.2.1**).<sup>13c</sup> An alternative procedure with higher yield of CB7 separated from the mixture was proposed by Day, in which a hot 20% glycerol aqueous solution was used to extract CB7.<sup>13a</sup> Proper guest molecules are chosen to bind to CB7 selectively in order to separate CB7 from the CB7/CB5 mixture, a process of precipitations and anion exchanges.<sup>42</sup> CB10 was isolated from the CB5•CB10 complex in 2005<sup>13e</sup> and the crystal structure of CB10 was reported in 2009<sup>13d</sup> by Isaacs's group. Day and coworkers used 1,12-dodecanediamine to eject CB5 from the CB10 cavity under conditions of low pH and recrystallized the free CB10 in concentrated HCl solution.<sup>43</sup>



**Scheme 1.2.1** General purification of the CBn mixtures <sup>13c</sup>

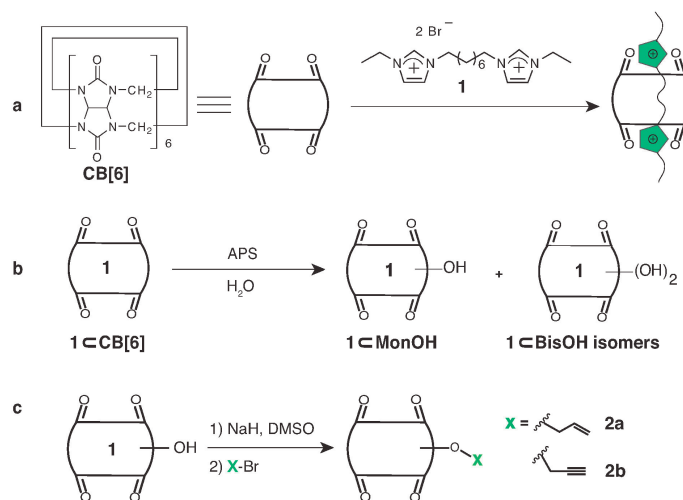
The CB products can be roughly determined by the mass spectroscopy, either matrix-assisted laser desorption/ionization (MALDI) or electrospray ionization (ESI) with time-of-flight analyzer (TOF). The observed  $m/z$  values usually reflect the CB molecule associated to small ions, such as  $\text{Na}^+$ . The purity of the CB products is analyzed by  $^1\text{H}$  NMR spectroscopy, based on the different chemical shifts of the methylene hydrogens along these cucurbituril members.<sup>13c,13b</sup> The molecular weight of the CB needs to be calibrated before use since CBs may contain water molecules, cations and HCl molecules. Our group recently reported a procedure for the determination of the effective molecular weights of CB7 and CB8 by UV-Vis titration.<sup>44</sup>

## 1.2.2 Functionalization of Cucurbiturils

One of the applications of the functionalized CBs is to attach CBs to solid phases in order to act as “glue” for biomolecule immobilization. It can be potentially used in the development of biochips, where the biomolecules are immobilized on the solid surfaces without losing their bioactivities. The extremely strong and specific interactions between avidin and biotin lead this pair to be one

of the widely used tools in the surface immobilization of biomolecules. Considering the high binding affinities of the CB hosts with selected guests, such as ferrocene-CB7 or adamantane-CB7 complexes with  $K$  values ranging  $10^9$ - $10^{15}$   $M^{-1}$ , Kim and coworkers proposed the use of the highly stable ferrocene-CB7 complex as a glue to immobilize biomolecules on the solid surface.<sup>45</sup>

The partial hydroxylation of the CBn is usually the first step in CBn functionalization. Kim has reported a decade ago that reaction of CB6 with  $K_2S_2O_8$  in water at 85 °C resulted in perhydroxy-CB6. Further modification of the -OH group on the façade of the CB6 macrocycle could lead to the successful attachment of CB6 to solid surfaces.<sup>46</sup> Later on, the same group reported the attachment of CB7 to self-assembled monolayers by a similar procedure.<sup>45</sup> Very recently, Scherman's group reported a guest-assisted synthetic procedure to monofunctionalize CB6 by controlling the amount of hydroxylation reagent  $(NH_4)_2S_2O_8$  and further chemical modification (**Scheme 1.2.2**).<sup>47</sup>



**Scheme 1.2.2** The procedure of CB6 monofunctionalization with guest assistance and further modification<sup>47</sup>

### 1.3 Summary and Outlook

In this chapter, we have briefly described the history and development of cucurbituril chemistry. Some of the cucurbituril members: CB6, CB7, CB8 and CB10 are extensively studied for their properties as host molecules to encapsulate various guest molecules with exceptionally high selectivity and binding affinities. The extraordinarily stable interactions between CB7 and some guests are found to be one of the strongest non-covalent interactions ever measured between synthetic small host-guest systems (up to  $10^{15} \text{ M}^{-1}$ ), which are comparable to the landmark avidin-biotin interactions. The enlarged cavity volumes of CB8 and CB10 allow the formation of ternary complexes, in which the two guests are either identical or not and interact through different forces, such as  $\pi$ - $\pi$  stacking or charge-transfer. Several groups have expanded cucurbituril family by functionalization of the original members. Good examples are the hydroxylation and further modifications of the facades of CB6 or CB7, respectively. These properties of cucurbituril family have led to the design of CB-based supramolecular systems consisting of biomolecules, which can be potentially used in molecular level medical devices such as biosensors and biochips.

The next three chapters will particularly focus on the studies of the interaction properties between CB7 with varying series of ferrocene-based guests. For instance, complex conformation, association kinetics and CB7-induced pKa shifts will be discussed in more details.

## CHAPTER 2

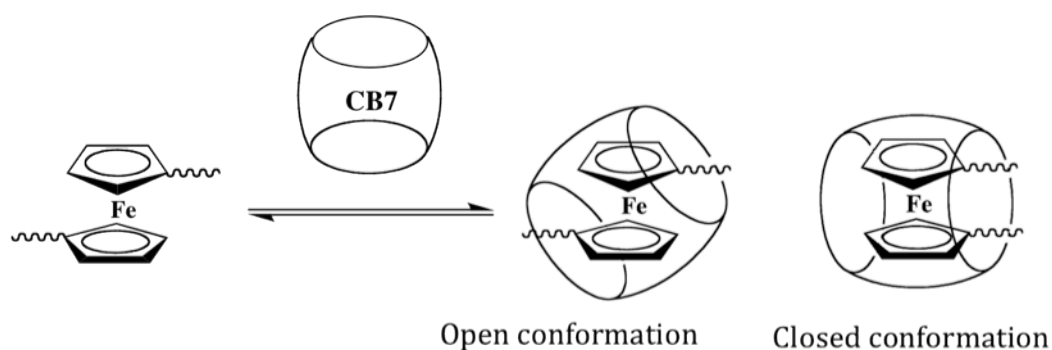
### Inclusion Complexation between Cyclic Ferrocene Derivatives and Cucurbit[7]uril (CB7)

#### 2.1 Background

The macrocyclic host cucurbit[7]uril (CB7) is one of the most interesting and important members in the cucurbituril family. It exhibits high binding affinity with several suitable guests, forming inclusion complexes in aqueous media, such as ferrocenyl and adamantyl derivatives.<sup>18a,48</sup> The equilibrium association constants (K) reach values up to  $10^{12}\sim 10^{13}$  M<sup>-1</sup> for cationic guests and  $10^{10}\sim 10^{11}$  M<sup>-1</sup> for neutral guests.<sup>18c</sup> In 2007, a synthetic dicationic guest 1,1'-bis(trimethylammoniomethyl) ferrocene was reported to have a K value of  $10^{15}$  M<sup>-1</sup>, comparable to that of the avidin-biotin system.<sup>19</sup> In this ferrocene-CB7 inclusion complex, the ferrocene moiety is nicely located inside the CB7 cavity through hydrophobic interactions, while the positive charge on each of the substituents interacts with each of the negatively charged portals of CB7 by electrostatic interactions. The X-ray crystal structure shows that each of the trimethylammoniomethyl arms protrudes through the CB7 cavity and consequently the dicationic ferrocene guest resides inside CB7 symmetrically.

In the last few years, the extraordinarily high binding affinity between ferrocene guests and CB7 in aqueous solution has led us to investigate the inclusion complexation behavior of a series of ferrocene derivatives with CB7 by NMR, electrochemistry and electrospray ionization mass spectrometry (ESI-MS)

methods.<sup>18c</sup> The results have given very promising evidence for the formation of the inclusion complexes with high K values. We have noted that bi-armed ferrocene derivatives with identical substituents on each of the cyclopentadienyl (Cp) rings always form CB7 inclusion complexes in an open, extended conformation, where each of the arms interacts with one of the portals of the CB7 cavity. The ferrocene-CB7 inclusion complexes with a closed conformation, in which the two arms protrude through the same CB7 opening, have never been reported. (**Scheme 2.1**)



**Scheme 2.1** Demonstration of open and closed conformation of the ferrocene-CB7 inclusion complex

With strong interest in the structural manipulation of the ferrocene-CB7 inclusion complexes and eventual development of supramolecular systems that can dissociate under mild conditions, a series of cyclic ferrocene guests **1-5** were designed and synthesized (**Figure 2.1**). In this series, the two Cp rings are connected through a linker, which can substantially limit the rotating motion of the two rings.

We anticipated that these cyclic ferrocene guests could form inclusion complexes with CB7 in which the linker is forced to stay on one side of the CB7 to adopt a closed conformation, leaving the other portal of the CB7 cavity free. In this chapter, we fully describe the synthetic procedures for the preparation of these cyclic ferrocene guests and the detailed investigation of the inclusion complexation with CB7 in aqueous media using NMR spectroscopy, electrochemistry, electrospray ionization mass spectrometry (ESI-MS) and computational chemical methods.

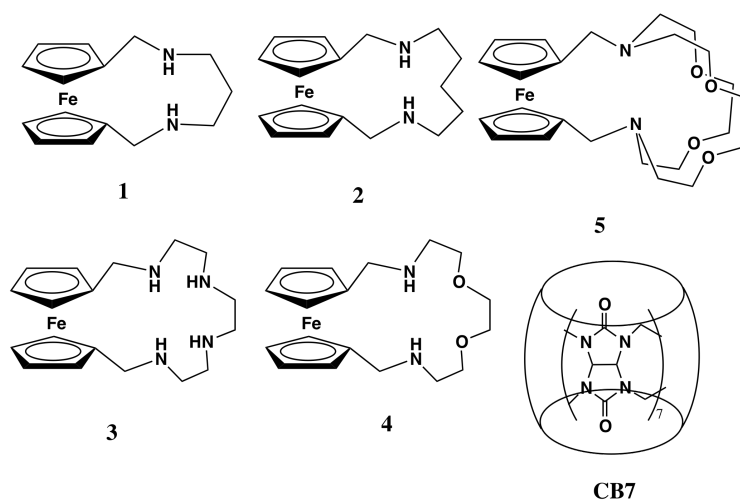


**Figure 2.1** Molecular structures of cyclic ferrocene guests 1-5

## 2.2 Forces Driving the Binding of Cyclic Ferrocene Guests and CB7

Hydrophobic interaction is one of the most important driving forces in the formation of ferrocene-CB7 inclusion complexes in aqueous media. Ferrocene is highly hydrophobic and nicely suitable for the very hydrophobic CB7 cavity. This strong interaction takes the association equilibrium constant  $K$  value of neutral

ferrocene guests and CB7 as high as  $10^9$ - $10^{10}$   $M^{-1}$ . By introducing one or two positive charges onto the side arms of ferrocene guests, the binding affinity could increase 2~3 orders of magnitude because of the addition of the electrostatic interactions (specifically, the ion-dipole interactions) around the portal area of CB7 between the positive charges and the negatively-charged carbonyl oxygens. (See some examples in **Figure 2.2**)

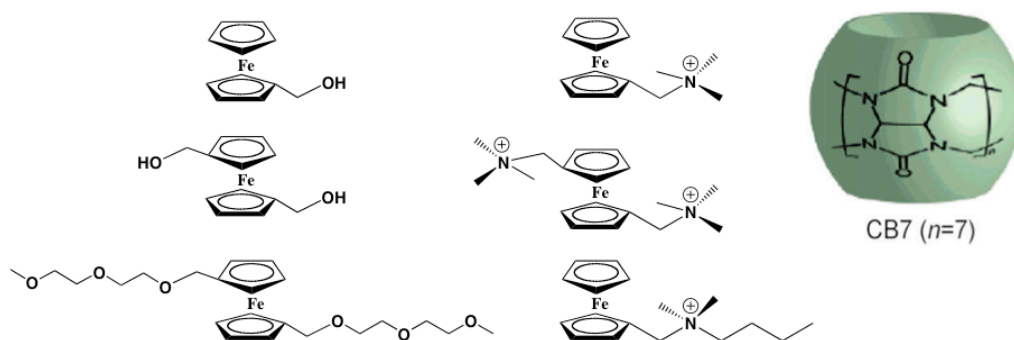


**Figure 2.2** Neutral and cationic ferrocene guests for CB7 with high binding affinity

Based on these complexation-driving forces, our cyclic ferrocene guests are designed to have two amino groups close to the ferrocene moiety, which can be fully charged, taking positive charges under acidic conditions (pH ~4). The linkers are of different sizes, which may affect the distance between the positive and negative charges, the flexibility of the whole guest molecule, as well as the insertion depth of the ferrocene moiety inside the CB7 cavity.



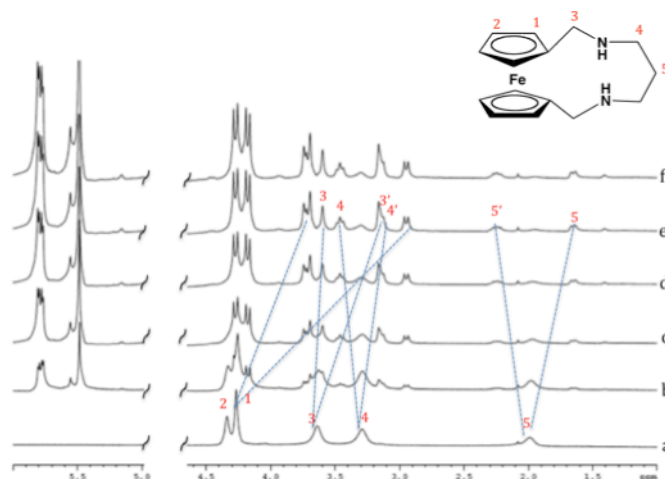
### 2.3 $^1\text{H}$ NMR Spectroscopic Experiments to Investigate the Complexation Behavior of Cyclic Ferrocene Guests 1-4 (Figure 2.1) and CB7

$^1\text{H}$  NMR spectroscopy is an extremely useful and direct way to determine not only whether the guest compound is bound by CB7, forming complexes, but also to afford considerable insight regarding the main binding site, that is, the main region of the guest included inside the CB7 cavity, as the corresponding proton resonances of this region typically shift upfield upon inclusion complexation. Similarly, the protons on the guest molecule that remain outside although in close proximity to the CB7 cavity portal in the complex experience downfield shifts. The observation of chemical shifts ( $\delta$ ) of the guest proton peaks in the absence and presence of the host can give information on the complexation behavior.

In this project, 1D proton NMR and 2D COSY were used to analyze the interactions between our cyclic ferrocene guests and the CB7 host in acidic aqueous media. All the NMR spectra were measured on a Bruker 500MHz spectrometer. 0.1 M NaCl/D<sub>2</sub>O was used as the solvent to provide the same media as that used in the electrochemical experiments. Chemical shifts ( $\delta$ ) for the  $^1\text{H}$  NMR spectra were referenced to TMS and CH<sub>3</sub>COONa ( $\delta$ = 2.08 ppm at pH=4). The peaks were assigned by using 2D COSY method.

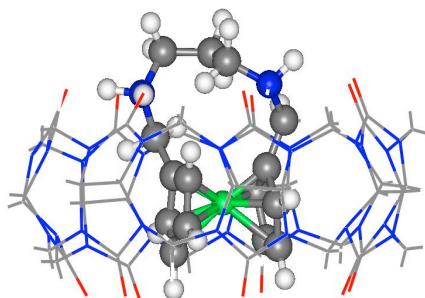
**Figure 2.3.1** shows the NMR spectroscopic changes associated with addition of gradually increasing concentrations of CB7 to a D<sub>2</sub>O solution (pH 4) of cyclic ferrocene guest **1**. Under these experimental conditions, guest **1** carries

two positive charges, as both nitrogens are protonated. The resulting pattern of the complexation-induced chemical shifts  $\delta$  of the guest protons on guest **1** is unexpectedly complicated, with all the proton resonances splitting from one single sharp peak to two peaks with different chemical shifts upon interaction with CB7. The ferrocene protons (Labeled 1 and 2 in **Figure 2.3.1**) undergo pronounced upfield shifts from 4.27 to 3.69 / 2.96 ppm and 4.34 to 3.74 / 2.93 ppm, respectively. This indicates the inclusion of the ferrocene moiety inside the CB7 cavity. The peak at 3.64 ppm, corresponding to the methylene protons between the Cp rings and the amino groups splits to two peaks with  $\delta$  values of 3.60 and 3.16 ppm in the **1**<sup>2+</sup>•CB7 complex. The chemical shifts of these two peaks reveal that one of the two methylene protons is located inside the cavity, while the other one remains around the CB7 portal, clearly less deeply included than the first. The peak splittings for methylene protons 4 and 5 on the macrocyclic linker are similar, that is, one peak shifts downfield, while the other moves upfield. For instance, the protons at position 4 split from 3.29 ppm to 3.46 and 3.13 ppm.



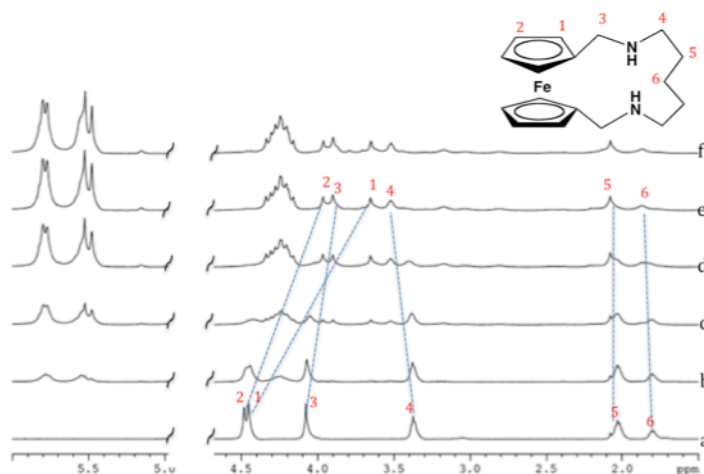
**Figure 2.3.1**  $^1\text{H}$  NMR spectra of 1 mM  $1^{2+}$  (a) in the absence and in the presence of (b) 0.25, (c) 0.5, (d) 0.75, (e) 1.0 and (f) 1.25 equiv. of CB7 in  $\text{D}_2\text{O}$  (pH  $\sim$ 4)

In order to understand these complicated peak splittings, we used computational methods to optimize the structure of the  $1^{2+}\cdot\text{CB7}$  complex at B3LYP/sto-3g\* level in the gas phase. The conformation of this complex with minimized energy in **Figure 2.3.2** clearly shows that the ferrocene moiety is positioned inside the CB7 cavity, while the macrocyclic linker -  $\text{CH}_2\text{NH}_2^+\text{CH}_2\text{CH}_2\text{CH}_2\text{NH}_2^+\text{CH}_2-$  stays around one of the CB7 portals. Due to the length and rigidity of this linker, the two protons on each of the methylene carbons adopt nonequivalent positions, which explains the splittings observed in the  $^1\text{H}$  NMR spectra. For instance, the two protons on the center methylene of the linker (Labeled 5) have different positions relative to the plane of the oxygens on the CB7 portal.



**Figure 2.3.2** Optimized conformation of  $1^{2+} \cdot \text{CB7}$  complex (B3LYP/sto3g\*)

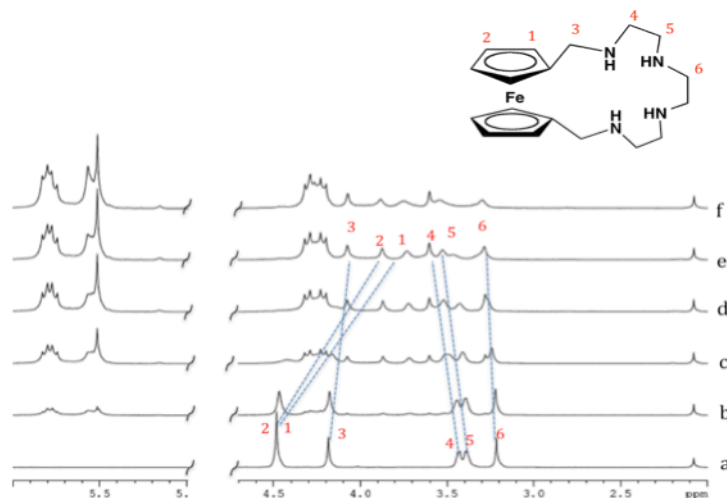
Increasing the linker length with only two more methylene groups (guest **2**) results in a much simpler pattern of proton resonances in the  $^1\text{H}$  NMR spectra upon addition of CB7 (see **Figure 2.3.3**). Methylene protons between those two nitrogens (labeled 4,5 and 6 in **Figure 2.3.3**) have downfield shifts without any splitting. This is probably due to the greater length and flexibility of the macrocyclic linker, which averages the position of those protons and results in a set of broad singlet peaks in the spectrum of  $2^{2+} \cdot \text{CB7}$ .



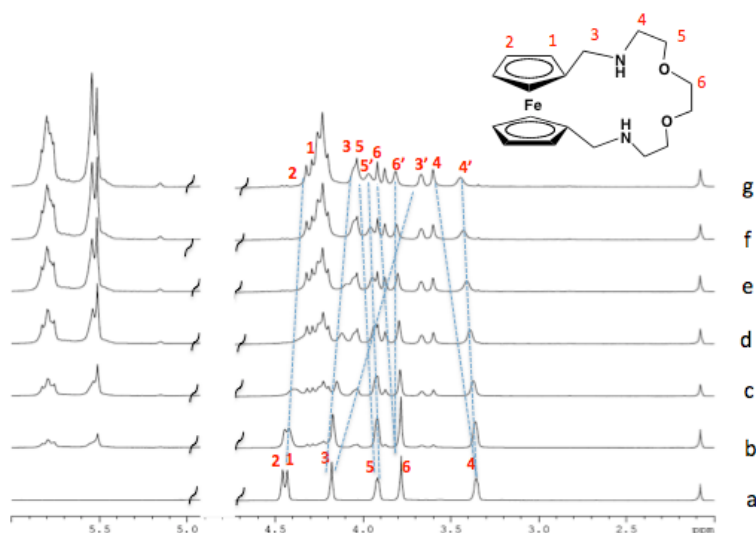
**Figure 2.3.3**  $^1\text{H}$  NMR spectra of 1 mM  $2^{2+}$  (a) in the absence and in the presence of (b) 0.25, (c) 0.5, (d) 0.75, (e) 1.0 and (f) 1.25 equiv. of CB7 in  $\text{D}_2\text{O}$  (pH  $\sim$ 4)

Guest **3**, in which the two Cp rings are connected by a longer and more rigid linker  $-\text{CH}_2\text{NH}_2^+\text{CH}_2\text{CH}_2\text{NH}_2^+\text{CH}_2\text{CH}_2\text{NH}_2^+\text{CH}_2\text{CH}_2\text{NH}_2^+\text{CH}_2-$  in acidic media exhibits a trend of proton chemical shift changes upon inclusion complexation by CB7 similar to that observed with guest **2** (**Figure 2.3.4**), that is, protons on the included ferrocene and adjacent methylenes show as upfield-shifted singlets, while those on the carbons between the nitrogens shift downfield due to their positions outside the CB7 cavity.

Compared to guest **3**, guest **4** with similar linker length shows smaller chemical shift changes. The ferrocene protons only shift upfield for 0.1 ppm, which may indicate that in this case, the ferrocene group of  $\mathbf{4}^{2+}$  does not go inside the CB7 cavity as deeply as  $\mathbf{3}^{4+}$ . Also, unlike guest **3**, the pattern of all proton resonances on the linker carbons of guest **4** splits to two downfield-shifted peaks upon CB7-complexation, which probably results from nonequivalent environment of the two protons on each of the methylene carbons caused the lower flexibility of the linker  $-\text{CH}_2\text{NH}_2^+\text{CH}_2\text{CH}_2\text{OCH}_2\text{CH}_2\text{OCH}_2\text{CH}_2\text{NH}_2^+\text{CH}_2-$  (**Figure 2.3.5**).



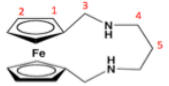
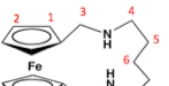
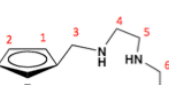
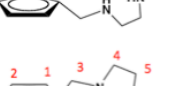
**Figure 2.3.4**  $^1\text{H}$  NMR spectra of 1 mM  $3^{4+}$  (a) in the absence and in the presence of (b) 0.25, (c) 0.5, (d) 0.75, (e) 1.0 and (f) 1.25 equiv. of CB7 in  $\text{D}_2\text{O}$  (pH  $\sim$ 4)



**Figure 2.3.5**  $^1\text{H}$  NMR spectra of 1 mM  $4^{2+}$  (a) in the absence and in the presence of (b) 0.25, (c) 0.5, (d) 0.75, (e) 1.0, (f) 1.2 and (g) 1.5 equiv. of CB7 in  $\text{D}_2\text{O}$  (pH  $\sim$ 4)

The complexation-induced chemical shifts ( $\delta$ ) of the protons on guests **1-4** in the presence of 1 equivalent of CB7 are collected in Table 2.3. In conclusion, the  $^1\text{H}$  NMR spectroscopic results show that these four cyclic ferrocene guests

with linkers of different length and flexibility all form inclusion complexes with CB7 in acidic media, with upfield shifts of the ferrocene protons and downfield shifts of the linker protons in  $^1\text{H}$  NMR spectra upon complexation. These data confidently indicate that the ferrocene group is included inside the CB7 cavity, while the linker is positioned outside around the opening. However, the pattern of proton resonances is strongly affected by the rigidity and length of the linkers, which may lead to a complicated peak splitting in case where the positions of the protons on the same carbon adopt nonequivalent positions.

Chemical shift $\delta$ (ppm)	1	2	3	4	5	6
	4.27 3.69/2.96	4.34 3.74/2.93	3.64 3.60/3.16	3.29 3.46/3.13	1.99 2.24/1.67	N/A
	4.45 3.65	4.48 3.96	4.07 3.90	3.37 3.52	2.03 2.08	1.80 1.87
	4.48 3.88	4.48 3.73	4.19 4.08	3.44/3.43 3.60	3.40/3.39 3.53	3.22 3.29
	4.43 4.32	4.46 4.29	4.18 4.10/3.67	3.36 3.41/3.60	3.92 4.04/3.95	3.78 3.88/3.80

**Table 2.3** Chemical shifts ( $\delta$ ) of protons of interest on the free guests 1-4 (data in black) and their CB7 inclusion complexes (data in red) in ppm in  $\text{D}_2\text{O}$  (pH  $\sim$ 4)

## 2.4 Electrochemistry of Free Cyclic Ferrocene Guests 1-4 and their CB7 Complexes

Ferrocene/ferrocenium (Fc/Fc<sup>+</sup>) and its derivatives are good redox-active species in both aqueous and organic media and widely used in electrochemical applications.<sup>49</sup> Our cyclic ferrocene guests are water-soluble and suitable for electrochemical experiments in aqueous media. The electrochemical behavior of ferrocene inclusion complexes has received considerable attention for more than two decades. Cyclic voltammetry (CV) provides a second effective method to determine the formation of complexes. In general, the half-wave potential ( $E_{1/2}$ ) of the ferrocene group is of interest in our CB7 complexation analysis. Formation of a ferrocene-CB7 complex usually will induce a more positive  $E_{1/2}$  and decreased currents when the ferrocene group is located inside the CB7 cavity.<sup>18b</sup> The more positive  $E_{1/2}$  shift reveals that the electrochemical oxidation of ferrocene residue is thermodynamically hindered by CB7-complexation, that is, the reduced form (Fe(II)) is more favored and stable inside the CB7 cavity. The one electron oxidation of ferrocene decreases the stability of complex. Also, due to the highly hydrophobic CB7 cavity, water molecules cannot solvate effectively and stabilize the oxidized form (Fe(III)) Fc<sup>+</sup> inside the CB7 cavity, which reflects that oxidized form is less favored inside the CB7 cavity. The decreased current levels upon CB7-inclusion-complexation indicate that the complex is bulkier and diffuses more slowly than the free ferrocene guests. The average value of peak potentials for the cathodic peak ( $E_{pc}$ ) and the anodic peak ( $E_{pa}$ ) affords the half-wave potential  $E_{1/2}$  of the corresponding redox couple. At  $E_{1/2}$ , the concentration of the



oxidized species is equal to that of the reduced species. According to the Nernst equation,  $E_{1/2}$  is equal to the formal potential ( $E^0$ ) and therefore characteristic of the redox system. In our investigation, a more positive value of  $E_{1/2}$  of the ferrocene group upon complexation is expected to indicate the formation of the ferrocene-included complexes.

#### 2.4.1. Cyclic Voltammetry on Conventional Glassy Carbon Electrode

Cyclic voltammetry of 1 mM guest  $1^{2+}$  solution shows that the half-wave potential  $E_{1/2}$  for the ferrocene oxidation shifts significantly from 361 mV to 471 mV in the presence of 1 equivalent of CB7 (**Figure 2.4.1**). The complexation leads to a more positive oxidation potential to convert ferrocene to ferrocenium, in other words, the host CB7 differentially stabilizes the reduced form of the ferrocene residue. The decreased current observed in the presence of CB7 confirms the inclusion interaction between this host and guest  $1^{2+}$ , that is, the complex has a smaller diffusion coefficient ( $D_{0 \text{ complex}}$ ) than the free ferrocene guest ( $D_{0 \text{ free}}$ ). This will be explained in the next section (**Section 2.4.2**) in more detail.

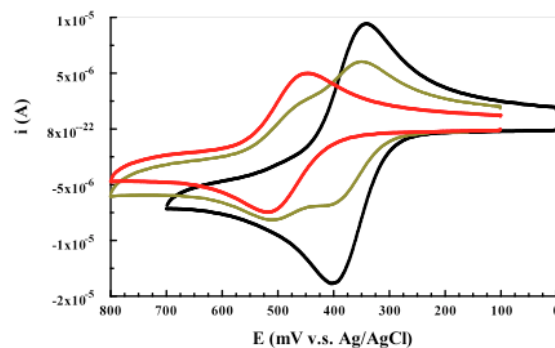


**Figure 2.4.1** Cyclic voltammetry of 1 mM  $1^{2+}$  with 0 (black), 0.5 (brown) and 1.0 (red) equiv. of CB7 in 0.1 M NaCl /H<sub>2</sub>O solution (pH ~4) at 25 °C. Scan rate: 100 mV/s

Cyclic voltammetry of guests **2-4** has also been recorded and analyzed (**Figure 2.4.2-2.4.4**). All the electrochemical data for guests **1-4** are collected in **Table 2.4**. Diminished complexation-induced currents are observed within all four guests, which confirm the formation of ferrocene-CB7 complexes in all cases. Surprisingly, the difference between  $E_{1/2}$  values ( $\Delta E_{1/2}$ ) of the ferrocene-CB7 complex and that of the free ferrocene guest vary considerably.  $\Delta E_{1/2}$  for guest **1** has a pronounced value of 110 mV. As the linker length increases, the value of  $\Delta E_{1/2}$  decreases except for **2**. With similar linkers, **3** and **4** have very similar electrochemical behavior with  $\Delta E_{1/2}$  values of 49 mV and 46 mV, respectively. However, there is no significant  $E_{1/2}$  change with **2**, which may be due to the greater flexibility of this five-carbon linker. In order to prove this assumption, we investigated the computational conformation structures of  $1^{2+}$ ,  $2^{2+}$ ,  $3^{4+}$  and  $4^{2+}$  using B3LYP/sto-3g\* method. The results will be discussed in **Section 2.7** in more detail.

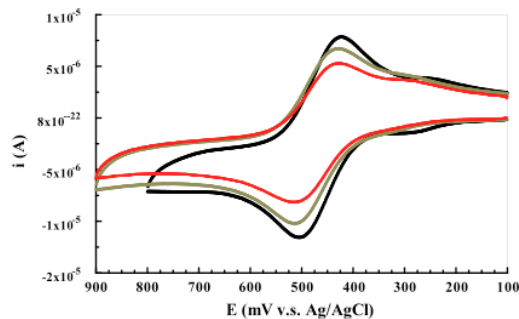


**Figure 2.4.2** Cyclic voltammety of 1 mM  $2^{2+}$  with 0 (black), 0.5 (brown) and 1.0 (red) equiv. of CB7 in 0.1M NaCl /H<sub>2</sub>O solution (pH ~4) at 25 °C. Scan rate: 100 mV/s

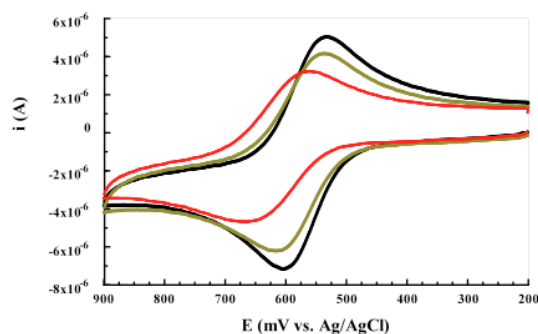


**Figure 2.4.3** Cyclic voltammety of 1mM  $3^{4+}$  with 0 (black), 0.5 (brown) and 1.0 (red) equiv. of CB7 in 0.1M NaCl /H<sub>2</sub>O solution (pH ~4) at 25 °C. Scan rate: 100mV/s

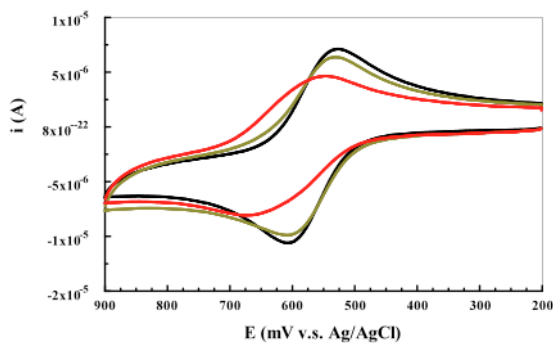


**Figure 2.4.4** Cyclic voltammety of 1mM  $4^{2+}$  with 0 (black), 0.5 (brown) and 1.0 (red) equiv. of CB7 in 0.1M NaCl /H<sub>2</sub>O solution (pH ~4) at 25 °C. Scan rate: 100mV/s

	Equiv. of CB7	E <sub>pc</sub> (mV)	E <sub>pa</sub> (mV)	ΔE (mV)	E <sub>1/2</sub> (mV)	ΔE <sub>1/2</sub>
<b>1<sup>2+</sup></b>	0	393	328	65	361	110
	1	507	434	73	471	
<b>2<sup>2+</sup></b>	0	504	425	79	465	4
	1	506	430	76	468	
<b>3<sup>4+</sup></b>	0	604	535	69	570	49
	1	670	567	103	619	
<b>4<sup>2+</sup></b>	0	608	508	79	569	46
	1	670	559	111	615	

**Table 2.4.1** Cyclic voltammetric data of compounds **1-4** in 0.1M NaCl /H<sub>2</sub>O solution (pH ~4) at 25 °C

#### 2.4.2. Cyclic Voltammetry on Pt Disk Ultramicroelectrode (UME) for Determination of Diffusion Coefficient (D<sub>0</sub>) of Free Guests 1-4 and their CB7 Complexes

The diffusion coefficient (D<sub>0</sub>) is related to the size of the molecule according to the Stokes-Einstein Equation for diffusion in solution (**Eq. 2.4.1**) and is a direct parameter to detect the formation of complex.

$$D_0 = \frac{K_B T}{6\pi\eta r} \quad \text{Eq. 2.4.1}$$

Here, D<sub>0</sub> is the diffusion coefficient, η is the viscosity and r is the radius of the spherical particle. This equation indicates that when the molecular size increases, the diffusion coefficient will decrease. The formation of the inclusion complex between a ferrocene guest and CB7 will result in a larger molecular size and should decrease the diffusion coefficient. In electrochemistry, diffusion coefficients of the redox-active species are usually measured by cyclic voltammetric methods using disk UMEs.

The diffusion coefficients of the cyclic ferrocene guests **1-4** ( $D_{0 \text{ free}}$ ) and their complexes with CB7 ( $D_{0 \text{ complex}}$ ) were measured and calculated using equation **Eq. 2.4.2**

$$i_{ss} = 4nFD_0Cr \quad \text{Eq.2.4.2}$$

Here,  $i_{ss}$  is the steady-state current,  $C$  is the concentration of the redox-active ferrocene guests,  $r$  is the radius of the disk UME surface,  $n$  is the number of electrons transferred and  $F$  is Faraday constant.

#### 2.4.2.1 The Radius Calibration by Ferrocenemethanol

According to **Eq.2.4.2**, the  $D_0$  value strongly depends on the accuracy of the radius of the UME. Thus, the first important step is to calibrate the radius of the Pt disk UME used in this experiment with a redox-active compound with a well-known diffusion coefficient value. Here, we chose ferrocenemethanol (Fc-OH), whose  $D_0$  value was determined by our group previously as  $7.8 \times 10^{-6} \text{ cm}^2/\text{s}$  in 0.1 M NaCl/H<sub>2</sub>O.<sup>18c</sup> The cyclic voltammetry on UME was recorded at a scan rate of 20 mV/s (**Figure 2.4.5**). Different concentrations of Fc-OH were used (1 mM and 2 mM). The steady-state current is 1.21 nA and 2.37 nA for 1 mM and 2 mM solutions, respectively. Applying the experimental data and all other constants to **Eq.2.4.2**, the average radius value of the Pt disk UME was found to be 4.7  $\mu\text{m}$ .

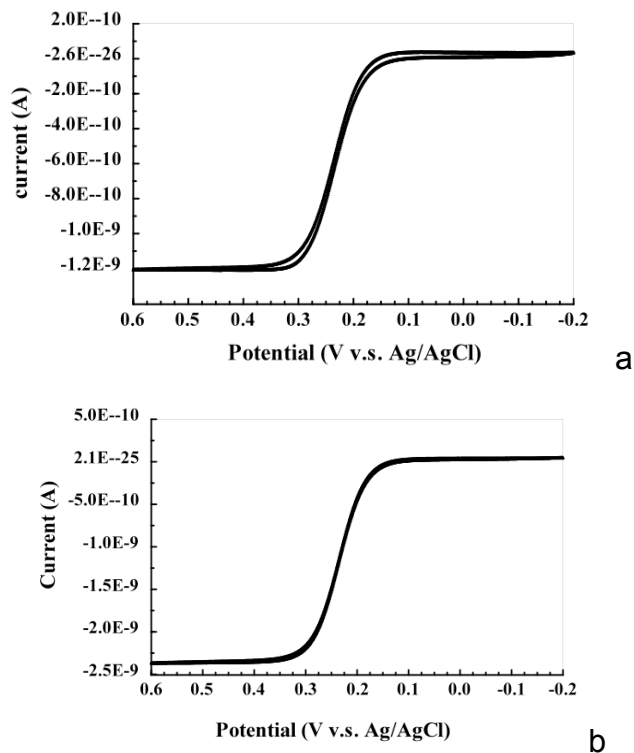


**Figure 2.4.5** Cyclic voltammetry on UME of (a) 1 mM and (b) 2 mM of Fc-OH in 0.1 M NaCl/H<sub>2</sub>O solution at 25 °C. Scan rate: 20 mV/s.

#### 2.4.2.2 Measurement of $D_0$ for Guests 1-4

The cyclic voltammetric responses on disk UME of free guests **1-4** and their CB7 inclusion complexes are shown in **Figure 2.4.6** and all the diffusion coefficient values are collected in **Table 2.4.2**. Clearly, upon formation of the ferrocene-CB7 inclusion complex, the steady-state currents decrease, which can be explained by the Stokes-Einstein equation as a result of the increased molecular size of the complexes.

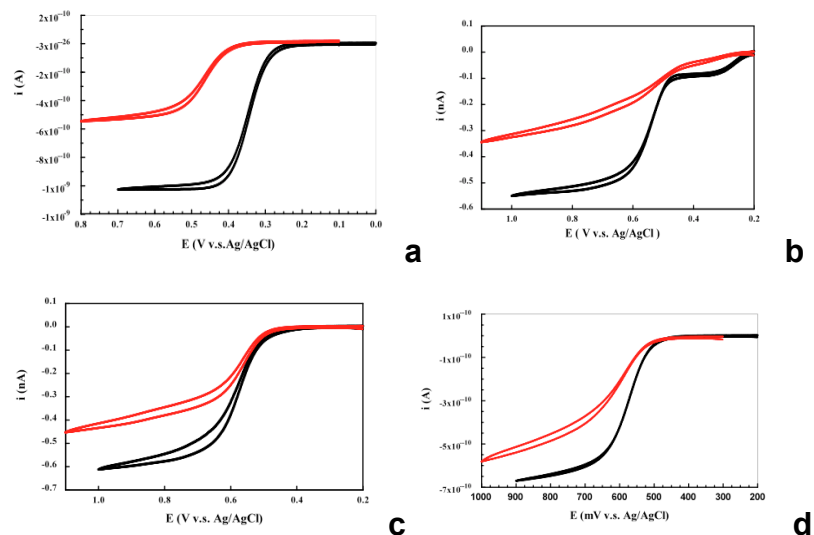


**Figure 2.4.6** Cyclic voltammetry on UME of 1 mM (a)  $1^{2+}$ , (b)  $2^{2+}$ , (c)  $3^{4+}$  and (d)  $4^{2+}$  in the absence (black) and presence of 1 equiv. of CB7 (red) in 0.1M NaCl /H<sub>2</sub>O solution (pH ~4) at 25 °C. Scan rate: 20 mV/s

cm <sup>2</sup> /s	$1^{2+}$	$2^{2+}$	$3^{4+}$	$4^{2+}$
<b>D<sub>0</sub> free</b>	$6.6 \times 10^{-6}$	$3.6 \times 10^{-6}$	$4.0 \times 10^{-6}$	$4.3 \times 10^{-6}$
<b>D<sub>0</sub> complex</b>	$3.5 \times 10^{-6}$	$2.5 \times 10^{-6}$	$3.2 \times 10^{-6}$	$4.0 \times 10^{-6}$

**Table 2.4.2** Diffusion coefficient values of free guests **1-4** and their CB7 complexes in 0.1M NaCl /H<sub>2</sub>O solution (pH ~4) at 25 °C. Scan rate: 20 mV/s.

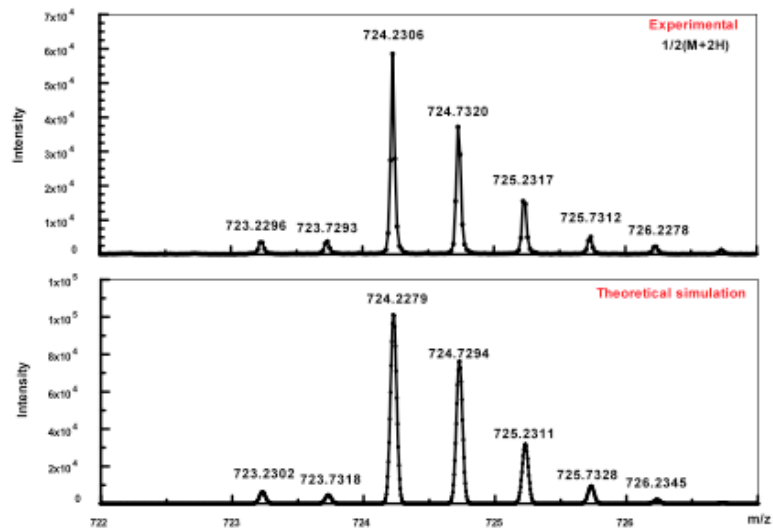
## 2.5 Electro spray Ionization Mass Spectrometry for Complexation Confirmation

Electrospray ionization mass spectrometry (ESI-MS) has played an important role in the investigation of large, non-covalent, host-guest complexes and other systems.<sup>50</sup> The electrospray ionization is a soft ionization technique with low ion internal energy that results in very limited or no fragmentations. ESI can transfer the whole complex to the gas phase in order to address their

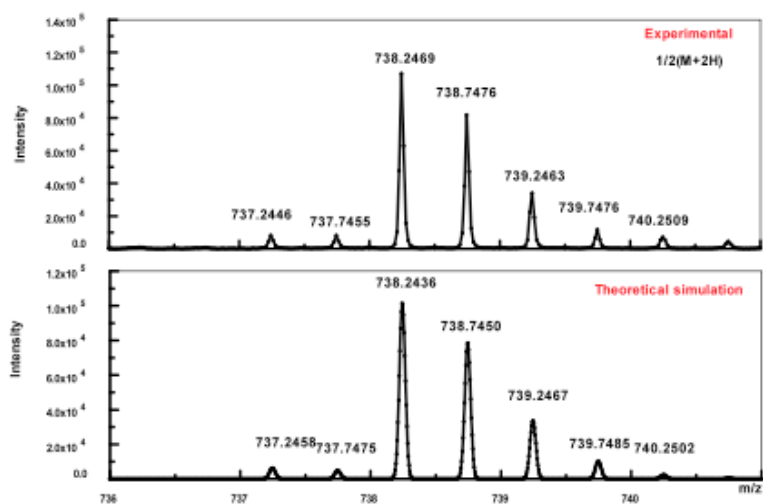
intrinsic properties without much influence from solvent molecules. By combining the pulsed operation of the time of flight analyzer (TOF), it can provide the possibility to ionize directly from the sample solution with mass range virtually unlimited. ESI-MS has been used to study complexes between cucurbiturils with ionic and neutral guests.<sup>25c, 51</sup> It efficiently provides valuable information on the complexation, the binding affinity and the stoichiometry of the complexes, etc.

Spectra in **Figure 2.5** depict the experimental m/z ratio of the complexes with two positive charges. Guests **1-4** are fully protonated at pH~4 to interact with the CB7 host, that is, guests **1**, **2** and **4** bring two positive charges to the whole complex, while guest **3** brings four positive charges. The m/z ratio value in each spectrum in **Figure 2.5** is equal to half of the molecular weight of complex. Here, M is the molecular weight of the deprotonated ferrocene guest plus CB7. The patterns of isotopic peaks in the experimental results perfectly match those obtained from theoretical simulation by using the chemical formula of the complexes. For example, the complex **1<sup>2+</sup>•CB7** shows a chemical formula:  $C_{57}H_{64}FeN_{30}O_{14}^{2+}$ , the m/z value found is 724.2306 and the calculated one is 724.2279. This confirms the formation of these very stable inclusion complexes.



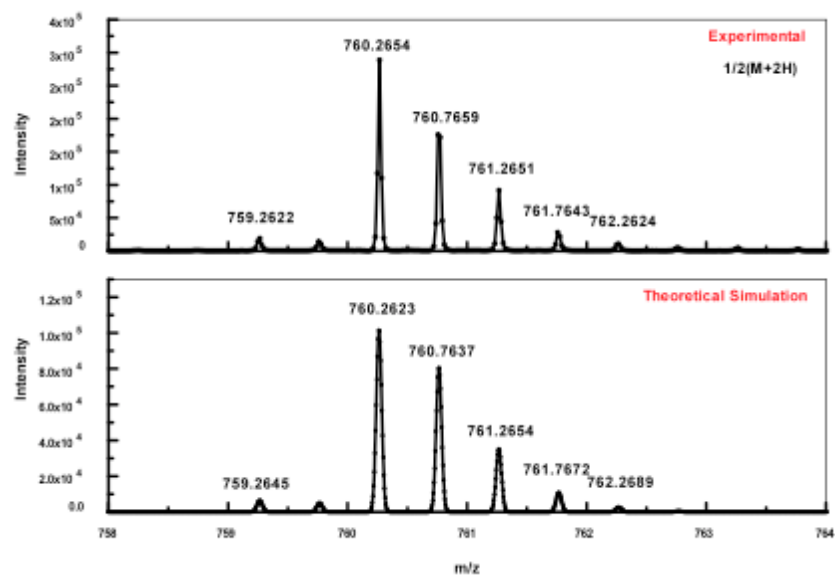


a

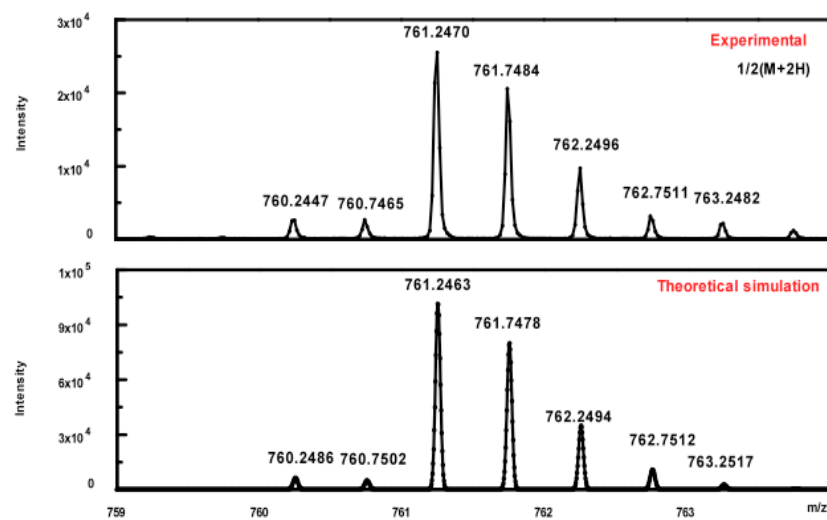


b

**Figure 2.5** Experimental and theoretical simulation of high-resolution ESI-TOF mass spectra of guest (a) **1** (b) **2** (c) **3** and (d) **4** with 1 equiv. of CB7 carrying two positive charges in the complexes in water solution (pH ~4)



C



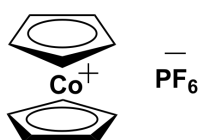
d

Figure 2.5 Continued

## 2.6 <sup>1</sup>H NMR Competition Experiments for Determination of the Association Equilibrium Constants

All the <sup>1</sup>H NMR, electrochemical and ESI-MS results in **Sections 2.3-2.5** have confirmed the formation of inclusion complexes between cyclic ferrocene guests **1-4** and CB7 host in a closed conformation manner (see **Scheme 2.1**). Upon the collection of the experimental data, we elected to determine the association equilibrium constants ( $K_{Fc}$ ) for each ferrocene-CB7 pair.

<sup>1</sup>H NMR competition experiments to measure the association equilibrium constants ( $K_{Fc}$ ) were performed at room temperature in 50 mM CD<sub>3</sub>COONa/D<sub>2</sub>O solution with the reference guest cobaltocenium (Cob<sup>+</sup>) (**Figure 2.6.1**). Each sample contains one of the ferrocene guests, Cob<sup>+</sup> and an insufficient amount of CB7 to bind both guests. Equations **2.6.1-2.6.4** define the thermodynamics of the host-guest and competition experiments, in the case that both of the K values are high and all the CB7 is consumed binding to these two guests.



**Figure 2.6.1** Reference guest cobaltocenium (Cob<sup>+</sup>)

$$K_{Fc} = \frac{[Fc @ CB7]_{eq.}}{[Fc]_{eq.}[CB7]_{eq.}} \quad \text{Eq. 2.6.1}$$

$$K_{Cob^+} = \frac{[Cob^+ @ CB7]_{eq.}}{[Cob^+]_{eq.}[CB7]_{eq.}} \quad \text{Eq. 2.6.24}$$

$$[CB7]_{total} = [Fc @ CB7]_{eq.} + [Cob^+ @ CB7]_{eq.} \quad \text{Eq. 2.6.3}$$

$$K_{Fc} = K_{Cob^+} \times \frac{[Fc @ CB7]_{eq.} [Cob^+]_{eq.}}{[Fc]_{eq.} [Cob^+ @ CB7]_{eq.}} \quad \text{Eq. 2.6.4}$$

$[Cob^+]$  and  $[Cob^+ @ CB7]$  need to be calculated in order to get the  $K_{Fc}$  values. According to **Eq. 2.6.5-2.6.7**, in NMR competition experiments,  $[Cob^+]$  and  $[Cob^+ @ CB7]$  can be calculated from the value of the observed chemical shift of  $Cob^+$  ( $\delta_{observed}$ ). The chemical shifts ( $\delta$ ) were recorded relative to the chemical shift of  $CH_3COONa$  at  $pH \sim 4$ . Under these acidic conditions,  $CH_3COONa$  is converted to  $CH_3COOH$  with  $\delta = 2.08$  ppm. The free and bound  $Cob^+$  have  $\delta$  values of 5.745 and 5.251 ppm, respectively. Because the free and bound  $Cob^+$  are in fast exchange in the NMR time scale, when both free and bound species exist, only one average peak with chemical shift  $\delta_{observed}$  can be observed.  $\chi$  is the molar fraction of  $Cob^+$ , which helps to get the value of  $[Cob^+]$  and  $[Cob^+ @ CB7]$ .

$$\delta_{observed} = \delta_{free} \chi_{free} + \delta_{bound} \chi_{bound} \quad \text{Eq. 2.6.5}$$

$$\chi_{free} + \chi_{bound} = 1 \quad \text{Eq. 2.6.6}$$

$$\delta_{observed} = 5.745 \chi_{free} + 5.251 \chi_{bound} \quad \text{Eq. 2.6.7}$$

According to **Eq. 2.6.4**, the  $K_{Fc}$  was calculated in the reference to the known value of  $K_{Cob^+}$  ( $5.7 \times 10^9 \text{ M}^{-1}$ ) in 50 mM  $CH_3COONa$  solution, which was measured by our group in 2006.<sup>52</sup> For each of the guests **1-4**, several data points were collected from separately prepared samples. The data were analyzed and

finalized by using Dixon's Test, which allows the removal of any discordant data point in the data set.

The values of the association equilibrium constant  $K_{Fc}$  for guests **1-4** in acidic media in **Table 2.6.2** shows a trend that the binding affinity decreases with the increasing length of the linker.

	<b>1<sup>2+</sup></b>	<b>2<sup>2+</sup></b>	<b>3<sup>4+</sup></b>	<b>4<sup>2+</sup></b>
<b><math>K_{Fc}</math> (<math>M^{-1}</math>)</b>	$1.5 \times 10^{10}$	$9.0 \times 10^8$	$5.7 \times 10^8$	$4.3 \times 10^9$

**Table 2.6** Association equilibrium constant  $K_{Fc}$  of guests **1-4** in 50 mM sodium acetate (pH 4) at 25 °C

## 2.7 Calculated Structures of Guests 1-4

In order to explain the observed results from electrochemical and NMR experimental results in **Section 2.3** and **2.4** and the binding affinity trend from **Section 2.6**, we performed computational calculations with four guests **1-4** using the B3LYP/sto-3g\* method. We expected that the flexibility and the length of the linkers of the guests would be key issues that affect the binding affinity between the cyclic ferrocene guests and the CB7 host.

**Figure 2.7** shows the energy-minimized structures of guests **1-4** in deprotonated form and protonated forms. Due to the rigidity of the diaminopropyl linker in guest **1** and the triethylenetetramino linker in guest **3**, the free rotational motion of the two Cp rings is substantially limited by the linker, thus, the two Cp rings show eclipsed conformations (seen **Figure 2.7 a** and **e**). In contrast, the two Cp rings of guest **2** are staggered (**Figure 2.7 c**). The diaminopentyl linker in

guest **2** is longer than the diaminopropyl linker and less rigid than the triethylenetetramino linker, which makes the ferrocene more flexible. Upon protonation in guests **1-3**, the additional proton on each nitrogen atom creates repulsions and push the overlapping Cp rings in **1** and **3** to a staggered conformation.

The overall molecular size of guest **1** is the smallest in this series with a relatively short and rigid linker. This allows the ferrocene moiety to be placed right inside the hydrophobic cavity of CB7 and the positive charges next to the cavity opening, which results in a large oxidation potential shift of around 110 mV and a high binding constant of  $10^{10} \text{ M}^{-1}$ .

Guest **2** has a longer linker of 5 carbons between the amino groups. This increases the bulkiness of the molecule. However, the larger flexibility and size of the linker is assumed to pull the ferrocene closer to the portal of CB7, although still inside the cavity. The oxidation of ferrocene is still easy even in the presence of CB7. In electrochemical experiment, no pronounced oxidation potential change of the ferrocene group was observed. Because of the combination of hydrophobic and electrostatic interactions, the binding affinity stays at  $10^8 \text{ M}^{-1}$ .

Guest **3** may bear up to four positive charges on the linker under acidic conditions. The two extra positive charges in **3** provide a stronger electrostatic interaction with the CB7 portal, thus, pushing the ferrocene more deeply towards the cavity center than in guest **2**, resulting in a positive oxidation potential shift of

49 mV and binding affinity of  $10^8 \text{ M}^{-1}$ . Guest **4** has similar conformation and electrochemical behavior as **3**.

The calculated conformations of guests **1-4** have helped us clarify the experimental observation in both  $^1\text{H}$  NMR and electrochemistry. The exact place where the ferrocene moiety will be located inside the CB7 cavity depends tightly on the bulkiness and rigidity of the linkers.

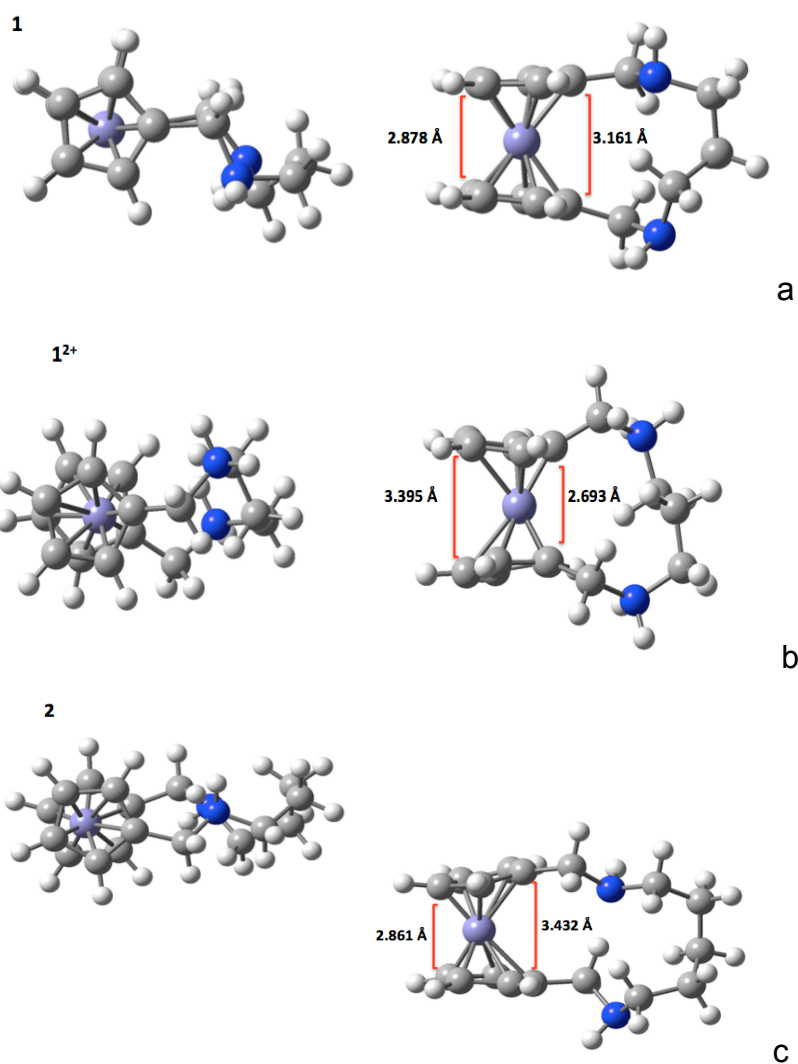


**Figure 2.7** Energy-minimized structures of guest **1-3** in deprotonated conformation (a, c, e) and protonated conformation (b, d, f) and guest **4** (g) in top and size view.

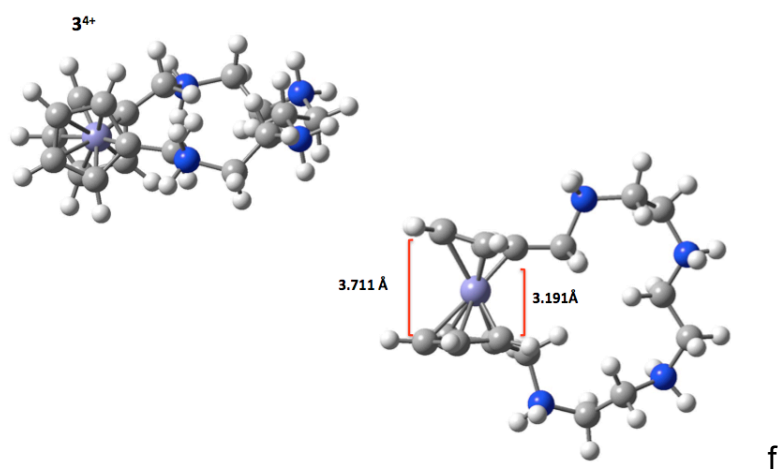
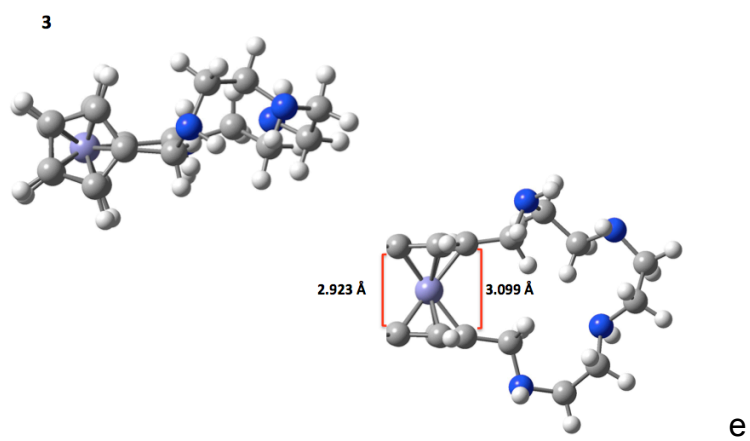
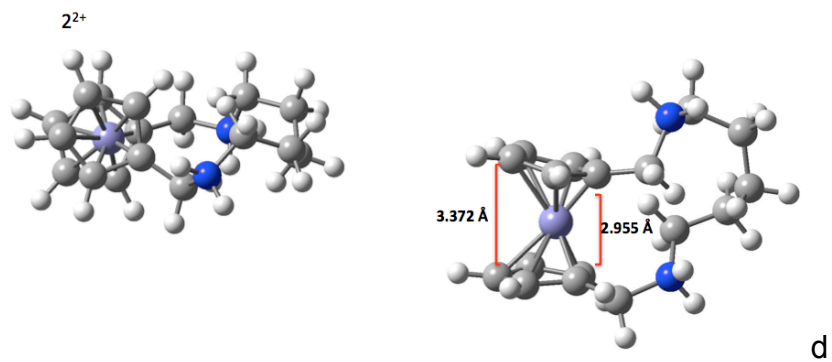


Figure 2.7 continued



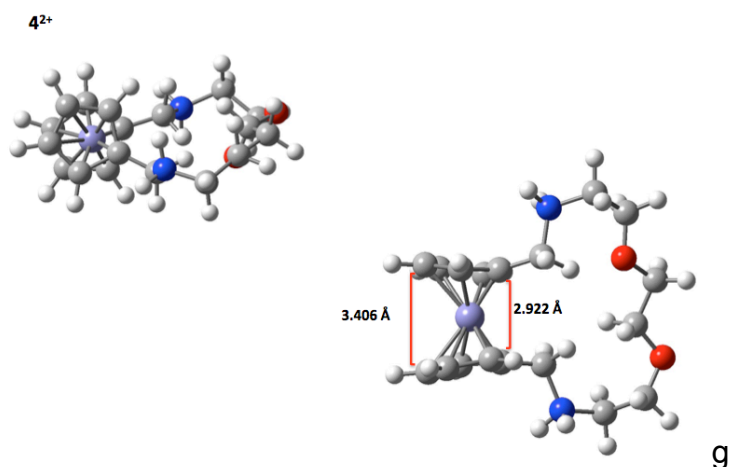
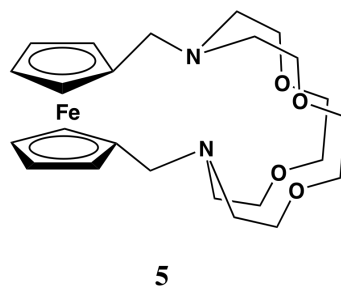


Figure 2.7 continued

## 2.8 Interaction between Guest 5 with CB7 and $\text{Ag}^+$

In further work, we investigated the cyclic ferrocene guest **5** having a bulkier tetraoxa-diazacyclooctadecane (cryptand) linker (**Figure 2.8.1**). This guest has already been reported as a ligand to coordinate metal ions, such as  $\text{Na}^+$ ,  $\text{K}^+$  and  $\text{Cu}^{2+}$  in non-aqueous media and  $\text{Ag}^+$  in aqueous solution.<sup>53</sup> These metal ions are included in the cryptand to form complexes. This work was done to 1) investigate how this bulky linker would affect the inclusion complexation with CB7; 2) see whether the addition of a positive charge metal ion could help to stabilize the complex between the ferrocene guest and CB7 and finally form a ternary complex.



**Figure 2.8.1** Molecular structure of guest **5** with a bulky linker

As stated before, the main driving forces for inclusion complexation between our cyclic ferrocene guests and CB7 are hydrophobic interactions and electrostatic interactions. We used linkers bearing positive charges under acidic conditions (pH~4) to induce the electrostatic interactions. However, under acidic conditions, the full protonation of guest **5** may interfere with the complexation of metal ion with cryptand linker.

It is important to determine the pKa range of **5** in order to set up a proper pH value for the experiments.  $^1\text{H}$  NMR spectra of guest **5** at pH range from 2-11 in **Figure 2.8.2** clearly indicates that guest **5** is fully protonated under pH 5 and has a pKa around 8, where there is a mixture of protonated species and deprotonated species.

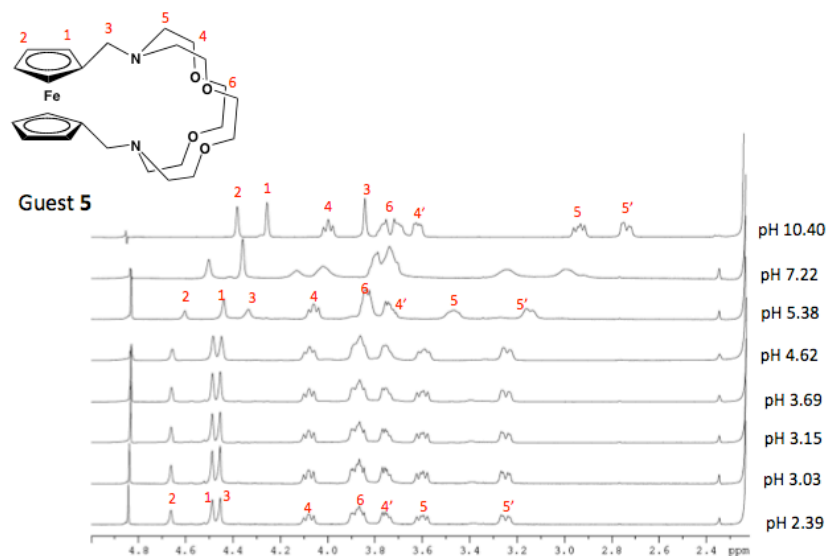


**Figure 2.8.2**  $^1\text{H}$  NMR spectra of guest **5** at pH range from 2-11.

We kept the first set of experiments under similar acidic conditions as guests **1-4**, and performed the  $^1\text{H}$  NMR titrations with CB7 or  $\text{Ag}^+$ , respectively. The spectra in **Figure 2.8.3** show that the proton peaks corresponding to the ferrocene Cp rings gradually disappear from their original positions in the presence of CB7. Also the peaks corresponding to protons on position 3 have a slight upfield shift, which is a sign of inclusion of the ferrocene moiety inside CB7, while, the peaks of the cryptand linker do not show significant changes due to the far distance from CB7.

The interaction between guest **5** and  $\text{Ag}^+$  in this media is not pronounced. No chemical shift changes are observed in  $^1\text{H}$  NMR titrations with  $\text{Ag}^+$  at pH  $\sim 4$  in **Figure 2.8.4 a-d**. Full protonation of guest **5** interrupts the coordination behavior between the cryptand linker and  $\text{Ag}^+$  under acidic conditions. Further addition of

CB7 host to the mixture of  $\text{Ag}^+$  and **5** forms the CB7 complex again (**Figure 2.8.4 e-f**).

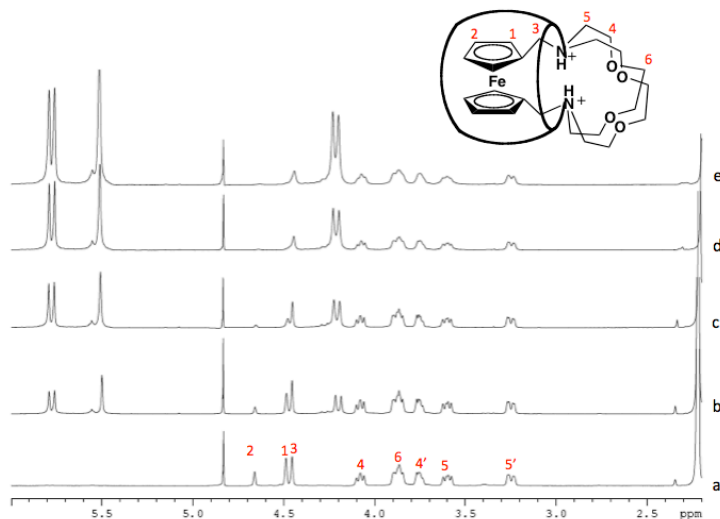


**Figure 2.8.3**  $^1\text{H}$  NMR spectra of 1 mM guest  $5^{2+}$  (a) in the absence and in the presence of (b) 0.25, (c) 0.5, (d) 1.0 and (e) 1.25 equiv. of CB7 in  $\text{D}_2\text{O}$  (pH  $\sim$ 4)

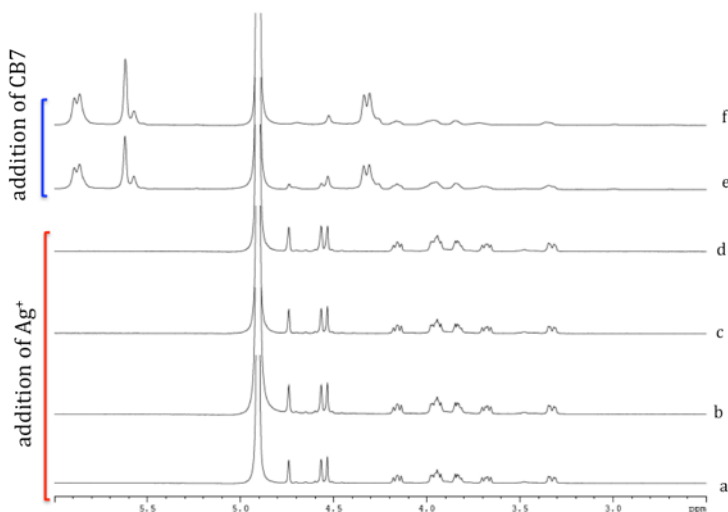


**Figure 2.8.4**  $^1\text{H}$  NMR spectra of 1 mM guest  $5^{2+}$  (a) in the absence and in the presence of (b) 0.25, (c) 0.5 and (d) 1.0 equiv. of  $\text{Ag}^+$  and then addition of  $<1$  (e) and  $>1$  equiv. of CB7 in  $\text{D}_2\text{O}$  (pH  $\sim$ 4)

By switching the pH value to  $\sim 8$ , the interaction between guest **5** and  $\text{Ag}^+$  becomes the predominant complexation behavior.  $^1\text{H}$  NMR spectra of  $\text{Ag}^+$  titration in **Figure 2.8.5** give strong evidence that the  $\text{Ag}^+$  is included inside the cryptand. The positive charge de-shields the protons on guest **5**, resulting in downfield chemical shifts of all the proton peaks. However, the binding of guest **5** and CB7 weakens thus, they cannot form inclusion complex any more due to the lack of electrostatic interactions between the amino groups and oxygen rim of CB7 (**Figure 2.8.6 a-d**). The coordination of a metal ion to the cryptand linker was observed again after adding  $\text{Ag}^+$  to a mixture of guest **5** and CB7 (**Figure 2.8.6 e**). Based on the phenomenon observed in this experiment, the metal ion does not strengthen the binding affinity between guest **5** and CB7 as expected.

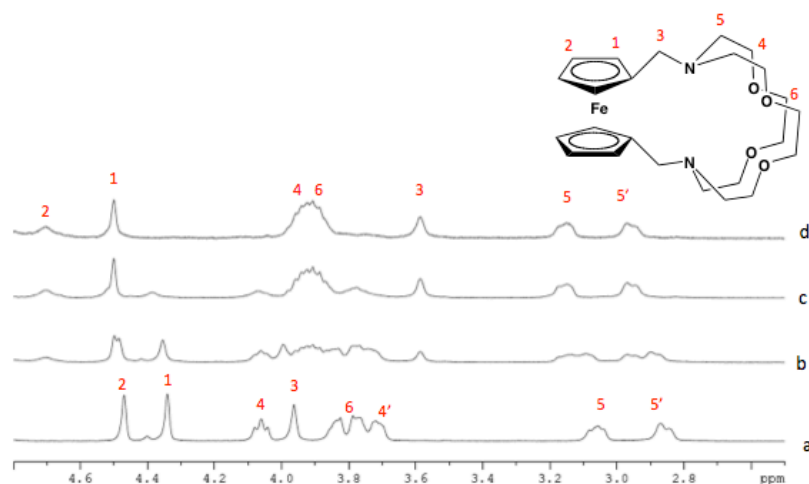


**Figure 2.8.5**  $^1\text{H}$  NMR spectra of 1 mM guest **5** in the (a) absence and presence of (b) 0.37, (c) 0.75, and (d) 1.0 equiv. of  $\text{Ag}^+$  in  $\text{D}_2\text{O}$  (pH  $\sim 8$ )

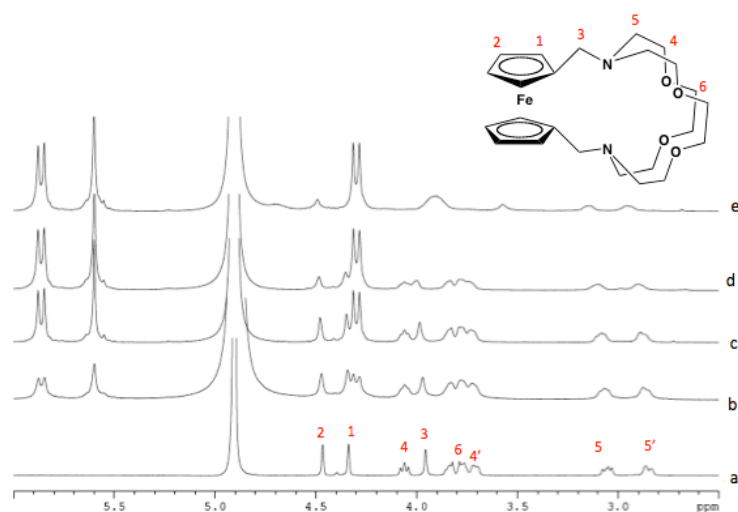


**Figure 2.8.6**  $^1\text{H}$  NMR spectra of 1 mM guest **5** (a) in the absence and in the presence of (b) 0.25, (c) 0.5 and (d) 1.0 equiv. of CB7 and then addition of (e) 1 equiv. of  $\text{Ag}^+$  in  $\text{D}_2\text{O}$  (pH  $\sim$ 8)

The electrochemical behavior of guest **5** interacting with either CB7 or  $\text{Ag}^+$  also leads to similar conclusions as the  $^1\text{H}$  NMR experiments. Ferrocene is bound inside the CB7 cavity but close to the opening because of the size of the linker, thus, the oxidation potential does not shift at pH $\sim$ 4 (**Figure 2.8.7**). At pH  $\sim$ 8, the oxidation potential shifts 127 mV positively in addition of 1 equivalent of  $\text{Ag}^+$  to the guest **5** solution (**Figure 2.8.8**), which indicates the formation of the complex between  $\text{Ag}^+$  and guest **5** as reported. However, there is no evidence that a complex of **5**, CB7 and  $\text{Ag}^+$  is formed either under acidic condition or around pKa range of guest **5**.

Even though the inclusion complexation between guest **5** and CB7 takes place in acidic media, the binding affinity of this complex is not as strong as guests **1-4**, therefore, unlike with guests **1-4**, the complex of guest **5** and CB7

could not be detected by ESI- MS. The size of the linker seems to play an important role in the binding affinity to CB7, bulky linker will affect the location of the ferrocene moiety and pull it off the highly hydrophobic CB7 cavity center.

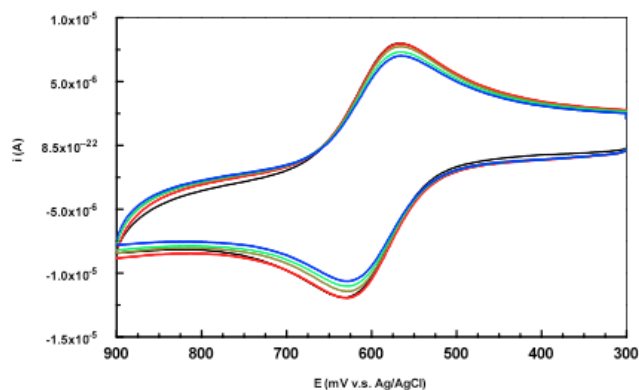


**Figure 2.8.7** Cyclic voltammety of 1 mM guest  $5^{2+}$  with 0 (black), 0.25 (red), 0.5 (brown), 1.0 (green) and 1.25 (blue) equiv. of CB7 in 1M  $\text{NaNO}_3$  / $\text{H}_2\text{O}$  solution (pH  $\sim$ 4) at 25  $^\circ\text{C}$ . Scan rate: 100mV/s

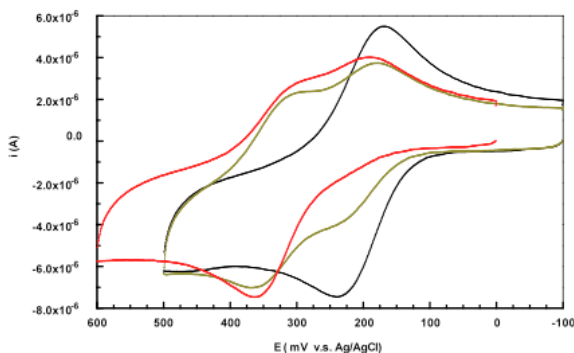


**Figure 2.8.8** Cyclic voltammety of 1 mM guest **5** with 0 (black), 0.5 (brown) and 1.0 (red) equiv. of  $\text{Ag}^+$  in 0.1M  $\text{NaNO}_3$  / $\text{H}_2\text{O}$  solution (pH  $\sim$ 8) at 25  $^\circ\text{C}$ . Scan rate:100 mV/s

## 2.9 Experimental

All the cyclic voltammetric experiments on glassy carbon working electrodes ( $0.07 \text{ cm}^2$ ) were recorded on a BAS-100 electrochemical station and the experiments on Pt ultramicroelectrodes (UMEs) were performed on a Scanning Electrochemical Microscope from CH Instruments under  $\text{N}_2$  protection at room temperature. The glassy carbon working electrode was polished by  $5 \mu\text{m}$   $\text{Al}_2\text{O}_3$  powder (0.05 MICRON, BUEHLER<sup>®</sup> MICROPOLISH<sup>®</sup>II) before every measurement. The radius of the Pt disk UME was calibrated with a ferrocenemethanol solution and polished before use. Pt counter electrode and Ag/AgCl reference electrode were used in all experiments. 0.1 M NaCl was used as the supporting electrolyte. HCl/ $\text{H}_2\text{O}$  solution was used to adjust the solution to acidic conditions ( $\sim\text{pH}$  4).

All the high-resolution ESI-MS spectra were obtained on Bruker MicroTOF-Q II. The CB7 complexes of guests **1-4** were prepared in acidic water ( $\text{pH}\sim 4$  adjusted by HCl solution) with concentration at the millimolar (mM) level. The theoretical isotopic simulation was performed based on the chemical formula of the complex.

### 2.9.1 Synthesis of Guest **1**<sup>54</sup>

Guest **1**. A mixture of 1,1'-ferrocenedicarboxaldehyde (150 mg, 0.62 mmol) and 1,3-diaminopropane (46 mg, 0.62 mmol) was refluxed with stirring at  $45^\circ\text{C}$  in absolute methanol (25 ml) under  $\text{N}_2$  atmosphere. A small amount of molecular sieves was added to the solution to absorb water. After 4h,  $\text{NaBH}_4$  (70



mg, 1.86 mmol) was added to the pale yellow mixture and the reaction mixture was refluxed for another 24h. The suspension was filtered through Celite and the resulting yellow solution was evaporated to remove methanol. Water and  $\text{CHCl}_3$  (15 ml/15 ml) were added to the orange oil and the organic phase was separated and collected. The water phase was extracted with  $\text{CHCl}_3$  (4×10 ml) and all the organic phase was collected.  $\text{CHCl}_3$  solutions were dried over  $\text{Na}_2\text{SO}_4$  and evaporated. The orange oil was purified on neutral  $\text{Al}_2\text{O}_3$  column with  $\text{CHCl}_3$ /methanol. A minor fast-running band was discarded and the major yellow band was gradually collected by changing the eluent to  $\text{CHCl}_3$ -methanol (9:1). After evaporation, a yellow solid was obtained. (80 mg, yield: 45.4%).  $^1\text{H}$  NMR ( $\text{D}_2\text{O}$ , 500 MHz):  $\delta$ =1.93-1.94 (m, 2H,  $\text{CH}_2$ ), 3.22-3.24 (m, 4H,  $\text{CH}_2$ ), 3.58 (s, 4H,  $\text{CH}_2$ ), 4.22 (s, 4H,  $\text{C}_5\text{H}_4$ ), 4.29 (s, 4H,  $\text{C}_5\text{H}_4$ ) ppm.  $^{13}\text{C}$  NMR ( $\text{D}_2\text{O}$ , 125 MHz):  $\delta$ =17.57 (1C,  $\text{CH}_2$ ), 42.02 (2C,  $\text{CH}_2$ ), 65.93 (4C,  $\text{C}_5\text{H}_4$ ), 68.06 (4C,  $\text{C}_5\text{H}_4$ ), 85.46 (2C,  $\text{C}_5\text{H}_4$ ) ppm. ESI-MS: found  $m/z = 285.1058$   $[\text{M}+\text{H}]^+$ ,  $\text{C}_{15}\text{H}_{21}\text{FeN}_2^+$ , calcd. 285.1049.

### 2.9.2 Synthesis of Guest 2

Guest 2. A mixture of 1,1'-ferrocenedicarboxaldehyde (150 mg, 0.62 mmol) and 1,5-diaminopentane (63 mg, 0.62 mmol) was refluxed with stirring at  $45^\circ\text{C}$  in absolute methanol (25 ml) under  $\text{N}_2$  atmosphere for 4h.  $\text{NaBH}_4$  (70 mg, 1.86 mmol) was added and the yellow mixture was refluxed for another 48h. The resulting yellow solution was evaporated to remove solvent. Water and  $\text{CHCl}_3$  (10 ml/10 ml) were added to the orange oil and the organic orange phase was collected. The aqueous phase was extracted with  $\text{CHCl}_3$  (4×10 ml). All the

organic phase was collected and then dried over  $\text{Na}_2\text{SO}_4$  and evaporated. The orange oily mixture was separated on neutral  $\text{Al}_2\text{O}_3$  column with  $\text{CHCl}_3$ /methanol. The long major yellow band was collected by elution with  $\text{CHCl}_3$ -methanol (4:1). A yellow solid product was obtained. (100 mg, yield: 51.7%).  $^1\text{H}$  NMR ( $\text{D}_2\text{O}$ , 500 MHz):  $\delta$ =1.88 (m, 2H,  $\text{CH}_2$ ), 1.95 (m, 4H,  $\text{CH}_2$ ), 3.15 (m, 4H,  $\text{CH}_2$ ), 3.76 (s, 4H,  $\text{CH}_2$ ), 4.36 (s, 4H,  $\text{C}_5\text{H}_4$ ), 4.43 (s, 4H,  $\text{C}_5\text{H}_4$ ) ppm.  $^{13}\text{C}$  NMR ( $\text{D}_2\text{O}$ , 125 MHz):  $\delta$ =20.76 (1C,  $\text{CH}_2$ ), 24.88 (2C, $\text{CH}_2$ ), 46.06 (2C, $\text{CH}_2$ ), 47.94 (2C, $\text{CH}_2$ ), 66.40 (4C,  $\text{C}_5\text{H}_4$ ), 68.39 (4C,  $\text{C}_5\text{H}_4$ ), 84.31 (2C,  $\text{C}_5\text{H}_4$ ) ppm. ESI-MS: found  $m/z = 313.1373$   $[\text{M}+\text{H}]^+$ ,  $\text{C}_{17}\text{H}_{25}\text{FeN}_2^+$ , calcd 313.1362.

### 2.9.3 Synthesis of Guest 3

Guest **3**. A mixture of 1,1'-ferrocenedicarboxaldehyde (150 mg, 0.62 mmol) and triethylenetetramine (91 mg, 0.62 mmol) in absolute methanol (25 ml) was refluxed with stirring at  $45^\circ\text{C}$  under  $\text{N}_2$  for 4h. Molecular sieves were added to absorb water.  $\text{NaBH}_4$  (94 mg, 2.56 mmol) was added to the brownish mixture and the mixture was refluxed for another 48h. The suspension was filtered through Celite and an orange oil was obtained after evaporation of methanol. Water and  $\text{CHCl}_3$  (15 ml/15 ml) were added to the oil and the organic orange phase was separated and collected. The water phase was extracted with  $\text{CHCl}_3$  (4×5 ml) and all the organic phase was collected and dried over  $\text{Na}_2\text{SO}_4$  and evaporated. The orange oil was purified on neutral  $\text{Al}_2\text{O}_3$  column with  $\text{CHCl}_3$ /methanol (1:1). After evaporation, a yellow powder was obtained. (70 mg, yield: 31.7%).  $^1\text{H}$  NMR ( $\text{D}_2\text{O}$ , 500MHz):  $\delta$ =3.11 (s, 4H,  $\text{CH}_2$ ), 3.16 (s, 8H,  $\text{CH}_2$ ), 3.88 (s, 4H,  $\text{CH}_2$ ), 4.38 (s, 4H,  $\text{C}_5\text{H}_4$ ), 4.40 (s, 4H,  $\text{C}_5\text{H}_4$ ) ppm.  $^{13}\text{C}$  NMR ( $\text{D}_2\text{O}$ ,

125 MHz):  $\delta$ =45.36 (4C, CH<sub>2</sub>), 45.53 (2C,CH<sub>2</sub>), 46.89 (2C,CH<sub>2</sub>), 69.19 (8C, C<sub>5</sub>H<sub>4</sub>), 81.75 (1C, C<sub>5</sub>H<sub>4</sub>) ppm. ESI-MS: found m/z = 357.1751[M+H]<sup>+</sup>, C<sub>18</sub>H<sub>29</sub>FeN<sub>4</sub><sup>+</sup>, calcd 357.1736.

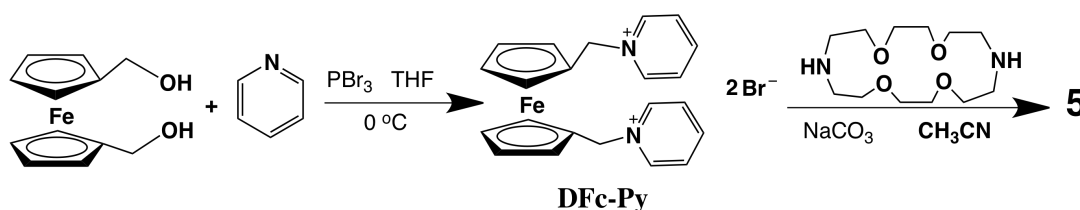
#### 2.9.4 Synthesis of Guest 4<sup>55</sup>

Guest **4**. 1,1'-ferrocenedicarboxaldehyde (209 mg, 0.86 mmol) and 2,2'-(ethylenedioxy)-bis(ethylamine) (128 mg, 0.86 mmol) were mixed together in freshly distilled CH<sub>3</sub>CN (50 ml) under N<sub>2</sub> atmosphere and kept stirring at room temperature in darkness for 48h. The CH<sub>3</sub>CN was removed afterwards. The resulting orange oil was re-dissolved in methanol (30 ml) followed by addition of NaBH<sub>4</sub> (97.60 mg, 2.58 mmol) with stirring under N<sub>2</sub> overnight. The methanol was removed and acetone was added to the oil and the solution was refluxed for another 2h. The solution was filtered through Celite and the resulting yellow solution was evaporated to remove acetone. Water and CHCl<sub>3</sub> (15 ml/15 ml) were added to the orange oil and the organic orange phase was collected. The water phase was extracted with CHCl<sub>3</sub> (4×5 ml) and all the organic phase was collected. CHCl<sub>3</sub> solutions were dried over Na<sub>2</sub>SO<sub>4</sub>. The CHCl<sub>3</sub> was finally removed. Then the dark orange oil was purified and separated by column chromatography on neutral Al<sub>2</sub>O<sub>3</sub> using methanol-CH<sub>2</sub>Cl<sub>2</sub> (1:20). The product was collected as an orange oil with roughly 50% yield. The orange oil (guest **4**) was converted into its hydrochloride salt **4**<sup>2+</sup> by bubbling HCl gas in the ethyl ether solution of **4**. A light brown precipitate was obtained by filtration. <sup>1</sup>H NMR (D<sub>2</sub>O, 500 MHz):  $\delta$ =3.36 (t, 4H, CH<sub>2</sub>), 3.78 (s, 4H, CH<sub>2</sub>), 3.92 (t, 4H, CH<sub>2</sub>), 4.18 (s, 4H, CH<sub>2</sub>), 4.43 (d, 4H, C<sub>5</sub>H<sub>4</sub>), 4.46 (d, 4H, C<sub>5</sub>H<sub>4</sub>) ppm. <sup>13</sup>C NMR (D<sub>2</sub>O, 125 MHz):

$\delta=45.79$  (1C, CH<sub>2</sub>), 47.16 (2C,CH<sub>2</sub>), 67.10 (2C, CH<sub>2</sub>), 69.96 (2C,CH<sub>2</sub>), 70.70(4C, C<sub>5</sub>H<sub>4</sub>), 70.82 (4C, C<sub>5</sub>H<sub>4</sub>), 76.82 (2C, C<sub>5</sub>H<sub>4</sub>) ppm. ESI-MS: found  $m/z = 180.0746$  [M]<sup>2+</sup>, C<sub>18</sub>H<sub>28</sub>FeN<sub>2</sub>O<sub>2</sub><sup>2+</sup>, calcd. 180.0755.

### 2.9.5 Synthesis of Guest 5

Guest **5** was synthesized in two steps. (**Scheme 2.9**)



**Scheme 2.9** Synthetic procedure of guest **5**

**Step 1:**<sup>56</sup> Synthesis of 1,1-bis(pyridiniummethyl) ferrocene dibromide (DFc-Py). A 4.5 ml freshly distilled THF solution of phosphorus tribromide (70  $\mu$ L, 0.73 mmol) was added dropwise into a 30 ml THF solution of 1,1'-ferrocenedimethanol (181 mg, 0.73 mmol) and pyridine (118  $\mu$ L, 1.46 mmol) under N<sub>2</sub> at 0°C in an ice bath. The yellow mixture was kept stirring for 1h at this temperature and then 3h at room temperature. The yellow precipitate formed during the process was collected by filtration and washed with CH<sub>2</sub>Cl<sub>2</sub>. The solid was dissolved in a small amount of water and purified through column chromatography on neutral Al<sub>2</sub>O<sub>3</sub>. Pyridine was washed out with ethyl acetate first and then DFc-Py with methanol. The product was confirmed by ESI-MS: found  $m/z=185.0572$  [M]<sup>2+</sup>, C<sub>22</sub>H<sub>22</sub>FeN<sub>2</sub><sup>2+</sup>, calcd. 185.0561, and ready for the **step 2**.

**Step 2:**<sup>53a</sup> A mixture of DFC-Py (101 mg, 0.19 mmol), 1,4,7,13-tetraoxa-7,16-diazacyclooctadecane (51 mg, 0.19 mmol) and NaCO<sub>3</sub> (41 mg, 0.38 mmol) was dissolved in 20 ml freshly distilled CH<sub>3</sub>CN and the solution was refluxed with stirring at 50°C under N<sub>2</sub> for 48h. The product conversion was followed conveniently by ESI-MS during the reaction. The solution was cooled down to room temperature and filtered. The solvent was evaporated and 10 ml water was added to the residue and extracted with CH<sub>2</sub>Cl<sub>2</sub> (4×5 ml). The collected organic layers were dried over Na<sub>2</sub>SO<sub>4</sub> and the CH<sub>2</sub>Cl<sub>2</sub> was evaporated. The mixture was separated by chromatography on neutral Al<sub>2</sub>O<sub>3</sub> column with solvents of increasing polarity. Unreacted 1,4,7,13-tetraoxa-7,16-diazacyclooctadecane was removed out first by CH<sub>2</sub>Cl<sub>2</sub>. Then acetone-CH<sub>2</sub>Cl<sub>2</sub> (1:1) was applied to separate compound **5** from other ferrocene by-products. Finally, **5** was eluted with isopropanol. The collected isopropanol solution of **5** was dried in a freeze drier, leaving an orange oil. Ethyl ether was added to the oil and converted the oil product into a dark yellow solid. <sup>1</sup>H NMR (D<sub>2</sub>O, pD~11, 500 MHz): δ=2.72-2.95 (m, 8H, CH<sub>2</sub>), 3.60-3.62 and 3.96-4.00 (m, 8H, CH<sub>2</sub>), 3.71-3.74 (m, 8H, CH<sub>2</sub>), 3.84 (s, 4H, CH<sub>2</sub>), 4.25 (s, 4H, C<sub>5</sub>H<sub>4</sub>), 4.38 (s, 4H, C<sub>5</sub>H<sub>4</sub>) ppm. <sup>13</sup>C NMR(D<sub>2</sub>O, pD~11, 125 MHz,): δ=49.58 (4C, CH<sub>2</sub>), 50.65 (4C, CH<sub>2</sub>), 68.58 (4C, C<sub>5</sub>H<sub>4</sub>), 68.84 (4C, CH<sub>2</sub>), 69.93(2C, CH<sub>2</sub>), 71.70(4C, C<sub>5</sub>H<sub>4</sub>), 82.84(2C, C<sub>5</sub>H<sub>4</sub>) ppm. ESI-MS: m/z =473.2077 [M+H]<sup>+</sup> and 237.1091 [M+2H]<sup>2+</sup>, C<sub>24</sub>H<sub>36</sub>FeN<sub>2</sub>O<sub>4</sub>. calcd. 437.2097 [M+H]<sup>+</sup> and 237.1085 [M+2H]<sup>2+</sup>.

## 2.10 Conclusion

This series of cyclic ferrocene guests **1-5** beautifully provides the possibility to form inclusion complexes with CB7 in a closed-conformation manner (see in **Scheme 2.1**).  $^1\text{H}$  NMR, electrochemical and ESI-MS results have proved the formation of these complexes with association equilibrium constants  $K_{\text{Fc}}$  of relatively high value, in the range of  $10^8$  to  $10^{10} \text{ M}^{-1}$  under acidic conditions. The binding affinity is tightly dependent on the length, rigidity and bulkiness of the linker. In general, increasing the length of the linker will result in a smaller  $K_{\text{Fc}}$  value, while bulkier or more flexible linkers will locate the ferrocene moiety more displaced away from the hydrophobic cavity center of CB7 and lead to a lower shift of the oxidation potential in cyclic voltammetry. One exception happened with guest **3** that no pronounced oxidation potential shift was observed upon complexation. This may indicate that the diaminopropyl linker is relatively flexible and well extended in order to allow the ferrocene group to reside inside the CB7 cavity closer to the other opening. Moreover, when the linker size reaches up to a certain point, the inclusion complexes between cyclic ferrocene guest and CB7 are no longer as stable as the ones with smaller linkers (for example, guest **5**).

## CHAPTER 3

### Complexation of a Series of Bi-armed Ferrocene Guests with Cucurbit[7]uril (CB7) and Cucurbit[8]uril (CB8)

#### 3.1 Background

The complexation behavior between cucurbit[7]uril (CB7) and ferrocene derivatives is very attractive in the study of host-guest systems due to the high binding affinities that lead to the formation of very stable inclusion complexes in aqueous media. For the single-armed ferrocene guests, when the interactions between CB7 and ferrocene are stronger than those with the substituent, the hydrophobic ferrocene residue is nicely fitted inside the very hydrophobic CB cavity, and the substituent protrudes through one of the CB7 portals, leaving the other portal open. On the other hand, one of cyclopentadiene rings (Cp) is unmodified, which may allow this side of the ferrocene residue freely to come in or out of the CB7 cavity without much interference from the substituent. For instance, our group has reported the binding interactions between the host CB7 and a series of ferrocene guests containing a relatively bulky dendrimer substituent of variable size.<sup>57</sup> The previous studies show that the association equilibrium constant (K) values are  $10^9$ - $10^{11}$  M<sup>-1</sup> for neutral ferrocene guests and reach up to  $10^{12}$ - $10^{13}$  M<sup>-1</sup> for monocationic guests due to the addition of the electrostatic interactions between the positive charge on the substituent and the negatively charged carbonyl rim on the portals of CB7. Inspired by the positive charge-induced increased binding affinity, a synthetic ferrocene guest, 1,1'-

bis(trimethylammoniomethyl) ferrocene, which has an identical trimethylammoniomethyl group ( $-\text{CH}_2\text{N}^+(\text{CH}_3)_3$ ) on each of the Cp rings, was reported to have an extraordinarily high binding affinity to CB7 in pure water, with a K value of  $10^{15} \text{ M}^{-1}$ .<sup>19</sup> The X-Ray structure of this complex clearly shows that ferrocene is located inside the CB7 cavity, with each of the trimethylaminomethyl groups protruding through each of the portals, resulting in a very symmetric conformation in which the ferrocene guest molecule is extended through the CB7 molecule. The appropriate positioning of a second positive charge to induce additional electrostatic interactions with the other opening of CB7 boosts a robust binding affinity, which has resulted in a strong interest to investigate the complexation between bi-armed ferrocene guests and CB hosts.

Predictably, the substituent would play an essential role in the interactions between bi-armed ferrocene guests and CB hosts. Unlike the single-armed ferrocene guests leaving one side of the ferrocene free, the bi-armed ferrocene guests, whose two Cp rings are both modified with an identical substituent make the complexation behavior of ferrocene guests and the CB hosts much more complicated. The binding behavior is strongly dependent on the properties of the substituents, such as, bulkiness, hydrophobicity, binding affinities to CBs and charges, which may affect the overall binding site, the binding affinity and the stoichiometry of the final complexes.

Understanding the substituent effects on ferrocene-CB complexes is of great importance not only because of the high binding affinity of ferrocene derivatives and CBs, but also because it could (1) provide information on how the



substituents could change the binding behavior, (2) facilitate the study of binding kinetics and eventually develop relatively simple guest-host systems that could mimic bio-systems for drug delivery and other medicinal applications.

### 3.2 Series of Bi-armed Ferrocene Guests

With the encouragement from the extremely high binding affinity of the CB7 complex of 1,1'-bis(trimethylammoniomethyl) ferrocene in pure water and the great interest on the effect of substituents on the binding behavior of the bi-armed ferrocene guests and CB hosts, we proposed a series of bi-armed ferrocene guests, in which the substituents have one cyclohexyl group on the nitrogen atom with different numbers (0-2) of methyl groups (see **Figure 3.2**). The addition of methyl groups to the substituent increases the size of the substituents and is expected to slow down or even stop the CBs from threading through the substituent and binding to the ferrocene group. The amine groups that are close to the ferrocene Cp rings ensure the positioning of the positive charges on the portal of the CB hosts under acidic conditions, which induce ion-dipole interactions to stabilize the complexes.

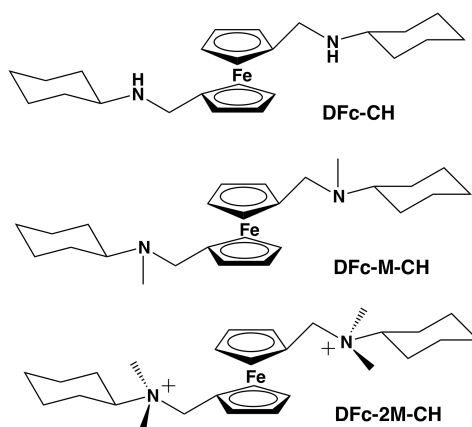


**Figure 3.2** Molecular structures of a series of bi-armed ferrocene guests: DFc-CH, DFc-M-CH and DFc-2M-CH

We investigated the interactions of this series of ferrocene guests with both CB7 and CB8 in acidic aqueous media. With one more glycoluril unit in the macrocycle, the portal diameter of CB8 opens up to 6.9 Å from that of CB7 (5.4 Å)<sup>13b</sup> and the cavity diameter is extended from 7.3 Å (CB7) to 8.8 Å (CB8), which is expected to help CB8 slip over larger substituent groups. Also, the enlarged volume of the cavity of CB8 will result in different binding affinities to ferrocene guests.

### 3.3 Studies on the Complexation Behavior between Bi-armed Ferrocene Guests and CB7 Host

This series of bi-armed ferrocene guests: DFc-CH, DFc-M-CH and DFc-2M-CH (**Figure 3.2**) and their binding behavior to CB7 were all analyzed by <sup>1</sup>H NMR spectroscopic, electrochemical and electrospray ionization mass spectrometric (ESI-MS) methods, respectively. All the samples were prepared

under acidic conditions at pH value of 4 in order to fully protonate the amine groups for the addition of electrostatic interactions.

$^1\text{H}$  NMR spectroscopy method is very useful for determination of not only whether the complexes are formed, but also where the main binding site is located. In CB complexes, as the main region of the guest is included inside the CBs cavity, the corresponding proton resonances of this region typically shift upfield upon inclusion complexation, while the protons on the guest molecule which remain outside although in close proximity to the CB cavity portal in the complex experience downfield shifts. The observation of chemical shifts ( $\delta$ ) of the guest proton peaks in the absence and presence of the host can provide information on the complexation behavior.

Electrochemical methods are widely used for the analysis of ferrocene-CB7 complexes. The redox process of the ferrocene/ferrocenium ( $\text{Fc}/\text{Fc}^+$ ) redox couple is well known to be reversible and fast in the absence of the CB7 host in cyclic voltammetry (CV), while, upon inclusion of the ferrocene group inside the CB cavity, CV typically shows a reversible or quasi-reversible behavior with more positive oxidation potential (indicated as the half-wave potential,  $E_{1/2}$ , see more details in **Chapter 2**) and diminished currents. The value of the half-wave potential shift between the free ferrocene guest and the complex depends on where the ferrocene group is located inside the CB7 cavity. For this series of bi-armed ferrocene guests in this chapter, if the CB7 can reach the ferrocene group, due to the highly symmetric structure, the ferrocene residue is expected to reside

nicely in the center of the cavity, which would lead to a relatively large positive shift in the oxidation potential of ferrocene.

ESI-MS can directly confirm the formation of the complexes by comparing the isotopic distribution pattern of the experimental results with the theoretical simulation based on the chemical formula and the charges of the complexes. Also, it can reflect the relative stabilities of the complexes. When the interaction between the host and guest are too weak, no peaks corresponding to the complex can be observed.

### 3.3.1 Interactions between DFC-CH and CB7

The guest DFC-CH has the simplest substituent in this series of bi-armed ferrocene guests and is expected to form inclusion complex with CB7 in relatively fast kinetics with the main binding site on the ferrocene group.

$^1\text{H}$  NMR titration results in **Figure 3.3.1.1** clearly shows that the addition of CB7 results in chemical shift changes of the proton resonances. The ferrocene protons and the adjacent methylene protons (labeled 1, 2 and 3 in **Figure 3.3.1.1**) present upfield shifts in the presence of one equivalent of CB7. For instance, the ferrocene protons shift from 4.41 to 3.66 ppm and 4.34 to 3.55 ppm while the methylene protons shift from 4.05 to 3.60 ppm. This indicates that the ferrocene group is completely included inside the CB7 cavity as well as the adjacent methylenes. Similarly, the protons on the cyclohexyl groups that remain outside of the cavity although in close proximity to the CB7 openings in the complex experience downfield shifts. The protons (labeled 4, 5, 5', 6 and 6'),

which are closer to the CB7 cavity portals, show downfield shift values of around 0.2 ppm, respectively. The protons (labeled 7, 8) far from the portals downfield shift only from 1.13 to 1.18 ppm. As expected, the proton resonance peaks of CB7 do not have any signal splitting due to the formation of the inclusion complex ferrocene-CB7, in which the CB7 host maintains its equatorial plane of symmetry.

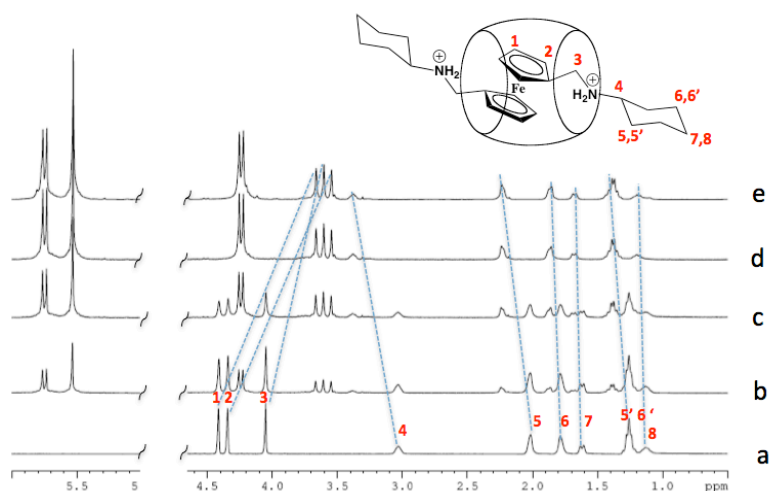


**Figure 3.3.1.1**  $^1\text{H}$  NMR spectra of 1 mM DFc-CH in the (a) absence and presence of (b) 0.25, (c) 0.5, (d) 1.0 and (e) 1.25 equiv. of CB7 in  $\text{D}_2\text{O}$  (pD 4.5)

The cyclic voltammetric results obtained with a 1 mM DFc-CH solution in the absence and presence of CB7 (**Figure 3.3.1.2**) indicate the formation of a complex between guest DFc-CH and host CB7. The addition of one equivalent of CB7 to the free DFc-CH solution immediately leads to a largely positive half-wave potential ( $E_{1/2}$ ) shift of 184 mV (from 565 mV to 749 mV) with substantially decreasing currents. This phenomenon suggests that the ferrocene group locates deeply inside the CB7 cavity and the oxidation process of ferrocene to

ferrocenium only can be achieved at higher potential. In other words, the reduced form of ferrocene (Fe(II)) is more favored upon complexation by CB7. The values of the half-wave potential shifts usually could reflect the position of the ferrocene inside CB7. With the two identical substituents, DFC-CH is placed right in the center of the cavity due to the equivalent interactions between these two methylammoniocyclohexyl groups and the cavity portals.

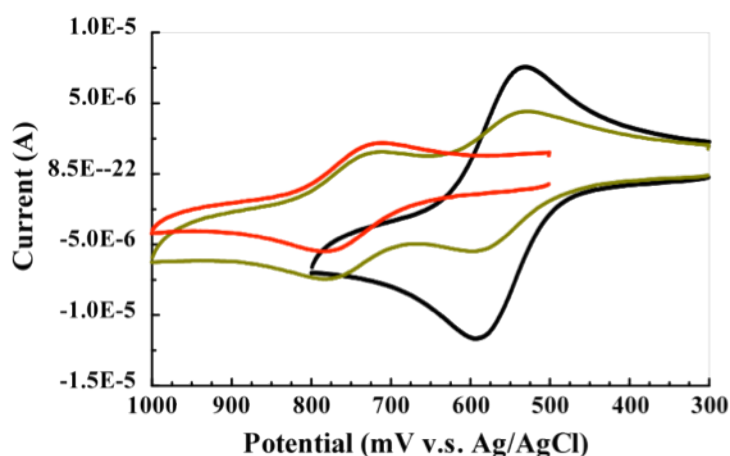


**Figure 3.3.1.2** Cyclic voltammetry of 1 mM DFC-CH with 0 (black), 0.5 (brown) and 1.0 (red) equiv. of CB7 in 0.1 M NaCl /H<sub>2</sub>O solution (pH ~4) at 25 °C. Scan rate: 100 mV/s

The experimental ESI-MS spectrum of the complex of DFC-CH•CB7 in **Figure 3.3.1.3** (top) shows the isotopic distribution pattern of this complex with two positive charges. The theoretical simulation is obtained according to the chemical formula of the complex. For instance, the DFC-CH•CB7 in acidic solution has a chemical formula C<sub>66</sub>H<sub>80</sub>FeN<sub>30</sub>O<sub>14</sub><sup>2+</sup> with a total molecular weight of 1573.38 g/mol. Due to the two positive charges on the complex, the observed

value of  $m/z$  is 786.29. The patterns of the isotopic peaks in both experimental and theoretical spectra are the same, which confirms the formation of the complex DFc-CH•CB7.

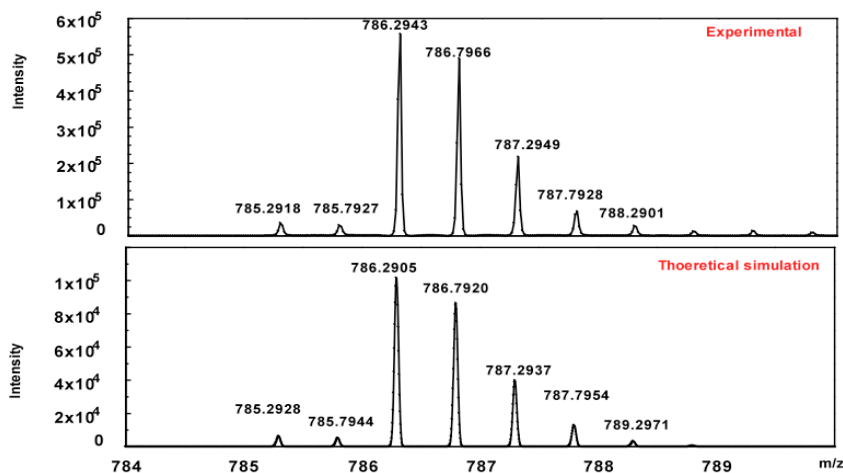


**Figure 3.3.1.3** Experimental and theoretical simulation of high-resolution ESI-TOF mass spectra of the bi-armed guest DFc-CH with 1 equiv. of CB7. The complex is diprotonated in water solution (pH ~4)

### 3.3.2 Interactions between DFc-M-CH and CB7

With identical substituents on each of the Cp rings of the ferrocene guests we have seen that the ferrocene resides inside the center of the CB7 cavity (**Section 3.3.1**). The relatively small substituent with one cyclohexyl group on DFc-CH does not block the CB7 from reaching and including the ferrocene to form a stable ferrocene-CB7 complex. Also, because the binding affinity between ferrocene and CB7 is much stronger than that between the substituent and CB7, the CB7 molecule has a strong tendency to bind the ferrocene group when there is no obstruction from the substituents. The complex DFc-CH•CB7 was formed

immediately after addition of the CB7 host, which suggests that the kinetics of the association is fast. This fast kinetics of formation of DFc-CH•CB7 leads us to investigate further the effects of the substituents on the complexation behavior between the bi-armed ferrocene guests and CB7. We added one methyl group to the nitrogen atom in order to enlarge the size of the substituent, which contains one methyl group and one cyclohexyl group directly attached to the amine nitrogen. The guest DFc-M-CH was analyzed in the same way as DFc-CH.

The  $^1\text{H}$  NMR CB7-titration experimental results for DFc-M-CH in **Figure 3.3.2.1** show the typical chemical shift ( $\delta$ ) changes of the proton resonances in the complexation process of ferrocene-CB7, that is, the peaks of the protons on ferrocene and adjacent methylene groups experience upfield shifts, while, the protons outside the CB7 shift downfield. Interestingly, the peak patterns of the proton resonances are different in this case. In detail, when the free DFc-M-CH exists in the acid solution, the chiral center N may affect the chemical environment of the two protons on the methylene group next to the ferrocene (labeled 3 in **Figure 3.3.2.1**,  $\delta = 4.12\sim 4.24$  ppm), causing the peak splitting. The additional methyl group on DFc-M-CH can rotate freely and results in a sharp singlet peak for the three methyl protons (Labeled 9,  $\delta = 2.63$  ppm). In addition of one equivalent of CB7, the complex DFc-M-CH•CB7 forms immediately. The methyl group is in close proximity to the portal of CB7 cavity that the proton peaks shift slightly downfield. However, the sharp singlet peak of methyl protons in free DFc-M-CH appears to be two peaks with  $\delta$  values of 2.67 and 2.69 ppm upon CB7-complexation. The differences in chemical shifts of these two peaks



(recorded in Hz with 300 MHz, 400MHz and 500 MHz  $^1\text{H}$  NMR spectrometers,  $\delta_{\text{Hz}}$ ) are 7.54, 10.36 and 13.28 Hz, respectively, which are proportional to the magnetic fields. This result reflects that the corresponding protons of these two peaks do not couple to each other; instead they belong to methyl groups in two nonequivalent environments resulting from the enantiomers caused by the chiral N center upon CB7-complexation.

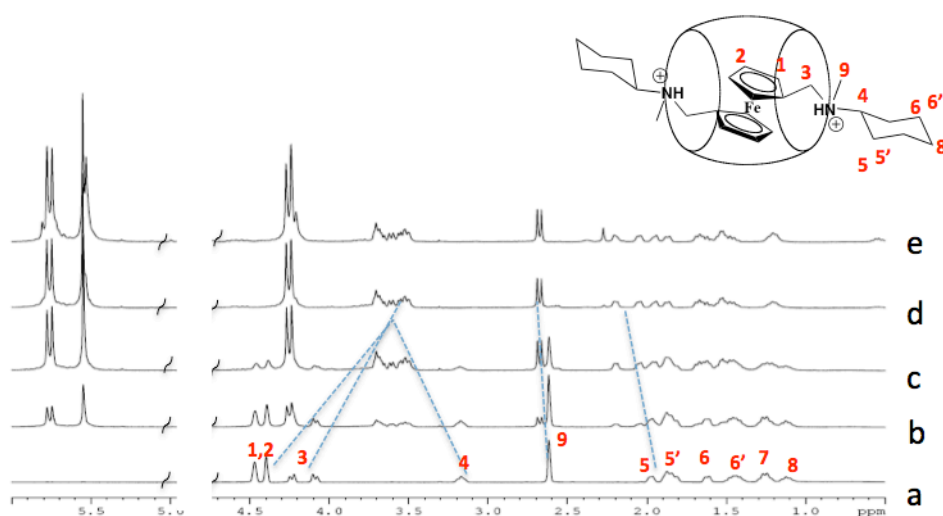


**Figure 3.3.2.1**  $^1\text{H}$  NMR spectra of 1 mM DFC-M-CH in the (a) absence and presence of (b) 0.25, (c) 0.5, (d) 1.0 and (e) 1.25 equiv. of CB7 in  $\text{D}_2\text{O}$  (pD 4.5)

The cyclic voltammetry of 1 mM DFC-M-CH in the 0.1 M NaCl/ $\text{H}_2\text{O}$  (pH  $\sim$ 4) solution was recorded on glassy carbon working electrodes (**Figure 3.3.2.2**). In the presence of CB7, the complex DFC-M-CH $\cdot$ CB7 forms, resulting in a more positive oxidation potential (+160 mV) of the ferrocene and diminished currents. The half-wave potential  $E_{1/2}$  shifts from 621 mV to 781 mV. As with DFC-CH, the two substituents force the ferrocene group to stay deeply inside the CB7 cavity and cause a large  $E_{1/2}$  shift.

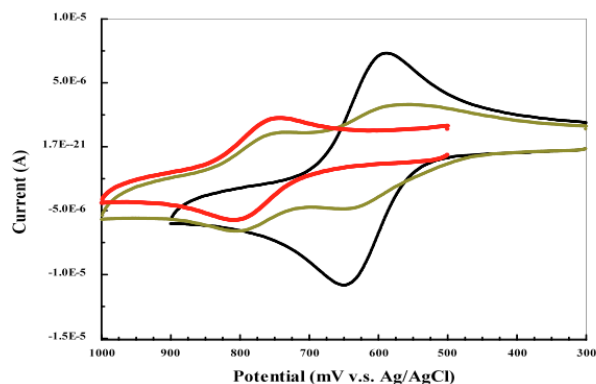


**Figure 3.3.2.2** Cyclic voltammetry of 1 mM DFc-M-CH with 0 (black), 0.5 (brown) and 1.0 (red) equiv. of CB7 in 0.1 M NaCl /H<sub>2</sub>O solution (pH ~4) at 25 °C. Scan rate: 100 mV/s

The ESI-MS spectra of the complex DFc-M-CH•CB7 in acidic media are shown in **Figure 3.3.2.3**. Based on the chemical formula C<sub>68</sub>H<sub>84</sub>FeN<sub>30</sub>O<sub>14</sub><sup>2+</sup>, the simulated spectrum shows an m/z value of 800.3062 for the main isotopic peak, which is close to the experimental result. The isotopic distribution patterns are the same in both experimental and theoretical simulated spectra. This result confidently confirms the formation of the stable inclusion complex DFc-M-CH•CB7.

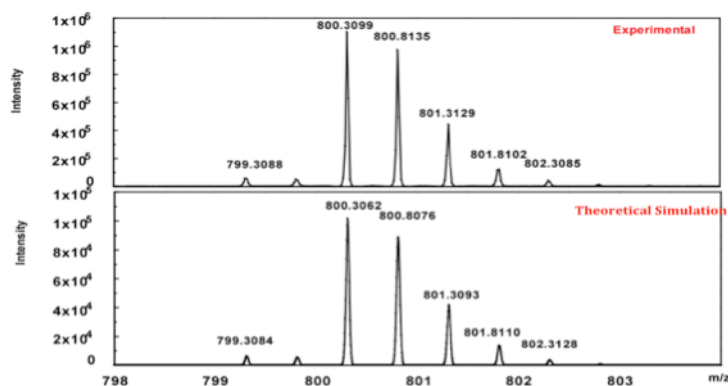


**Figure 3.3.2.3** Experimental and theoretical simulation of high-resolution ESI-TOF mass spectra of the bi-armed guest DFc-M-CH with 1 equiv. of CB7. The complex is diprotonated in water solution (pH ~4)

### 3.3.3 Interactions between DFc-2M-CH and CB7

Further addition of one methyl group to the amine leads to a bulkier bi-armed ferrocene guest DFc-2M-CH. As reported before, the bi-armed ferrocene 1,1'-bis(trimethylammoniomethyl) ferrocene, who has three methyl groups on the substituent, exhibits an extraordinarily high binding affinity with CB7. The  $\text{-CH}_2\text{N}^+(\text{CH}_3)_3$  groups do not stop CB7 threading through to bind to the ferrocene group. However, by changing one methyl group to a bulkier cyclohexyl group in our case may change the binding behavior.

Initially, similar  $^1\text{H}$  NMR spectroscopic and electrochemical procedures were performed for the analysis of DFc-2M-CH with CB7 as we did for DFc-CH and DFc-M-CH in this series. Every measurement was performed immediately after the addition of CB7 into the DFc-2M-CH solution. Unexpectedly, neither  $^1\text{H}$  NMR nor electrochemical results showed that the ferrocene group was bound to CB7. All the results indicate the main binding site moved to the bimethylcyclohexylammoniomethyl substituent. For instance, the cyclic voltammetry of DFc-2M-CH in **Figure 3.3.3** was recorded right after the addition of CB7. The half-wave potential of the ferrocene/ferrocenium redox couple shifts to a more negative value, which commonly suggests that the ferrocene group remains outside the CB7 cavity and one of side arms is located inside the CB7 cavity instead. The position of CB7 in this case results in an easier oxidation process of ferrocene due to the negatively charged CB7 portal, which is close to the ferrocene center undergoing oxidation. Also, in the  $^1\text{H}$  NMR spectra, the

typical upfield shifts of the ferrocene protons and the downfield shifts of the substituent protons upon CB7-complexation were not observed.

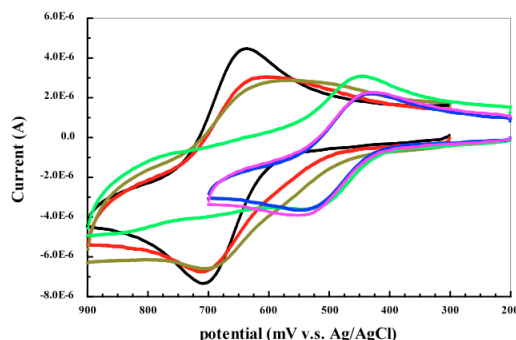


**Figure 3.3.3** Cyclic voltammetry of 1 mM DFc-2M-CH with 0 (black), 0.25 (red), 0.5 (brown), 0.75 (green), 1.0 (purple) and 1.25 (blue) equiv. of CB7 in 0.1 M NaCl /H<sub>2</sub>O solution (pH ~4) at 25 °C. Scan rate: 100 mV/s, recorded right after the addition of CB7

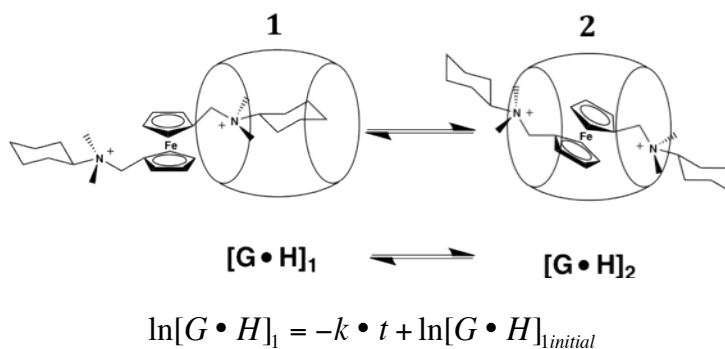
However, according to the well-known high binding affinity of bicationic ferrocene derivatives and CB7 driven the hydrophobic interactions and additional electrostatic interactions, we assumed that the main binding site of DFc-2M-CH and CB7 should still be on the ferrocene. The bulkier substituent may only affect the complexation kinetics, not the overall binding site. In other words, the results above were recorded before the association equilibrium was reached.

### 3.4 Study of the Complexation Kinetics between DFc-2M-CH and CB7

#### 3.4.1 Determination of the Rate Constant $k$ for Complexation of DFc-2M-CH with CB7

With the above assumptions in **Section 3.3.3**, we decided to further study the kinetics of the complexation of DFc-2M-CH with CB7. The inclusion

complexation of DFC-2M-CH with one equivalent of CB7, in which the main binding site is on the ferrocene residue (labeled as species **2** in **Scheme 3.4.1**), follows a first order reaction as proposed in **Scheme 3.4.1**. A practical approach to determine the reaction rate constant  $k$  is to prepare the characteristic kinetics plots according to the rate integrated laws. For a first order reaction, a plot of the natural logarithm of the initial complex (labeled as species **1** in **Scheme 3.4.1**) concentration  $\ln[G \cdot H]_1$ , where the CB7 is mainly bound on the substituent, against time  $t$ , should produce a straight line (see Equation of this line in **Scheme 3.4.1**). The slope of this line gives the approximate value of the rate constant  $k$ . The half-life time  $t_{1/2}$  is independent of the initial concentration of species **1** ( $[G \cdot H]_{i \text{ initial}}$ ) in the first order reaction and can be calculated as  $t_{1/2} = \frac{\ln 2}{k}$  accordingly.



**Scheme 3.4.1** The conversion between two isomeric complexes

A set of data from the  $^1\text{H}$  NMR spectra of DFC-2M-CH in the presence of one equivalent of CB7 was collected in the time period from 0 minute to 120 minutes upon mixing. The integration of specific guest signals allowed us to

follow the concentration change of the given species with time  $t$  and to calculate the association rate constant  $k$ . In detail, we integrated the proton peaks corresponding to the protons on ferrocene and the adjacent methylene group at 3.44~3.80 ppm (12 protons in total) for the inclusion complex DFC-2M-CH•CB7 (species **2**). The relative integral values  $I_{complex}$  are all referred to the integral value of the protons on CB7  $I_{CB7}$  at 5.30 ~6.00 ppm (28 protons in total). The concentration of the complex **2**  $[G\cdot H]_2$  can be calculated by the equation **Eq.3.4.1.1**. Here, we use the total CB7 concentration value  $[H]_{initial}$  in **Eq.3.4.1.1**. The value of  $[G\cdot H]_1$  then can be calculated directly with **Eq. 3.4.1.2**.

$$\frac{12 \times [G \cdot H]_2}{28 \times [H]_{initial}} = \frac{I_{complex}}{I_{CB7}} \quad \text{Eq. 3.4.1.1}$$

$$[G \cdot H]_1 = [H]_{initial} - [G \cdot H]_2 \quad \text{Eq. 3.4.1.2}$$

Taking the natural logarithmic value of  $[G\cdot H]_1$  and time  $t$  (min), the characteristic kinetics plot for the complexation of DFC-2M-CH with CB7 is obtained as shown in **Figure 3.4.1.1**. According to the best linear fitting of the data with a correlation coefficient value of 0.99872, the association rate constant  $k$  for the complexation between DFC-2M-CH and one equivalent of CB7 is found to be about  $0.015 \text{ min}^{-1}$ . The half-life time is estimated to be 50 minutes.

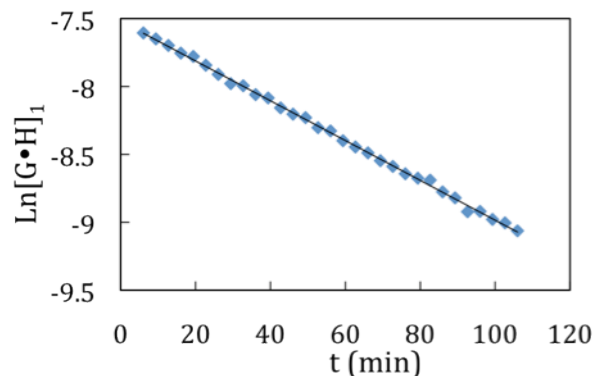


**Figure 3.4.1.1** Characteristic kinetics plot of complexation of DFc-2M-CH with 1euqiv. of CB7 at 25 °C

Based on the kinetic parameters obtained above, the complexation of DFc-2M-CH•CB7 will reach equilibrium roughly around 5 hours. <sup>1</sup>H NMR spectra of DFc-2M-CH with one equivalent of CB7 at equilibrium indicated that CB7 molecules eventually go through the substituents and bind to the ferrocene group, leaving each of the bulky substituents protruding through the CB7 cavity portals (**Figure 3.4.1.2**). Interestingly, the chemical shifts of the proton resonances of the two methyl groups on each of the substituents move from 2.82 ppm to 2.70 ppm (labeled 8 in **Figure 3.4.1.2**). The upfield shifts suggest that the methyl groups point toward the CB7 cavity, not like the methyl groups in DFc-M-CH, which remain outside the CB7 cavity upon complexation and experience slight downfield shifts (see **Figure 3.3.2.1** on page 70).

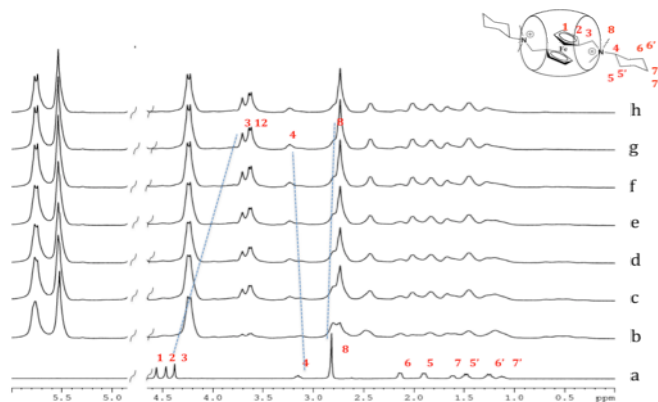


**Figure 3.4.1.2**  $^1\text{H}$  NMR spectra of 1 mM of DFc-2M-CH in the absence (a) and presence of 1 equiv. of CB7 recorded at (b) 0, (c) 30, (d) 50, (e) 60, (f) 80, (g) 110 and (h) 130 mins at 25 °C

The ESI-MS results in **Figure 3.4.1.3** confirm the formation of the complex DFc-2M-CH•CB7. The experimental isotopic peak distribution of the complex is very similar to the theoretic simulation. According to the chemical formula of this complex,  $\text{C}_{70}\text{H}_{88}\text{FeN}_{30}\text{O}_{14}^{2+}$ , the most intense peak was found to be 814.3242, very close to the value of 814.3219 obtained in the theoretical simulation.

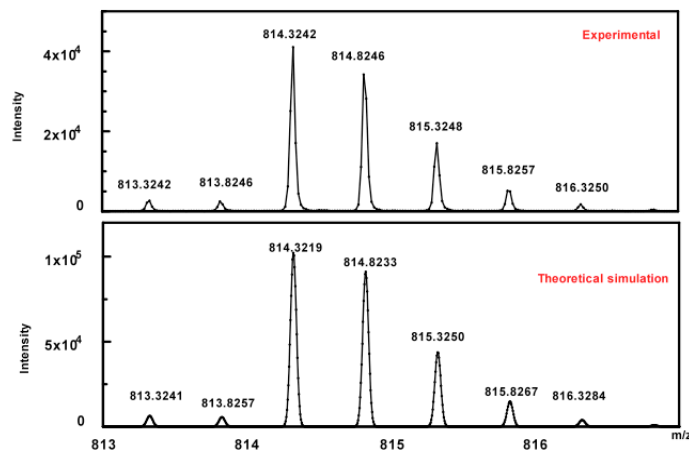
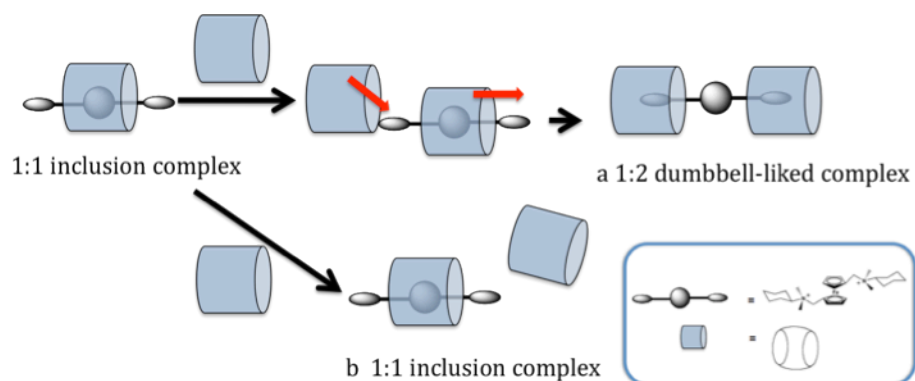


**Figure 3.4.1.3** Experimental and theoretical simulation of high-resolution ESI-TOF mass spectra of the bi-armed guest DFc-2M-CH with 1 equiv. of CB7. The complex carries two positive charges in water solution (pH ~4)



### 3.4.2 Analysis of the Complexation of DFC-2M-CH with two Equivalents of CB7

Since the formation of the 1:1 inclusion complex of DFC-2M-CH and CB7 is pronouncedly slowed down by the bulkier substituents, it is attractive to investigate further whether the CB7 can be removed from the ferrocene group and moved back to the side arms when an extra equivalent of CB7 is added to the solution to form a 2:1 dumbbell-like complex, or if the 1:1 inclusion complexes still dominate the binding due to the high binding affinity, leaving the excess CB7 free in the solution (**Scheme 3.4.2**).



**Scheme 3.4.2** Schematic complexation pathways possible for DFC-2M-CH in the presence of 2 equiv. of CB7 to form (a) 1:2 dumbbell-like complex and (b) 1:1 inclusion complex.

$^1\text{H}$  NMR spectroscopy was used to analyze the complexation behaviors stated above. The spectra in black in **Figure 3.4.2.1** clearly show that the 1:1 inclusion complex gradually formed after a certain time upon addition of one equivalent of CB7 into the free DFC-2M-CH solution. The complex is very stable without any dissociation or decomposition after one day. An extra equivalent of

CB7 then was added to this inclusion complex solution. The  $^1\text{H}$  NMR spectra were recorded immediately upon addition of CB7, after 10 hours and after one day. The major high intensity peaks, which correspond to the 1:1 inclusion complex, are still observed in the spectra. However, some new peaks of low intensity developed in the regions of 5.03-5.15 ppm and 0.36-0.68 ppm, respectively. Based on the patterns of these new peaks and their chemical shifts, it seems that a very small amount of 1:2 complex is formed. The ferrocene protons downfield shifts from 4.51-4.62 to 5.03-5.15 ppm and the cyclohexyl protons experience an upfield shift. This phenomenon indicates that the 1:1 inclusion complex is much favored upon addition of one equivalent of CB7 to the 1:1 inclusion complex, that is, the extra CB7 can barely push the bound CB7 away from ferrocene to the side arm due to the much weaker interactions between CB7 and the cyclohexyl substituent.

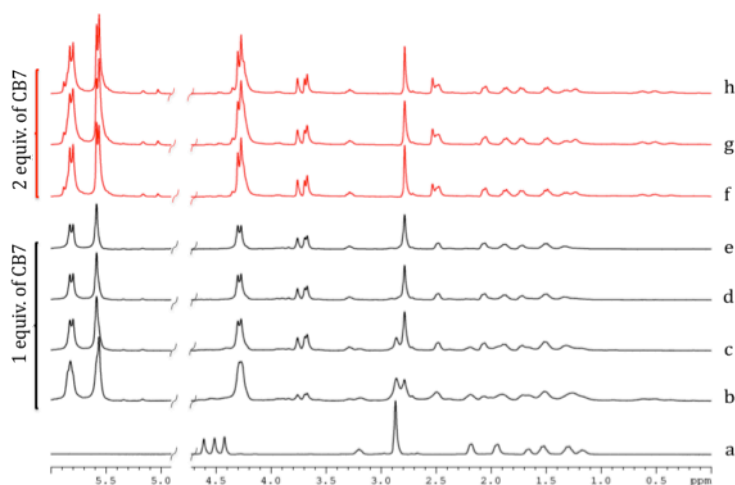


**Figure 3.4.2.1**  $^1\text{H}$  NMR spectra of DFc-2M-CH in the (a) absence and presence of 1 equiv. of CB7 (black) after (b) 0 min, (c) 30 min, (d) 5h, (e) 1 day and then addition of 1 equiv. of CB7 (red) after (f) 0 min, (g) 10h and (h) 1day at 25 °C

In order to prove our prediction on the binding processes, a series of  $^1\text{H}$  NMR spectra of DFc-2M-CH was recorded in the presence of two equivalents of CB7 over a period of time (**Figure 3.4.2.2**). As soon as the CB7 was added into the free DFc-2M-CH solution, due to the slow kinetics of the inclusion complexation, a similar amount of 1:1 complex and 1:2 complex formed in the solution according to the peak intensity corresponding to these two species. As time elapsed, more and more 1:1 complex forms with noticeable growing peaks around 3.70 ppm, which correspond to the ferrocene protons in the CB7-bound DFc-2M-CH. The spectrum recorded after one day clearly shows that the major complex is the 1:1 inclusion complex with a very small amount of 1:2 complex.

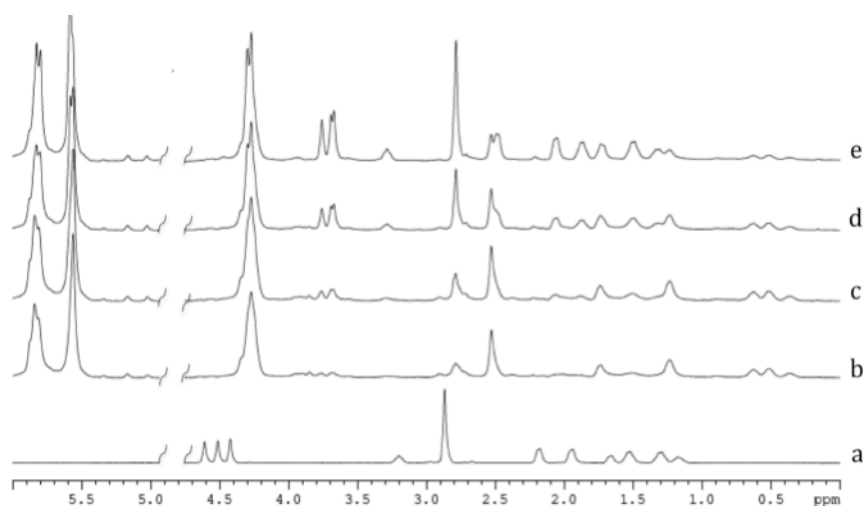


**Figure 3.4.2.2**  $^1\text{H}$  NMR spectra of DFc-2M-CH in the (a) absence and presence of 2 equiv. of CB7 after (b) 0 min, (c) 30 min, (d) 3 h, (e) 1 day at 25  $^{\circ}\text{C}$

Cyclic voltammetric results also are very useful to analyze the binding behavior for the redox active guests such as ferrocene. In general, the oxidation potential of ferrocene/ferrocenium redox couple will shift to more positive potential values when forming the CB-inclusion complex. On the other hand, it will shift more negatively when the CBs are bound on the side arms with the ferrocene group exposed outside the CB cavity. **Figure 3.4.2.3** shows the changes observed in the presence of CB7. The addition of one equivalent of CB7 leads to a positive shift in the half-wave potential,  $E_{1/2}$ , of +130 mV, from 672 mV to 802 mV, with diminished currents compared to that of the free DFC-2M-CH. However, a pair of poorly defined redox peaks was found in the presence of 2 equivalents of CB7. The  $E_{1/2}$  value is estimated around 469 mV, which is about 200 mV more negative than that of the free DFC-2M-CH. This indicates a very small amount of 1:2 complex formed. However, the major redox peaks are still those for the 1:1 inclusion complex, which suggest the same conclusion, that the 1:1 inclusion complexation dominates even with two equivalents of CB7 added.

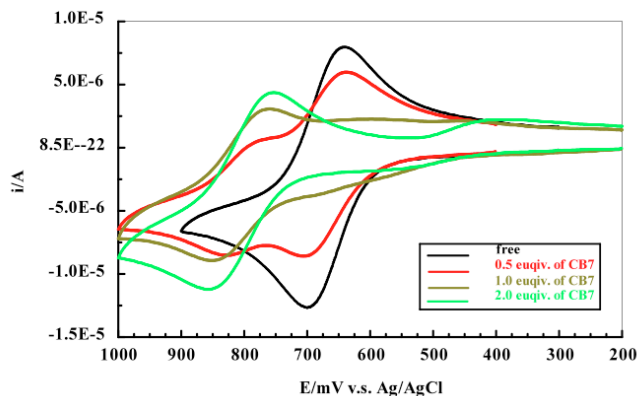


**Figure 3.4.2.3** Cyclic voltammetry of 1 mM DFC-2M-CH in the absence (black) and the presence of 0.5 (red), 1.0 (brown) and 2.0 (green) equiv. of CB7 in 0.1 M NaCl/H<sub>2</sub>O solution recorded at equilibrium 25 °C. Scan rate: 100mV/s

### 3.5 Interaction between the Bi-armed Ferrocene Guests and CB8

We have already shown that this series of bi-armed ferrocene guests could form stable 1:1 inclusion complexes with CB7. However, the bulkiness of the side arms strongly affects the binding kinetics with CB7, as the bulkier side arms may slow down the kinetics of the complexation between the bi-armed ferrocene guest and CB7. It would be interesting to enlarge the host cavity by using the next member of the cucurbituril family, CB8. How would CB8 affect the complexation behavior with our bi-armed ferrocene guests?

With the strong interest on these questions, we studied the complexation behavior of the ferrocene guests and CB8 by taking advantage of  $^1\text{H}$  NMR spectroscopic and electrochemical techniques.

#### 3.5.1 Study on Complexation with CB8 by $^1\text{H}$ NMR spectroscopy

$^1\text{H}$  NMR spectroscopic titration experiments were used to analyze the complexation behavior of these bi-armed ferrocene guests and CB8. Due to the lower solubility of CB8 in water, all the samples were prepared in pure  $\text{D}_2\text{O}$  at 0.1 mM of the guest concentrations.

The spectra in **Figure 3.5.1.1** show a clear 1:1 inclusion complexation behavior between DFc-CH and CB8 even in the presence of 2 equivalents of CB8. The protons on ferrocene and methylene groups (labeled 1, 2 and 3) experience upfield shifts, from 4.41 to 3.68 ppm, 4.32 to 3.62 ppm and 4.05 to 3.52 ppm, respectively, which indicates that the ferrocene is included inside the CB8 cavity. Similarly, the protons on the cyclohexyl groups, for example, the

protons labeled 4, downfield shift from 3.03 to 3.22 ppm, suggesting the cyclohexyl groups remain outside of the CB8 cavity. Addition of CB8 to the 1:1 complex solution doesn't change the binding site. This observation confirms that DFC-CH and CB8 form a 1:1 inclusion complex with the overall binding site on the ferrocene group.

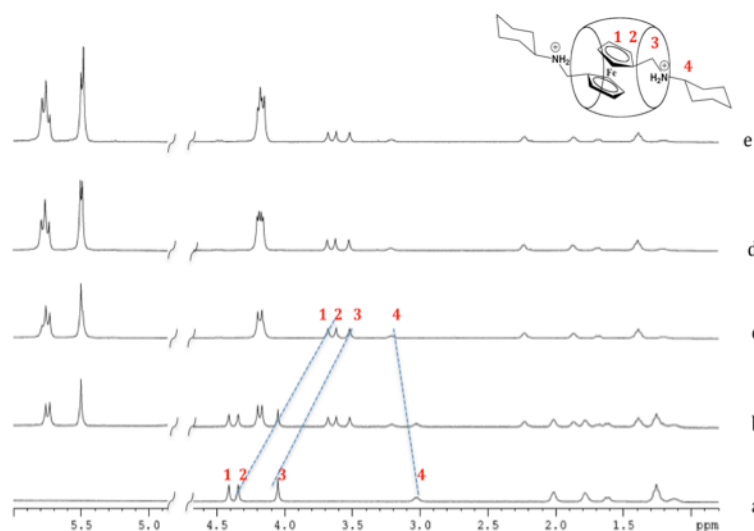


**Figure 3.5.1.1**  $^1\text{H}$  NMR spectra of 0.1 mM DFC-CH in the (a) absence and presence of (b) 0.5, (c) 1.0, (d) 1.5 and (e) 2.0 equiv. of CB8 in  $\text{D}_2\text{O}$  (pD 4.5)

The  $^1\text{H}$  NMR spectra of the DFC-M-CH with the presence of CB8 also indicate the fact that the DFC-M-CH can only form the 1:1 inclusion complex with CB8 (**Figure 3.5.1.2**). However, the peak pattern of the proton resonances is different from that of the inclusion complex DFC-M-CH•CB7. In detail, the protons on ferrocene, methylene and cyclohexyl groups have similar chemical shifts changes and pattern as those of DFC-M-CH•CB7, however, the singlet peak corresponding to the methyl group (labeled 5 in **Figure 3.5.1.2**) upfield shifts from 2.62 to 2.56 ppm upon complexation with CB8, which is opposite of the

CB7-complex, in which a downfield shift from 2.62 to 2.67~2.69 ppm was observed. Also, unlike the doublet peak in the CB7-complex, the peak remains a singlet in the CB8 complex. The difference in the behavior of the methyl protons reveals that the methyl groups are located in the very close proximity to the CB8 cavity, pointing into the cavity. The CB8 complexation does not slow down the proton exchange on the N-H due to the larger opening of CB8 and weaker binding affinity, which results in the singlet peak pattern of methyl protons.

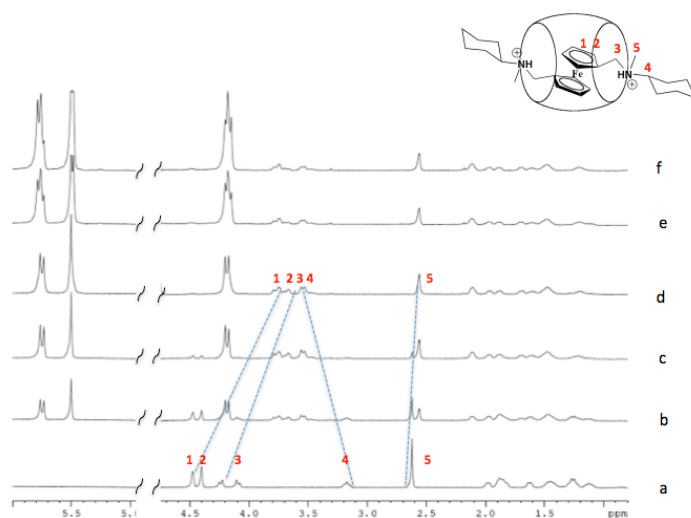


**Figure 3.5.1.2**  $^1\text{H}$  NMR spectra of 0.1 mM DFC-M-CH in the (a) absence and presence of (b) 0.3, (c) 0.6, (d) 1.0, (e) 1.5 and (f) 2.0 equiv. of CB8 in  $\text{D}_2\text{O}$  (pD 4.5)

An exciting behavior was observed in the complexation between DFC-2M-CH with CB8. As described before in **Section 3.4**, the two methyl groups on each of the substituents substantially affect the kinetics of CB7 binding to the center ferrocene group of DFC-2M-CH. Thus, the formation of the 1:1 inclusion complex eventually takes place with a half-life time of 50 minutes. Switching the host to CB8, with a larger cavity, provides a possibility that the binding becomes faster

and the CB8 molecules could go through the substituent without too much obstruction. The  $^1\text{H}$  NMR spectra (**Figure 3.5.1.3** a-d) show that the addition of one equivalent of CB8 immediately leads to the 1:1 inclusion complexation. The ferrocene group is bound inside the CB8 cavity, according to the upfield shifts of the proton peaks on the ferrocene and the methylene groups. The slight upfield shifts from 2.82 to 2.69 ppm of the proton peaks on the methyl groups (labeled 8) indicate the relative positioning of the methyl protons toward the CB8 cavity. However, the binding site of the DFc-2M-CH with CB8 gradually moves with continuous addition of CB8 to the 1:1 inclusion complex solution to reach 2 equivalents of CB8 in the solution. The spectrum **f** in **Figure 3.5.1.3** shows that the proton peaks of the cyclohexyl groups (labeled 4,5,6,7) and the methyl groups (labeled 8) largely shift upfield, for instance, the protons labeled as 6 shift from 2.13 to 1.34 ppm. Simultaneously, the proton peaks of the ferrocene group and adjacent methylene shift upfield slightly compared to the free DFc-2M-CH. The ferrocene proton peaks are believed to overlap with the CB8 peaks around 4.30 ppm and the methylene protons (labeled 3) shift from 4.38 to 4.01 ppm. This result shows that the binding site between DFc-2M-CH and CB8 moves from the ferrocene to the side arms upon addition of 2 equivalents of CB8 host, where a 1:2 dumbbell-like complex forms. The extra CB8 molecule will push the centrally bound CB8 on the ferrocene group to one side of the guest molecule to bind the side arm. More importantly, the change in binding site may indicate that the enlarged cavity of CB8 weakens the binding affinity of the ferrocene group to CB8. In other words, the binding affinity between the



bimethylcyclohexylamminomethyl group and CB8 is close to that of ferrocene with CB8.

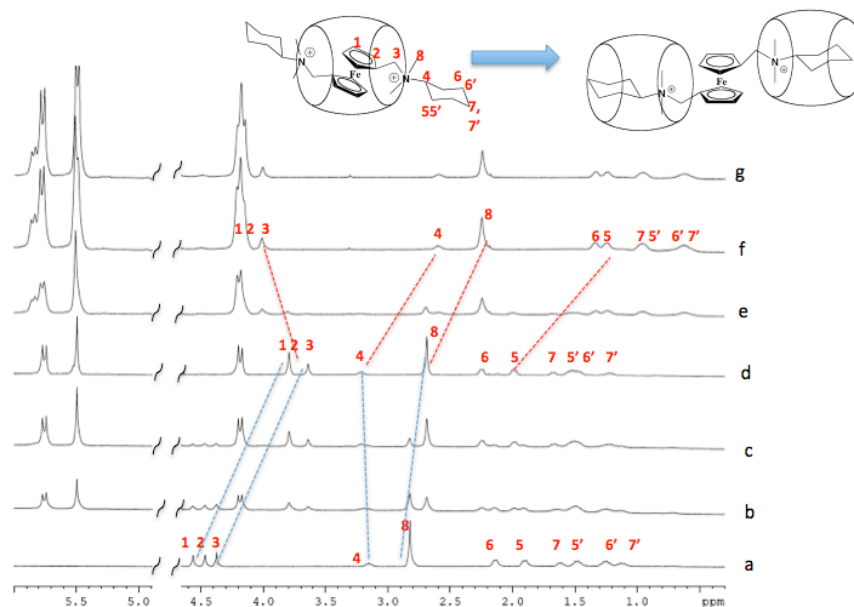


**Figure 3.5.1.3**  $^1\text{H}$ NMR spectra of 0.1mM DFc-2M-CH (a) in the absence and in the presence of (b) 0.44, (c) 0.88, (d) 1.0, (e) 1.76, (f) 2.65 and (g) 3.52 equiv. of CB8 in  $\text{D}_2\text{O}$  (pD 4.5)

### 3.5.2 Study of the Complexation with CB8 by Square-Wave Voltammetry

Square-wave voltammetry (SWV) relies on potential excitation functions that combine the features of a large-amplitude square wave modulation with a simple staircase waveform.<sup>58</sup> The current is collected at the end of each potential plateau. Plotting the difference of the currents in each potential cycle against the average potential will give peak-shaped voltammograms with excellent sensitivity. Ideally, the current function of the voltammograms is symmetrical around the half-wave potential  $E_{1/2}$ , therefore, the peak potential is equal to the

$E_{1/2}$  value of the redox couple. The high sensitivity of SWV could help us successfully investigate the complexation behavior between the ferrocene guests and CB8 at low concentrations forced by the low solubility of CB8 in aqueous media.

The square wave voltammetric results in **Figure 3.5.2.1** and **Figure 3.5.2.2** indicate the formation of 1:1 inclusion complexes DFc-CH•CB8 and DFc-M-CH•CB8, respectively. The addition of one equivalent of CB8 to the guest solution results in positive shifts in the  $E_{1/2}$ . That is, from 572 to 720 mV for DFc-CH and from 628 to 716 mV for DFc-M-CH, which commonly results from the inclusion complex, in which the ferrocene group is included inside the CB8 cavity, which makes the oxidation of the ferrocene more difficult. The addition of an extra amount of CB8 into the complex solution does not cause any further changes in the  $E_{1/2}$  value, thus, only 1:1 inclusion complexation can be observed in both DFc-CH and DFc-M-CH even with 2 equivalents of CB8.

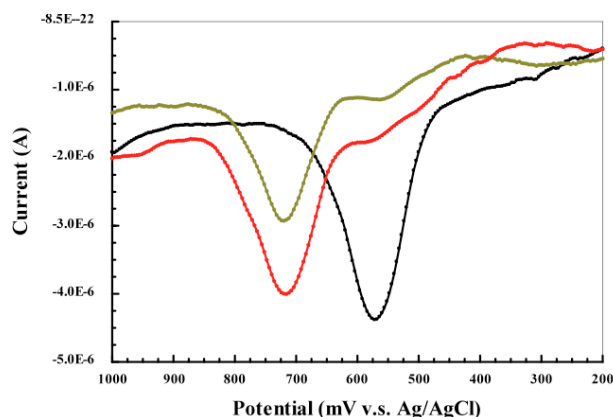


**Figure 3.5.2.1** Square Wave Voltammetry of 0.1 mM Fc-CH in the absence (black) and the presence of 1 (brown) and 2 (red) equivalent of CB8 in 50 mM NaCl/H<sub>2</sub>O pH 4 at 25 °C. Scan rate: 60 mV/s

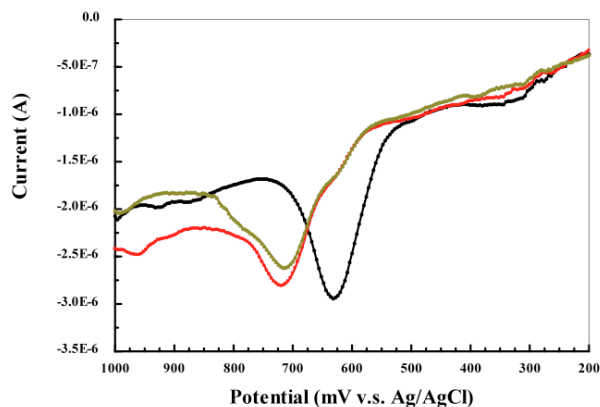


**Figure 3.5.2.2** Square Wave Voltammetry of 0.1 mM Fc-M-CH in the absence (black) and the presence of 1 (brown) and 2 (red) equivalent of CB8 in 50 mM NaCl/H<sub>2</sub>O pH 4 at 25 °C. Scan rate: 60 mV/s

The square wave voltammetric results with DFC-2M-CH (**Figure 3.5.2.3**) are very different in the presence of CB8 from those obtained with DFC-CH and DFC-M-CH. The  $E_{1/2}$  value of DFC-2M-CH does not pronouncedly shift in the presence of one equivalent of CB8. The respective  $E_{1/2}$  values are 680 mV for free guest and 688 mV for the bound guest. The addition of the second equivalent of CB8 results in a pronounced negative shift in  $E_{1/2}$  from 680 mV to 316 mV. This large shift indicates that the oxidation of the ferrocene to ferrocenium becomes much easier than that for the free DFC-2M-CH. The lower oxidation potential results from two contributions: the direct exposure of ferrocene group in the solution; the negatively charged carboxyl oxygens on the portals of CB8. The SWV results confirm that DFC-2M-CH forms a 1:1 inclusion complex in the presence of 1 equivalent of CB8 as well as a 1:2 dumbbell-liked complex in the presence of 2 equivalents of CB8.

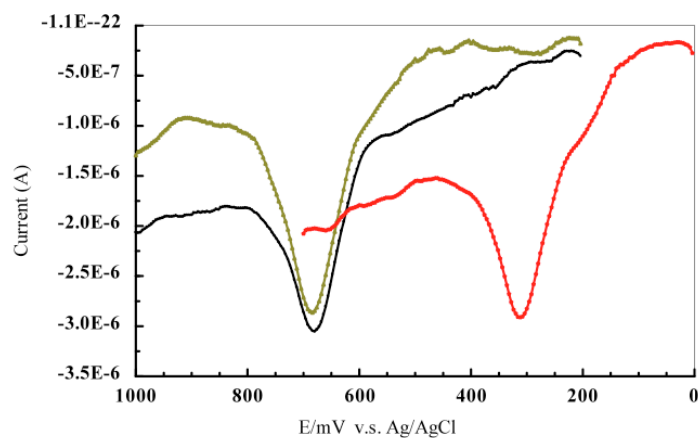


**Figure 3.5.2.3** Square Wave Voltammetry of 0.1 mM Fc-2M-CH in the absence (black) and the presence of 1 (brown) and 2 (red) equivalent of CB8 in 50 mM NaCl/H<sub>2</sub>O pH 4 at 25 °C. Scan rate: 60 mV/s

### 3.5.3 Complexation between Bi-armed Ferrocene Guests with CB8 by ESI-MS

The formation of the 1:1 inclusion complexes DFc-CH•CB8, DFc-M-CH•CB8 and DFc-2M-CH•CB8 are confirmed directly by using the ESI-TOF mass spectroscopy. All the experimental results for the  $m/z$  values and the isotopic peak distributions of the complexes are the same as those simulated from the molecular formulas (**Figure 3.5.3.1-Figure 3.5.3.3**). However, the ESI-MS failed to detect the 1:2 dumbbell-liked complex of DFc-2M-CH•2CB8.

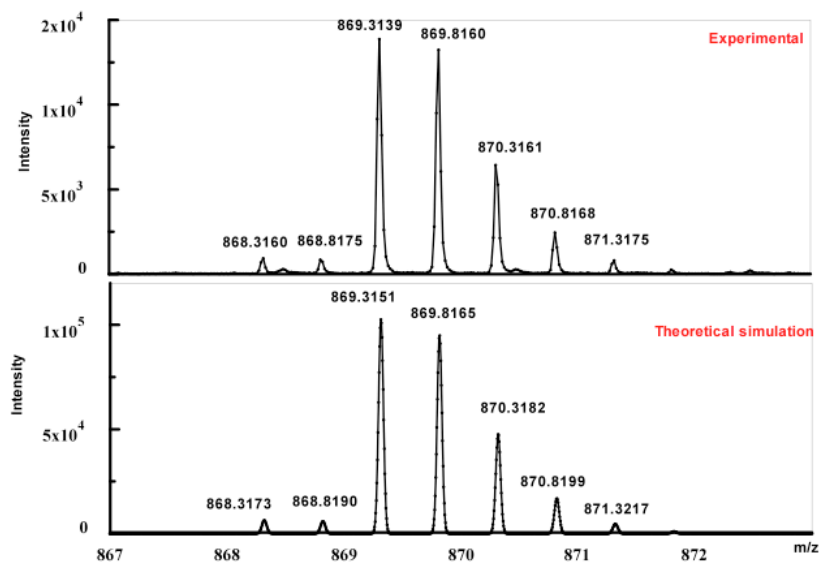


**Figure 3.5.3.1** Experimental and theoretical simulation of high-resolution ESI-TOF mass spectra of the complex DFC-CH•CB8. The complex is diprotonated in water solution (pH ~4)

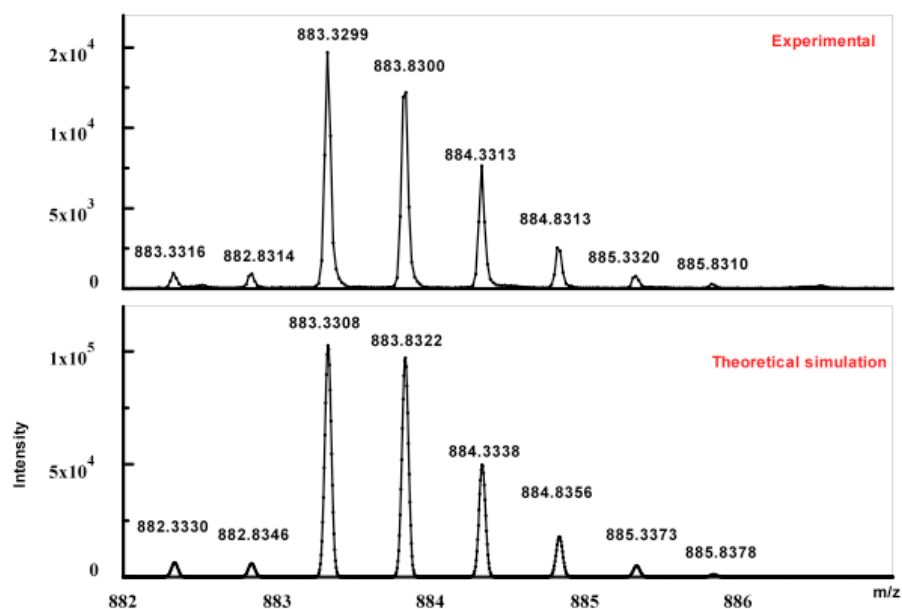


**Figure 3.5.3.2** Experimental and theoretical simulation of high-resolution ESI-TOF mass spectra of the complex DFC-M-CH•CB8. The complex is diprotonated in water solution (pH ~4)

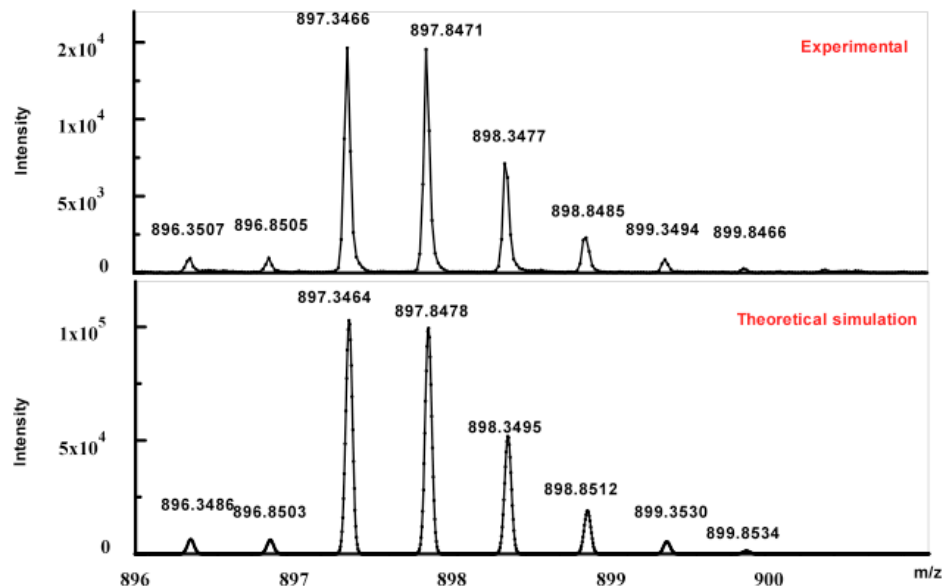


**Figure 3.5.3.3** Experimental and theoretical simulation of high-resolution ESI-TOF mass spectra of the complex DFc-2M-CH•CB8. The complex carries two positive charges in water solution (pH ~4)

### 3.6 Determination of Association Equilibrium Constant $K$ of Model Compounds

So far, we have discussed the complexation behavior of our bi-armed ferrocene guests with two hosts of different sizes: CB7 and CB8, respectively. Clearly, the bulkiness of the substituent, or more specifically, the degree of methylation of the amine group plays a very important role in the complexation behavior. For instance, the bulky side arm in DFc-2M-CH with two methyl groups can tremendously slow down the kinetics for 1:1 inclusion complexation between DFc-2M-CH and CB7 with a half-life time 50 minutes. Also, it moves the CB8 binding site of DFc-2M-CH from ferrocene to the side arms in the presence of

two equivalents of CB8, forming the 1:2 dumbbell-like complex (shown in **Scheme 3.4.2** on page 77).

These results prompted us to a further investigation of the binding affinities of some model molecules (**Figure 3.6.1**) with CB7 and CB8. These model molecules were chosen because they are building blocks of our guest molecules. The guests cyclohexylamine (NH<sub>3</sub>-CH) and trimethylcyclohexylamine (3M-CH) were all confirmed to form 1:1 complexes with CB7 (and CB8) by <sup>1</sup>H NMR titration experiments. The guest DFC-3M is well known to form an extremely stable inclusion complex with CB7 in aqueous media and also was confirmed to form 1:1 complex with CB8. By determining the association equilibrium constant K values of these complexes, we may gain insight on the observed complexation behavior of our bi-armed ferrocene guests with CB7 and/or CB8.

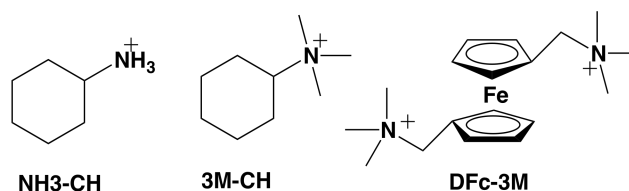


**Figure 3.6.1** Molecular structures of the model molecules

### 3.6.1 Determination of Association Equilibrium Constants for the Complexes of the Model Molecules and CB hosts by UV-Vis Competition Experiments

The binding affinities of these model molecules are predicted to be relatively high according to the previous experiments. Therefore, cobaltocenium

(Cob<sup>+</sup>, see **Figure 3.6.1.1**) was selected as the reference guest to determine the K values of the complexes of the model molecules with CB7 or CB8 in UV-Vis spectroscopic binding competition experiments. The equilibrium association constant between Cob<sup>+</sup> and CB7 has been reported as  $5.7 \times 10^9 \text{ M}^{-1}$  in 50 mM sodium acetate aqueous solution,<sup>59</sup> while the K value was obtained recently by our group to be  $1.9 \times 10^8 \text{ M}^{-1}$  in the same media for the complex Cob<sup>+</sup>•CB8, using a competition method with reference guest 1-adamantylamine.<sup>44</sup> The highly stable Cob<sup>+</sup>-CB complexes induce decreased molar absorptivity coefficients of Cob<sup>+</sup> at 261 nm, compared to that for the free Cob<sup>+</sup>, which leads to titration plots based on the absorbance against the concentrations of the CB host at a constant concentration of Cob<sup>+</sup> guest. Due to the high stability of Cob<sup>+</sup>-CB complexes, the titration plots always exhibit two straight lines intersecting at the equivalence point, where the exact 1 equivalent of CB host is added.

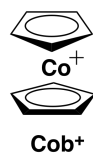
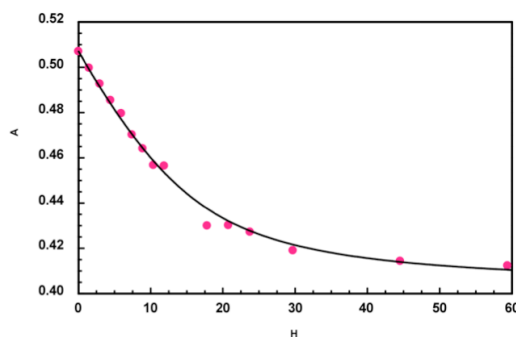


**Figure 3.6.1.1** Cobaltocenium as the reference guest in the binding competition experiments

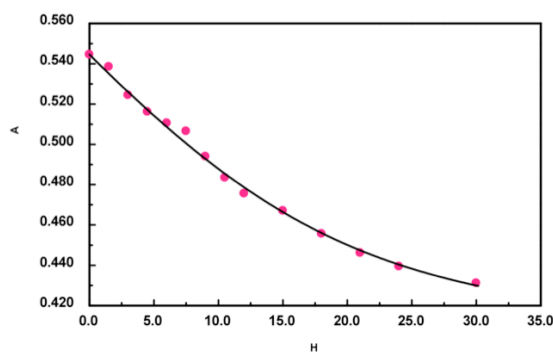
In the competition experiments with Cob<sup>+</sup>, the addition of another guest leads to the possibility to fit the experimental data of the Cob<sup>+</sup> absorbance at 261 nm to a competitive 1:1 binding model, in which the unknown association equilibrium constant K can be calculated (**Figure 3.6.1.2-Figure 3.6.1.5**). For



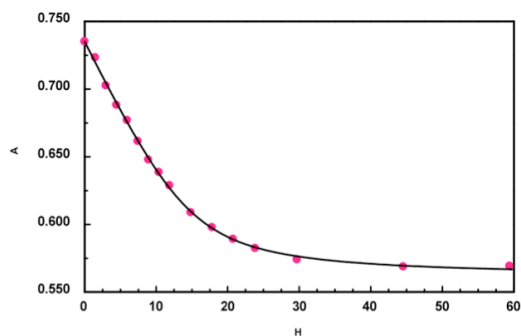
example, the curve in **Figure 3.6.1.2** shows the best fit of the resulting UV-Vis titration experimental data for the competitive 1:1 binding model. The fitting affords a ratio of 51.2 between the K values for the CB7 complexes of  $\text{Cob}^+$  and  $\text{NH}_3\text{-CH}$ . According to the K value of  $\text{Cob}^+$ -CB7 complex ( $5.7 \times 10^9 \text{ M}^{-1}$  in 50 mM  $\text{CH}_3\text{COONa} / \text{H}_2\text{O}$  solution at 25 °C), we obtained an association equilibrium constant of  $1.1 \times 10^8 \text{ M}^{-1}$  for the association of the complex  $\text{NH}_3\text{-CH}\cdot\text{CB7}$  in 50 mM  $\text{CH}_3\text{COONa} / \text{H}_2\text{O}$  solution.



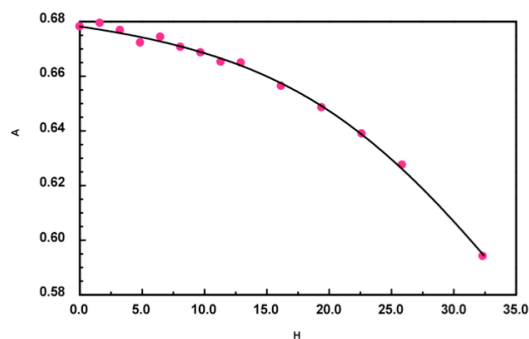
**Figure 3.6.1.2** Plot of absorbance values of  $14.9 \mu\text{M}$   $\text{Cob}^+$  in the presence of  $200 \mu\text{M}$   $\text{NH}_3\text{-CH}$  and increasing CB7 concentrations ( $0\text{-}60 \mu\text{M}$ ) in 50 mM  $\text{CH}_3\text{COONa}/\text{H}_2\text{O}$  solution at 25 °C. Dots are experimental points and the line represents the best fit to the competitive 1:1 binding model



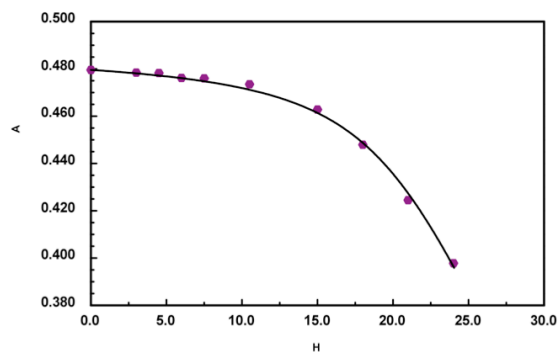
**Figure 3.6.1.3** Plot of absorbance values of  $15 \mu\text{M}$   $\text{Cob}^+$  in the presence of  $20 \mu\text{M}$   $3\text{M-CH}$  and increasing CB7 concentrations ( $0\text{-}30 \mu\text{M}$ ) in 50 mM  $\text{CH}_3\text{COONa}/\text{H}_2\text{O}$  solution at 25 °C. Dots are experimental points and the line represents the best fit to the competitive 1:1 binding model



**Figure 3.6.1.4** Plot of absorbance values of 14.9  $\mu\text{M}$   $\text{Cob}^+$  in the presence of 220  $\mu\text{M}$   $\text{NH}_3\text{-CH}$  and increasing CB8 concentrations (0-60  $\mu\text{M}$ ) in 50 mM  $\text{CH}_3\text{COONa}/\text{H}_2\text{O}$  solution at 25  $^\circ\text{C}$ . Dots are experimental points and the line represents the best fit to the competitive 1:1 binding model

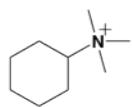
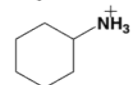
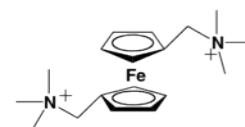


**Figure 3.6.1.5** Plot of absorbance values of 21.3  $\mu\text{M}$   $\text{Cob}^+$  in the presence of 16.2  $\mu\text{M}$  3M-CH and increasing CB8 concentrations (0-35  $\mu\text{M}$ ) in 50 mM  $\text{CH}_3\text{COONa}/\text{H}_2\text{O}$  solution at 25  $^\circ\text{C}$ . Dots are experimental points and the line represents the best fit to the competitive 1:1 binding model



**Figure 3.6.1.6** Plot of absorbance values of 15  $\mu\text{M}$   $\text{Cob}^+$  in the presence of 20  $\mu\text{M}$  DFC-3M and increasing CB8 concentrations (0-25  $\mu\text{M}$ ) in 50 mM  $\text{CH}_3\text{COONa}/\text{H}_2\text{O}$  solution at 25  $^\circ\text{C}$ . Dots are experimental points and the line represents the best fit to the competitive 1:1 binding model



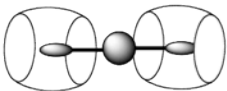

The 1:1 binding model was applied to all UV-Vis competition experiments for the K value determinations with good fitting (see **Figure 3.6.1.2-3.6.1.5**). A similar UV-Vis competition experiment was also performed to DFc-3M. However, the extremely slow decreasing trend at the beginning in **Figure 3.6.1.6** indicates that the DFc-3M binds CB8 much stronger than  $\text{Cob}^+$ , so that there is no competition between them, DFc-3M is much favored and forms a more stable CB8-complex. In order to obtain reliable association equilibrium constant for DFc-3M with CB8, a  $^1\text{H}$  NMR competition with 1-(1-adamantyl)-pyridinium bromide (Ad-Py) was done and gave a K value of  $1.5 \times 10^{11} \text{ M}^{-1}$ . All the K values for the model molecules with CB7 or CB8 are collected in **Table 3.6.1** through the similar calculating procedure as stated above.

	CB7	CB8
	$1.1 \times 10^9 \text{ M}^{-1}$	$1.4 \times 10^9 \text{ M}^{-1}$
	$1.1 \times 10^8 \text{ M}^{-1}$	$1.4 \times 10^6 \text{ M}^{-1}$
	$3.0 \times 10^{15} \text{ M}^{-1**}$	$5.4 \times 10^9 \text{ M}^{-1}$ (UV-Vis) $1.5 \times 10^{11} \text{ M}^{-1}$ (NMR)

**Table 3.6.1** Association equilibrium constant K values of complexes of model molecules with CB7 and CB8 in 50 mM  $\text{CH}_3\text{COONa} / \text{H}_2\text{O}$  solution (pH 4) at 25  $^\circ\text{C}$ . \*\*K value is from reference 19 obtained in pure water

### 3.6.2 Discussion on the Complexation Behavior of Bi-armed Ferrocene guests with CB hosts (CB7 and CB8)

The  $K$  values of the above model molecules obtained in **Section 3.6.1** can be used to help us understand the complexation behaviors of our bi-armed ferrocene guests. According to the  $K$  values of the model guests as building blocks, we roughly calculated the free energy values of the complexes between fully methylated bi-armed ferrocene guest (DFc-2M-CH) and CB7 (or CB8) in 1:1 inclusion conformation, 1:1 exclusion conformation and 1:2 dumbbell-like conformation (**Table 3.6.2**). For the 1:2 complex, we estimated the free energy by using pure statistical relation between the first association equilibrium constant  $K_1$  and the second association equilibrium constant  $K_2$  ( $K_1 = 4K_2$ ), where the guest contains two identical and un-interacting binding sites for the host.

	CB7	CB8
 1:1 inclusion complex	-88.3 kJ/mol	-63.8 kJ/mol
 1:1 exclusion complex	-51.6 kJ/mol	-52.2 kJ/mol
 1:2 dumbbell-like complex	-101.5 kJ/mol	-102.7 kJ/mol
		

**Table 3.6.2** Estimated free energy values of the complexes between fully methylated bi-armed ferrocene guest (DFc-2M-CH) and CB7 (or CB8) at 25 °C

The free energy values in **Table 3.6.2** show that (1) the 1:1 inclusion complex (-88.3 kJ/mol) is much preferred over the exclusion complex (-51.6 kJ/mol) with CB7 due to the much lower free energy of the former, (2) the 1:2 complex with CB7 was not observed because of electrostatic repulsion between the two CB7 hosts even though the free energy of the 1:2 complex (-101.5 kJ/mol) is statistically lower than that of the inclusion complex. However, when switching the host to CB8, the large difference between inclusion complex (-63.8 kJ/mol) and 1:2 complex (-102.7 kJ/mol) leads to the formation of the 1:2 complex in the presence of 2 equivalents of CB8.

### **3.6.3 Determination of the K Values of Complexes DFc-CH•CB7, DFc-M-CH•CB7 and DFc-2M-CH•CB7 by <sup>1</sup>H NMR Competition Experiments**

The K values of the complexes DFc-CH•CB7 and DFc-M-CH•CB7 were also obtained, using <sup>1</sup>H NMR competition method with the reference guest 1-(1-adamantyl)-pyridinium bromide (Ad-Py) ( $K_{\text{Ad-Py}}$  value of  $2.0 \times 10^{12} \text{ M}^{-1}$ ). The integrals of the proton resonance peaks of the free and CB7-bound Ad-Py were used to calculate the K values:  $1.5 \times 10^{12} \text{ M}^{-1}$  for DFc-CH•CB7 and  $1.4 \times 10^{12} \text{ M}^{-1}$  for DFc-M-CH•CB7 in 50 mM CH<sub>3</sub>COONa/H<sub>2</sub>O acidic solution at 25 °C. These two K values are as expected in the sense that bicationic ferrocene guests could form extremely stable CB7-complexes.

The slow association kinetics of the complex DFc-2M-CH•CB7 results in a more complicated yet predictable phenomenon in the presence of Ad-Py. For instance, the <sup>1</sup>H NMR spectra in **Figure 3.6.3.1** show that upon formation of the

complex Ad-Py•CB7, the addition of the DFc-2M-CH barely competes with Ad-Py for CB7, the complex Ad-Py•CB7 is much favored over the DFc-2M-CH•CB7. Similarly, after the formation of the complex DFc-2M-CH•CB7, the addition of Ad-Py can hardly drag the CB7 out from the DFc-2M-CH, thus, Ad-Py is left free in the mixed solution.

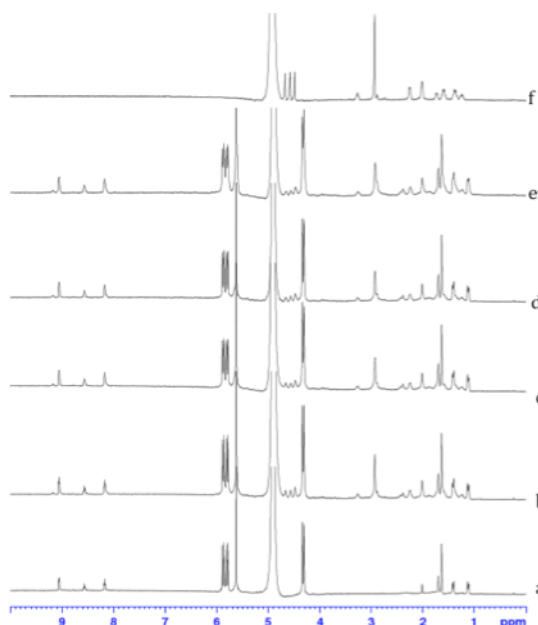


**Figure 3.6.3.1**  $^1\text{H}$  NMR spectra of (a) 0.5 mM Ad-Py in the presence of 0.5 mM CB7 and then addition of 0.5 mM DFc-2M-CH at (b) 0 h, (c) 4 h, (d) 8 h, (e) 32 h and (f) 0.5 mM free DFc-2M-CH in 50 mM  $\text{CH}_3\text{COONa}/\text{H}_2\text{O}$  at 25 °C (pD 4.5)

These phenomena may be the result from the low ground state energy of the complexes of Ad-Py•CB7 and DFc-2M-CH•CB7, both with high stabilities. The potential energy diagram of the complexation in **Figure 3.6.3.2** demonstrates that both complexes have a very low potential energy, while the intermediate state is at a relatively higher energy level, where CB7 threads through the side arm of the bi-armed ferrocene guest. Thus, either the complex

Ad-Py•CB7 or the complex DFC-2M-CH•CB7 is preferred. CB7 cannot jump over the energy barrier between the ground state of complex and the intermediate state to form the other complex.

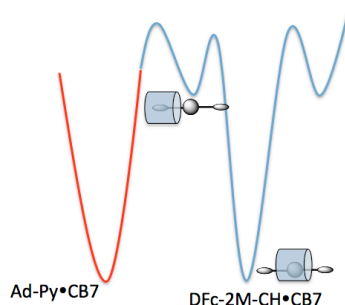


**Figure 3.6.3.2** Potential energy diagram of the complexation of DFC-2M-CH and Ad-Py with CB7

### 3.7 Experimental

1,1'-ferrocenedicarboxaldehyde, cyclohexylamine,  $\text{NaBH}_4$ ,  $\text{NaBH}_3\text{CN}$ , MeI, N-methyl-cyclohexylamine, N,N-dimethylcyclohexylamine and all the solvents are commercial available. All the amines were purified through basic  $\text{Al}_2\text{O}_3$  powder before use.

Cyclic voltammetric and square wave voltammetric experiments were performed on BAS-100 electrochemical station at 25 °C. Glassy carbon working electrodes, Pt counter electrode and Ag/AgCl reference electrodes were used. The glassy carbon electrodes were polished by 5  $\mu\text{m}$   $\text{Al}_2\text{O}_3$  powder (0.05 MICRON, BUEHLER® MICROPOLISH®II) before every measurement.

The pH measurements in H<sub>2</sub>O and D<sub>2</sub>O were done using a PHR-146 Micro Combination pH Electrode on Accumant<sup>®</sup> model 50 pH/ion/conductivity meter from Fisher Scientific, calibrated using standard buffers, pH 4, 7 and 10.

<sup>1</sup>H NMR spectra were obtained on a Bruker 500MHz spectrometer. DCl and D<sub>2</sub>O were purchased from Cambridge Isotope Inc.

### 3.7.1 Synthesis of DFC-CH

Cyclohexylamine (370 μL, 320 mg, 3.28 mmol) was dissolved in 20 mL methanol. HCl/H<sub>2</sub>O solution was used to adjust the solution pH value to around 5, followed by addition of 1,1'-ferrocenedicarboxaldehyde (132 mg, 0.54 mmol). Molecular sieves were used to absorb water in the reaction. The orange mixture was refluxed at 45 °C for 4 h under N<sub>2</sub> protection. NaBH<sub>4</sub> (123 mg, 3.28 mmol) was then added to the solution yielding in a yellow mixture. The solution was stirred for 24 h at 45°C and then cooled down. After filtration through Celite, methanol was removed. The orange oil was washed and extracted by ethyl ether/ water and the organic layers were collected for product purification. The mixture was separated through a neutral Al<sub>2</sub>O<sub>3</sub> column with ethyl ether/methanol (1:9). The major product (DFC-CH) was collected and dried, resulting in a yellow solid (132 mg, yield 60%). <sup>1</sup>H NMR (D<sub>2</sub>O, 500 MHz): δ=1.13 (t, 2H, CH<sub>2</sub>), 1.25 (m, 6H, CH<sub>2</sub>), 1.60~1.63 (d, 2H, CH<sub>2</sub>), 1.77 (s, 2H, CH<sub>2</sub>), 2.01 (s, 2H, CH<sub>2</sub>), 2.99 (s, H, CH), 4.01 (s, 2H, CH<sub>2</sub>), 4.33 (s, 4H, C<sub>5</sub>H<sub>4</sub>), 4.40 (s, 4H, C<sub>5</sub>H<sub>4</sub>) ppm. <sup>13</sup>C NMR (D<sub>2</sub>O, 125 MHz): δ=23.87 (1C, CH<sub>2</sub>), 24.50 (2C, CH<sub>2</sub>), 29.05 (2C, CH<sub>2</sub>), 43.58 (C,



CH), 56.06 (2C, CH<sub>2</sub>), 70.55 (4C, C<sub>5</sub>H<sub>4</sub>), 70.70 (4C, C<sub>5</sub>H<sub>4</sub>), 77.7 (2C, C<sub>5</sub>H<sub>4</sub>) ppm.

ESI-MS: found  $m/z = 205.1174$  [M+2H]<sup>2+</sup>, C<sub>24</sub>H<sub>38</sub>FeN<sub>2</sub><sup>2+</sup>, calcd. 205.1166.

### 3.7.2 Synthesis of DFc-M-CH

N-methyl-cyclohexylamine (390  $\mu$ L, 335 mg, 2.94 mmol) was dissolved in 20 mL methanol. HCl/H<sub>2</sub>O solution was used to adjust the solution pH value to around 5, followed by addition of 1,1'-ferrocenedicarboxaldehyde (119 mg, 0.49 mmol). Molecular sieves were used to absorb water in the reaction. The orange mixture was refluxed at 45°C for 4 h under N<sub>2</sub> protection. The mild reducing agent NaBH<sub>3</sub>CN (186 mg, 2.96 mmol) was then added to the solution yielding a yellow mixture. The solution was stirred for 24 h at 45 °C and then cooled down. After filtration through Celite, methanol was removed. The orange oil was washed and extracted by CH<sub>2</sub>Cl<sub>2</sub>/ water and the organic layers were collected for product purification. The mixture was separated on a neutral Al<sub>2</sub>O<sub>3</sub> column with CH<sub>2</sub>Cl<sub>2</sub>/methanol (1:10). DFc-M-CH was collected as a yellow solid (107 mg, yield 50%). <sup>1</sup>H NMR (D<sub>2</sub>O, 500 MHz):  $\delta$ =1.10~1.12 (m, 2H, CH<sub>2</sub>), 1.24~1.27 (m, 4H, CH<sub>2</sub>), 1.41~1.48 (m, 4H, CH<sub>2</sub>), 1.61~1.63 (d, 2H, CH<sub>2</sub>), 1.87 (m, 6H, CH<sub>2</sub>), 1.97~1.98 (d, 2H, CH<sub>2</sub>), 3.17 (t, 2H, CH), 4.08~4.25 (m, 4H, CH<sub>2</sub>), 4.40 (s, 4H, C<sub>5</sub>H<sub>4</sub>), 4.47 (s, 4H, C<sub>5</sub>H<sub>4</sub>) ppm. <sup>13</sup>C NMR (D<sub>2</sub>O, 125 MHz):  $\delta$ =24.31 (10C, CH<sub>2</sub>), 34.79 (2C, CH), 52.79 (2C, CH<sub>2</sub>), 63.27 (2C, CH<sub>3</sub>), 71.21 (4C, C<sub>5</sub>H<sub>4</sub>), 71.74 (4C, C<sub>5</sub>H<sub>4</sub>), 75.54 (2C, C<sub>5</sub>H<sub>4</sub>) ppm. ESI-MS: found  $m/z = 2219.1377$  [M+2H]<sup>2+</sup>, C<sub>26</sub>H<sub>42</sub>FeN<sub>2</sub><sup>2+</sup>, calcd. 219.1343.

### 3.7.3 Synthesis of DFc-2M-CH

DFc-2M-CH was synthesized by methylation of DFc-M-CH. DFc-M-CH (66 mg, 0.15 mmol) was dissolved in 15 mL CH<sub>2</sub>Cl<sub>2</sub> under N<sub>2</sub> atmosphere. Methyl sulfate (57 μL, 76 mg, 0.60 mmol) was added into the solution and stirred for 24 h. A brown precipitate was formed. The solid was collected by filtration and washed with CH<sub>2</sub>Cl<sub>2</sub>. A resulting light brown solid was obtained. (36 mg, yield: 43%). <sup>1</sup>H NMR (D<sub>2</sub>O, 500 MHz): δ=1.10~1.12 (m, 2H, CH<sub>2</sub>), 1.23~1.26 (m, 4H, CH<sub>2</sub>), 1.46~1.48 (m, 4H, CH<sub>2</sub>), 1.60~1.62 (d, 2H, CH<sub>2</sub>), 1.88~1.91 (d, 4H, CH<sub>2</sub>), 2.12~2.14 (d, 4H, CH<sub>2</sub>), 2.81 (s, 12H, CH<sub>3</sub>), 3.15 (t, 2H, CH), 4.37 (s, 4H, CH<sub>2</sub>), 4.46 (s, 4H, C<sub>5</sub>H<sub>4</sub>), 4.55 (s, 4H, C<sub>5</sub>H<sub>4</sub>) ppm. <sup>13</sup>C NMR (D<sub>2</sub>O, 125 MHz): δ=24.22 (2C, CH<sub>2</sub>), 24.78 (C, CH<sub>2</sub>), 25.62 (4C, CH<sub>2</sub>), 46.60 (2C, CH), 62.24 (2C, CH<sub>2</sub>), 71.18 (4C, CH<sub>3</sub>), 71.73 (4C, C<sub>5</sub>H<sub>4</sub>), 73.06 (4C, C<sub>5</sub>H<sub>4</sub>), 73.64 (2C, C<sub>5</sub>H<sub>4</sub>) ppm. ESI-MS: found m/z =233.1503 [M]<sup>2+</sup>, C<sub>28</sub>H<sub>46</sub>FeN<sub>2</sub><sup>2+</sup>, calcd. 233.1533.

### 3.7.4 Synthesis of 3M-CH

N,N-dimethylcyclohexylamine (500 mg, 589 μL, 3.98 mmol) was dissolved in 50 mL CH<sub>2</sub>Cl<sub>2</sub>, followed by addition of MeI (837 mg, 367 μL, 5.89 mmol). The mixture was stirred under N<sub>2</sub> for 24 h at room temperature. A white precipitate was formed and washed with acetone. The white product was collected (856mg, yield: 80%). ESI-MS: found 142.1593[M]<sup>+</sup>, C<sub>9</sub>H<sub>20</sub>N<sup>+</sup>, calcd.142.1596

### 3.7.5 Synthesis of DFC-3M

DFC-3M was synthesized by methylation of 1,1'-dimethylaminomethylferrocene (DFC-M). 1,1'-ferrocenedicarboxaldehyde (200 mg, 0.83 mmol) was dissolved in MeNH<sub>2</sub> (244 mg, 7.86 mmol) EtOH solution (30 mL) in N<sub>2</sub> atmosphere. The red solution was refluxed for 1 h at 45 °C. After cooling down to 0 °C, NaBH<sub>4</sub> (125 mg, .3.30 mmol) was added in one portion. The mixture was stirred for 12 h at 45 °C. EtOH was evaporated and the residue was extracted with water and ethyl ether (10 mL/10 mL). The aqueous solution was further extracted with ethyl ether (3×10 mL). All the organic solutions were collected and dried over Na<sub>2</sub>SO<sub>4</sub>, then the solvent was removed. The left red oil was separated on a neutral Al<sub>2</sub>O<sub>3</sub> column with ethyl ether/MeOH (1:5) as the eluent. A major yellow band was collected and resulted in a yellow solid product DFC-M (158 mg, 0.58 mmol, yield: 70%). The product was confirmed by <sup>1</sup>H NMR spectroscopy and ready for the next step.

The DFC-M (158 mg, 0.58 mmol) was re-dissolved in CH<sub>2</sub>Cl<sub>2</sub> (30 mL) under N<sub>2</sub> protection at room temperature. MeI (361 μL, 824 mg, 5.8 mmol) was added into the yellow solution. The reaction was covered by aluminum foil and stirred in the dark for 24 h. A yellow precipitate formed. After filtration and washing with CH<sub>2</sub>Cl<sub>2</sub>, a yellow solid was collected as iodide salt (67 mg, yield: 20%). <sup>1</sup>H NMR (D<sub>2</sub>O, 500 MHz): δ=2.94 (s, 18H, CH<sub>3</sub>), 4.36 (s, 4H, CH<sub>2</sub>), 4.47 (s, 4H, C<sub>5</sub>H<sub>4</sub>), 4.56 (s, 4H, C<sub>5</sub>H<sub>4</sub>) ppm. ESI-MS: found m/z =165.0881 [M]<sup>2+</sup>, C<sub>18</sub>H<sub>30</sub>FeN<sub>2</sub><sup>2+</sup>, calcd. 165.0874.

### 3.8 Conclusion

In this chapter, we systematically investigated the complexation behavior of a series of bi-armed ferrocene guests with CB7 and CB8. These guests, featuring identical side arms on each of the Cp rings, exhibit varying CB-complexation behavior closely dependent on the properties of the side arms. In general, the addition of methyl group(s) to our ferrocene guests could result in changes of complexation kinetics, overall binding site and stoichiometry of the complexes.

Electrochemical,  $^1\text{H}$  NMR spectroscopic and ESI-MS methods were used in our study of the complexation. They provide easy and direct ways to confirm the formation of the complexes as well as the analysis of stoichiometry of the complexes. The competition experiments with UV-Vis titration and  $^1\text{H}$  NMR spectroscopy successfully helped us to obtain the association equilibrium constant  $K$  values of some model molecules as building blocks of our bi-armed ferrocene guests, which assist in the rationalization of the complexation behavior observed in this project.

## CHAPTER 4

### Cucurbit[7]uril (CB7) Complexation-Induced pKa Shift of N-methylaminomethylferrocene (MFC)

#### 4.1 Background

One of the reasons why host-guest inclusion complexation is so fascinating to supramolecular chemists is perhaps because such simple assemblies can help researchers understand and mimic biological events. Especially complexes that possess high binding affinity in aqueous media, but could dissociate under mild conditions, are attracting much attention from supramolecular chemists. By modifying the state of the guests, one may increase/decrease the binding affinity in the host-guest system. One simple way to alter the guest reactivity is to modify the acidity constant ( $K_a$  or  $pK_a = -\log K_a$ ) by formation of the host-guest inclusion complex, which may afford catalytic and bio-mimetic applications of host-guest complexes.  $pK_a$  shifts can be achieved in two principal ways. The first approach comes from unspecific hydrophobic interactions, which result from immersion of organic water-soluble guests into a non-polar environment. This effect will disfavor ionized states and result in increasing or decreasing  $pK_a$  values. The second approach involves specific electrostatic interactions between the acidic or basic functional groups of the guests and the negatively or positively charged regions of the host and results in  $pK_a$  shifts due to electrostatic repulsions or attractions.  $pK_a$  value shifts as large as 5 units resulting from unspecific hydrophobic and specific electrostatic

effects have been reported in biological systems.<sup>60</sup> There is a very rapidly developing interest in the potential application of pKa shifts induced by inclusion complexation of the guests. Especially, pKa shifts induced upon complexation by cyclodextrin (CDs) and cucurbiturils (CBs) have drawn much attention. For instance, Nau's group has tremendously contributed to the complexation-induced pKa shifts by CDs and CBs and their further applications in drug delivery studies.<sup>61</sup> The CD-complexation-induced pKa shifts of azoalkane derivatives were reported to have a value around 1 in 2002.<sup>62</sup> Also, a similar pKa shift value of 1 induced by CB6-complexation was reported by the same group.<sup>63</sup> Several dyes such as phenazine-based dye neutral red and acridine orange were studied for the pKa shifts induced by the CB7-complexation with values of 2~3.<sup>64,21d</sup> The pKa shift of thiabendazole (TBZ), one of the drugs concerned benzimidazoles, was reported as high as 4 pKa units upon complexation by CB7(see figure 4.1.1).<sup>65</sup> Very recently, Bhasikuttan and coworkers has reported a CB7-assisted a pKa shift of 5.2 of coumarin 6 dye.<sup>66</sup>

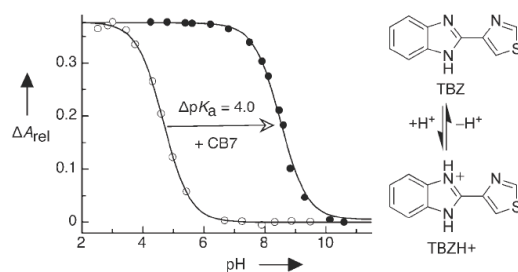


**Figure 4.1.1** pH titration by monitoring the UV absorption band of TBZ ( $\lambda_{\text{mon}}=318$  nm, 15 mm, in water) in the absence (open circles) and presence of 2.5 mM CB7 (filled circles). The pertinent protonation equilibrium is shown on the right<sup>63</sup>

The complexation between ferrocene derivatives and cucurbit[7]uril (CB7) has been investigated in the last few years, especially with neutral and cationic ferrocene guests, which can form highly stable CB7 complexes with association equilibrium constants ( $K$ ) in the range of  $10^9$ - $10^{10}$  and  $10^{12}$ - $10^{13}$   $M^{-1}$ , respectively. The ultra high thermodynamic stability of these ferrocene-CB7 complexes leads to extremely long complex lifetimes and very slow dissociation rates. It would be very desirable to modulate the complex binding affinities by relatively simple chemical processes in order to facilitate their dissociation on demand under mild conditions. With this goal in mind, we employed a simple model ferrocene guest, N-methylaminomethyl ferrocene (MFC, **Figure 4.1.2**), which is an analogue to the fully methylated ferrocene guest with a  $K$  value of  $3.3 \times 10^{11}$   $M^{-1}$  in 50 mM sodium acetate solution.<sup>18a</sup> It is particularly interesting to determine the changes in binding affinities between the CB7 host and various forms of MFC, which result from the amine protonation/deprotonation reactions, as well as the reversible one-electron redox of the ferrocene group in this model guest.

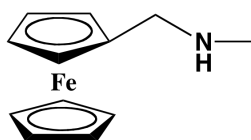


**Figure 4.1.2** Molecular structure of N-Methylaminomethyl ferrocene (MFC)

## 4.2 Thermodynamic “Four-State Model” of Protonation and Complexation of MFc and CB7

The interest in study of the pKa shifts of the guests in the absence and presence of the host is that it could help (1) understand the binding behavior between the guest and host under different acidic/basic conditions; (2) provide a way to predict the binding affinity under certain conditions; (3) eventually develop practical methods to dissociate and re-associate relatively simple guest-host systems with high binding affinity under mild or biological conditions. Theoretically, the association equilibrium constants ( $K$  for neutral species and  $K^+$  for cationic species) and the acidity constants ( $K_{a(\text{free})}$  for free guest and  $K_{a(\text{complex})}$  for its complex) can fit into a thermodynamic “four-state model”, including a closed cycle of protonation of free guest and its complex as well as the complexation of neutral species and cationic species and could successfully depict the relations between the  $K$ ,  $K^+$ ,  $K_{a(\text{free})}$  and  $K_{a(\text{complex})}$ .

For our model guest MFc and host CB7, the thermodynamic “four-state model” of the protonation of MFc and the complexation by CB7 is shown in **Scheme 4.2**. Here, the closed thermodynamic cycle will result in a zero total Gibbs energy ( $\Delta G_{\text{total}}=0$ ). According to the equations in **Eq. 4.2.1-4.2.5**, ideally, the changes in the binding affinities upon protonation/deprotonation of amine in the ferrocene guest can be estimated from the measurement of pKa shift upon CB7-complexation. Alternatively, the complexation would substantially affect the ability of the guest in the host-guest system to release a proton, that is, the value of the pKa will shift upon complexation.



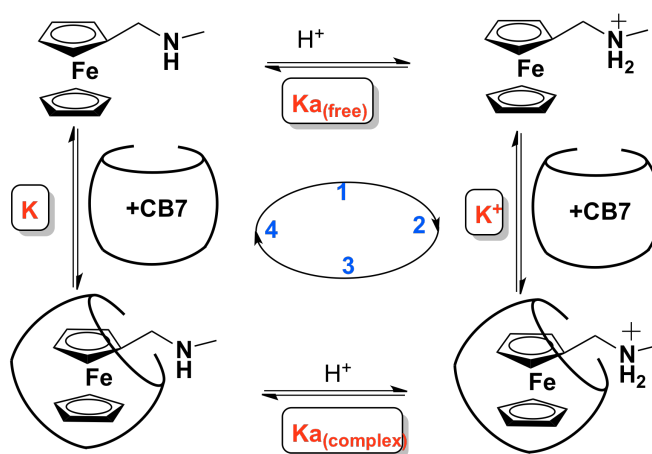
$$\Delta G_{total} = -\Delta G_1 + \Delta G_2 + \Delta G_3 - \Delta G_4 = 0 \quad \text{Eq. 4.2.1}$$

$$\Delta G = -RT \ln K \quad \text{Eq.4.2.2}$$

$$\ln \frac{K}{K^+} = \ln \frac{K_{a(\text{complex})}}{K_{a(\text{free})}} \quad \text{Eq. 4.2.3}$$

$$pKa = -\lg Ka \quad \text{Eq. 4.2.4}$$

$$K^+ = K \times 10^{pKa(\text{complex}) - pKa(\text{free})} \quad \text{Eq. 4.2.5}$$



**Scheme 4.2** Thermodynamic “four-state model” of protonation of MFc and complexation with CB7

### 4.3 Determination of Association Equilibrium Constants by $^1\text{H}$ NMR Competition Experiment

We firstly determined the association constants  $K^+$  and  $K$  for the complexes  $\text{MFcH}^+\cdot\text{CB7}$  and  $\text{MFcH}\cdot\text{CB7}$ , respectively. This can directly indicate the changes in binding interactions between the host CB7 and two forms of the

guest. Specifically, a decrease in binding affinity is expected between CB7 and the cationic guest MFcH<sup>+</sup> upon deprotonation of the amine group.

The <sup>1</sup>H NMR competition method was chosen to measure the values of K<sup>+</sup> and K experimentally. The equilibrium association constants between some ferrocene guests and CB7 have been reported to be 10<sup>12-13</sup> M<sup>-1</sup> for cationic species and 10<sup>9-11</sup> M<sup>-1</sup> for neutral species by our group and other groups.<sup>18</sup> It is of much importance to choose suitable reference guests for the competition experiments. The reference guest should (1) possess similar high binding affinity to the host molecule as that of the guest under investigation to compete effectively for the host; (2) exhibit a clear <sup>1</sup>H NMR spectrum that can provide the information on concentrations of both free and bound species; (3) have a well known equilibrium association constant.

Based on the predicted values for K<sup>+</sup> and K, we have chosen 1-(1-adamantyl)-pyridinium bromide (Ad-Py) with K<sub>Ad-Py</sub> value of 2.0×10<sup>12</sup> M<sup>-1</sup><sup>18a</sup> and cobaltocenium hexafluorophosphate (Cob<sup>+</sup>) with K<sub>Cob<sup>+</sup></sub> value of 5.7×10<sup>9</sup> M<sup>-1</sup><sup>59</sup> as the reference guests for MFcH<sup>+</sup> and MFc to bind CB7, respectively (**Figure 4.3.1**). All the <sup>1</sup>H NMR experiments were performed in 50 mM CD<sub>3</sub>COONa/D<sub>2</sub>O solutions. DCl and NaOD solutions were used to adjust the pD of the solutions in order to fully protonate or deprotonate the MFc.

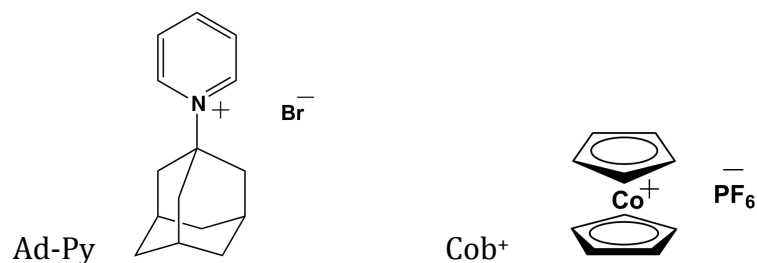


**Figure 4.3.1** Reference guests 1-(1-adamantyl)-pyridinium bromide (Ad-Py) (left) and cobaltocenium hexafluorophosphate (Cob<sup>+</sup>)

In basic solution, only the deprotonated species MFc is expected in the solution. It will compete with Cob<sup>+</sup> for an insufficient amount of CB7 host, which ensures all the CB7 is bound by both guests. As stated previously in **Section 2.6** on page 40-41, the chemical shift of the average peak of free and bound Cob<sup>+</sup> provides information on the concentrations of the free and bound Cob<sup>+</sup>. Following a similar procedure to that described in **Section 2.6**, the estimated K value of MFc was found to be  $3.4 \times 10^9 \text{ M}^{-1}$  in 50 mM CD<sub>3</sub>COONa solution at room temperature.

In acidic solution, all of the neutral MFc is converted to its protonated form MFcH<sup>+</sup>, which will compete with Ad-Py for the host CB7. The cationic guest MFcH<sup>+</sup> and the reference guest Ad-Py fully bind an insufficient amount of CB7. Unlike Cob<sup>+</sup>, free and CB7-bound Ad-Py molecules exhibit slow exchange in the NMR time scale, that is, separated sets of peaks for both free and bound species are observed in the <sup>1</sup>H NMR spectrum simultaneously. Integrals of the proton resonance peaks of a given proton on both free and bound species provide information on the relative number of protons, thus, can be used to

calculate the concentrations. According to the integrals of the free and bound species, one can calculate the equilibrium association constant. For instance, **Figure 4.3.2** shows a  $^1\text{H}$  NMR spectrum of a sample containing 0.5 mM MFCh $^+$ , 0.5 mM Ad-Py and 0.5 mM CB7 in 50 mM CD $_3$ COONa/D $_2$ O solution (pH  $\sim$ 4). The adamantyl group is included inside the CB7 cavity and part of the pyridinium is close to the opening, leading to upfield shifts of the protons (labeled 1 and 2 in **Figure 4.3.2**). These two sets of peaks on Ad-Py were chosen to calculate the molar fractions of free Ad-Py ( $\chi_{\text{free}}$ ) and bound Ad-Py ( $\chi_{\text{bound}}$ ), respectively.

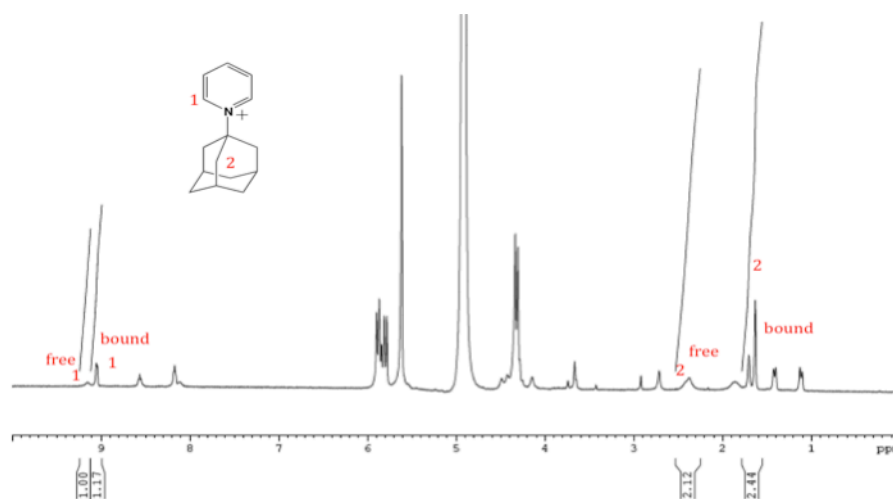


**Figure 4.3.2**  $^1\text{H}$  NMR spectrum of a sample containing 0.5 mM MFCh $^+$ , 0.5 mM Ad-Py and 0.5 mM CB7 in 50 mM CD $_3$ COONa/D $_2$ O solution (pH  $\sim$ 4) at 25  $^\circ\text{C}$ .

Based on the integrals shown in the  $^1\text{H}$  NMR spectrum above, the concentrations of free Ad-Py ( $[\text{Ad}]_{\text{free}}$ ) and bound Ad-Py ( $[\text{Ad}]_{\text{complex}}$ ) can be determined by the following equations(**Eq. 4.3.1-4.3.2**). Here, taking peak 1 for example.

$$[Ad]_{free} = 0.5mM \times \chi_{free} = 0.5mM \times \frac{1.00}{1.00 + 1.17} = 0.23mM \quad \text{Eq. 4.3.1}$$

$$[Ad]_{complex} = 0.5mM - 0.23mM = 0.27mM \quad \text{Eq. 4.3.2}$$

Peak 2 also gave the same results. Due to the insufficiency of the CB7 host and the high binding affinities between these two guests and CB7, CB7 is fully consumed by both guests. According to the equations **Eq.2.6.1-2.6.4** listed in **Section 2** on page 40-41,  $[Ad]_{free}$ ,  $[Ad]_{complex}$  and all other concentrations are applied to find the equilibrium association constant  $K^+$  of  $MFcH^+$  to be  $1.3 \times 10^{12} M^{-1}$  in 50 mM  $CD_3COONa$  solution at room temperature.

As expected, there is no effective binding competition taking place in basic media between neutral guest MFc and Ad-Py due to the very different binding affinities of these two guests with CB7 ( $K = 3.4 \times 10^9 M^{-1}$  for MFc and  $K_{Ad-Py} = 2.0 \times 10^{12} M^{-1}$ ). The  $^1H$  NMR spectrum in **Figure 4.3.3** clearly shows that all the Ad-Py molecules totally dominate the inclusion complexation by CB7 and only the proton peaks corresponding to the bound species are found. Also, the fully deprotonated MFc is left totally free from CB7-complexation when a much stronger guest Ad-Py exists in the solution. The neutral MFc failed to compete with Ad-Py for CB7 because of its  $\sim 3$  order of magnitude lower binding affinity.

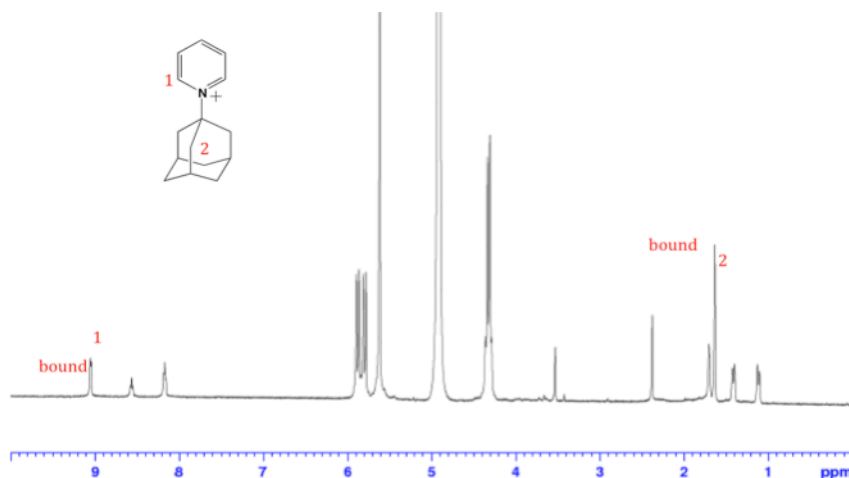


**Figure 4.3.3**  $^1\text{H}$  NMR spectrum of a sample containing 0.5 mM MFc, 0.5 mM Ad-Py and 0.5 mM CB7 in 50 mM  $\text{CD}_3\text{COONa}/\text{D}_2\text{O}$  solution (pH  $\sim$ 12) at 25  $^\circ\text{C}$ .

#### 4.4 Determination of the $\text{pK}_a$ of Free Cationic $\text{MFcH}^+$ and Complex $\text{MFcH}^+\cdot\text{CB7}$ by Cyclic Voltammetry

As stated previously in **Section 4.2**, determination of the  $\text{pK}_a$  shift upon complexation can help estimate the changes in binding affinities upon deprotonation.

The electrochemical process for one-electron oxidation of the free ferrocene residue is known to be extremely fast and reversible in cyclic voltammetry (CV), while, upon complexation with host CB7, the redox process of the ferrocene/ferrocenium ( $\text{Fc}/\text{Fc}^+$ ) couple is still fast and exhibits reversible or quasi-reversible behavior. By recording the half wave potential ( $E_{1/2}$ ) of  $\text{Fc}/\text{Fc}^+$  redox couple in both free MFc and the  $\text{MFc}\cdot\text{CB7}$  complex the media with increasing pH values, the values of  $\text{pK}_{a(\text{free})}$  and  $\text{pK}_{a(\text{complex})}$  could be estimated.

Generally, the  $E_{1/2}$  value will have a rapid change at pH value around the pKa value, where the amounts of MFc and MFcH<sup>+</sup> are equal.

All the CV experiments were performed in 0.1 M NaCl/H<sub>2</sub>O solutions with pH values of 4-13 at room temperature. Glassy carbon electrodes are used as working electrodes and Pt electrodes and Ag/AgCl electrodes are used as counter electrode and reference electrode, respectively. As anticipated, the CV behavior of free guest MFc recorded in media of pH range 4-13 shows typical ferrocene redox peaks with the potential difference ( $\Delta E$ ) between the anodic peak ( $E_{pa}$ ) and the cathodic peak ( $E_{pc}$ ) potentials equal to ~60 mV (**Figure 4.4.1, a**), which indicates that the one-electron oxidation of free guest MFc is reversible under these experimental conditions. Increasing the pH of the solutions eventually leads to a rapid shift of the half-wave potential around a pH value of 9. This phenomenon results from the deprotonation from MFcH<sup>+</sup> to MFc, that leads to higher electron density around the ferrocene group and makes it easier to release one electron. In other words, the proton on the MFcH<sup>+</sup> differentially stabilizes the reduced form of the ferrocene residue.

Addition of one equivalent of CB7 to the MFc solution fully converts the free guest to its CB7 inclusion complex (MFc•CB7). The CV behavior of MFc•CB7 exhibits more positive oxidation potentials with diminished currents compared to those of the free MFc in media in the pH range of 4-13. (**Figure 4.4.1, b**). This confirms the formation of the inclusion complex MFc•CB7. The  $\Delta E$  values for this complex are all around 90mV, which shows a clearly quasi-reversible behavior in CV. Meanwhile, the  $E_{1/2}$  values move to more negative

values as pH of the solution increases due to the deprotonation from  $\text{MFcH}^+\cdot\text{CB7}$  to  $\text{MFcH}\cdot\text{CB7}$ .

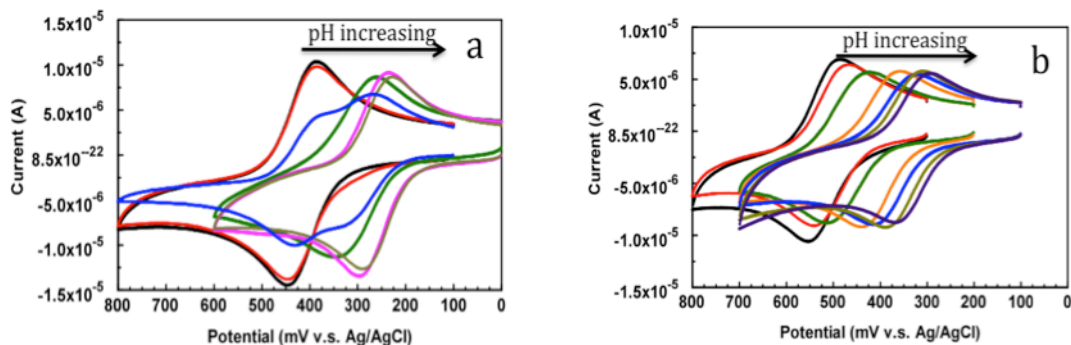


**Figure 4.3.1** Cyclic voltammetry on glassy carbon electrodes of 1 mM (a) free MFc and (b) complex  $\text{MFc}\cdot\text{CB7}$  in 0.1 M  $\text{NaCl}/\text{H}_2\text{O}$  solution of pH values range of 4-12 at 25 °C. Scan rate: 100mV/s

The  $\text{pK}_a$  values could be found from the plots of  $E_{1/2}$  values obtained in the CV experiments versus the pH values (**Figure 4.3.2**). Theoretically, the  $\text{pK}_a$  value is found as the pH value corresponding to the inflection point in the  $E_{1/2}$  vs pH plot. For instance, the  $E_{1/2}$  values in the curve of free MFc in **Figure 4.4.2 a** drop sharply from 406 mV to 260 mV when the pH value only changes from 8.6 to 10, which gives an approximate  $\text{pK}_{a(\text{free})}$  value of 9.3.

However, the curve in the  $E_{1/2}$  vs pH plot for the inclusion complex  $\text{MFcH}\cdot\text{CB7}$  does not show a clear rapid change in a small range of pH values as that in the case of free MFc (**Figure 4.4.2 b**). The  $E_{1/2}$  values of the CB7-bound MFc gradually decrease from 520 mV to 325 mV in the pH range of 8 to 13 without a clear plateau after the deprotonation that could provide the



information of the  $pK_a$  value. Due to the slowly decreasing curve, the value of  $pK_{a(\text{complex})}$  is left uncertain in these cyclic voltammetric experiments.

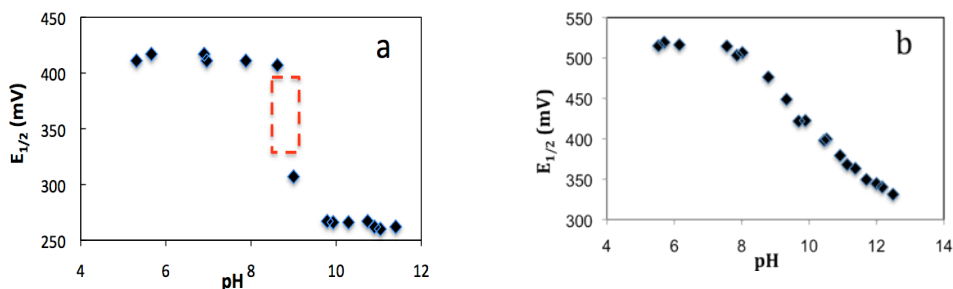


**Figure 4.3.2** Plot of the  $E_{1/2}$  values vs pH values of 1 mM (a) free MFC and (b) complex MFC•CB7 for determination of the  $pK_{a(\text{free})}$  and  $pK_{a(\text{complex})}$  at 25 °C. The red dotted square in plot a is the pH range where two pairs of redox peaks were observed

The cyclic voltammetry of MFC in the absence and the presence of variable concentrations of CB7 were recorded at pH values of 5, 9 and 12 in order to provide more clear evidence for the  $pK_a$  shifts upon inclusion complexation between MFC and CB7 (**Figure 4.4.3**). In pH 5 or pH 12 solutions, the addition of CB7 leads to positive shifts in  $E_{1/2}$  values (+112 mV and +127 mV respectively), larger  $\Delta E$  and diminished current levels as explained above. This indicates that the inclusion complexation between MFC and CB7 takes place in both fully protonated form  $\text{MFCH}^+$  and deprotonated form MFC with high binding affinity. However, an interesting phenomenon is observed at pH 9 (see in **Figure 4.4.3 b**). In the absence of CB7, two pairs of cathodic and anodic peaks appear in the CV, which correspond to  $\text{MFCH}^+$  and MFC, respectively. While, in the presence of CB7, the complex is formed,  $E_{1/2}$  value then goes back to the same position as that at pH 5, which indicates that the included

MFcH<sup>+</sup> requires more basic media to be deprotonated, that is, a higher pKa value results upon complexation.

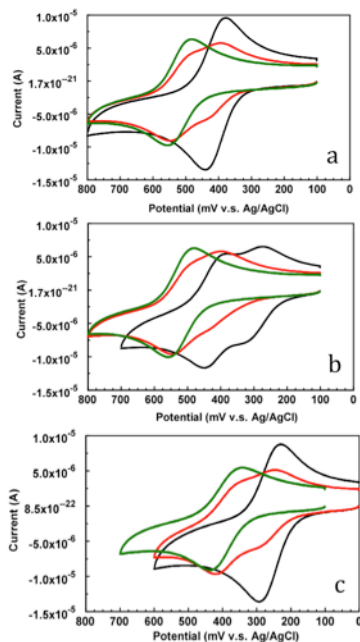


**Figure 4.4.3** Cyclic voltammetric behaviors of 1 mM MFc in the absence (black) and the presence of 0.5 (red) and 1.0 (green) of equiv. of CB7 in 0.1 M NaCl/H<sub>2</sub>O solution of pH values of (a) 5, (b) 9 and (c) 12 at 25 °C. Scan rate: 100mV/s

#### 4.5 Determination of the pKa of Free cationic MFcH<sup>+</sup> and Complex MFcH<sup>+</sup>•CB7 using <sup>1</sup>H NMR Spectroscopy

<sup>1</sup>H NMR spectroscopy is a very useful tool for complexation studies and widely used to investigate the complexation of ferrocene guests and CB7. It cannot only indicate whether the complex is formed, but also the location of the main binding site. Furthermore, it provides us with a very simple way to determine the pKa values of free MFcH<sup>+</sup> and complex MFcH<sup>+</sup>•CB7. In general,

the chemical shifts ( $\delta$ ) of the proton resonances are dependent on the pD (deuteriated pH in D<sub>2</sub>O, pD = pH + 0.4) of the solutions. The chemical shifts will have a large rapid change in a small range of pD values around the pKa. By plotting the chemical shifts of certain protons in solutions of varying range of pD against the pD values, the theoretical pKa value can be found.

The <sup>1</sup>H NMR spectra in **Figure 4.5.1 a** show that the chemical shifts of all the protons on free MFC shift upfield in solutions of increasing pD values. Especially in the pD range from 8.5-11, the chemical shifts afford a pronounced change. For instance, in the  $\delta$  vs pD plot in **Figure 4.5.1 c**, the proton chemical shifts of -CH<sub>2</sub>- changes from 4.14 ppm to 3.62 ppm in a small pD range of 8.5-11, giving a pKa value of 9.3, which is comparable with the results from the electrochemical study.

A similar trend of proton chemical shifts of MFC is observed in the <sup>1</sup>H NMR spectra of 1 mM complex MFC•CB7 (**Figure 4.4.2**). Unlike free MFC, the changes in the proton chemical shifts are quite small in this case (around 0.01 ppm for both protons on -CH<sub>3</sub> and -CH<sub>2</sub>-), which indicates that the inclusion complexation by CB7 has weakened the influence from the magnetic field on the guest protons, that is, the ferrocene residue is shielded inside the CB7 while the side arm -NH<sub>2</sub><sup>+</sup>CH<sub>3</sub> is close to the opening of CB7 and stabilized by the carbonyl groups. Taking the protons on the methyl group as an example (see **Figure 4.4.2 b**), the  $\delta$  value suddenly drops down from 2.89 ppm to 2.88 ppm at a pD value around 12. However, this sudden drop of  $\delta$  value is not convincing enough to find the pKa<sub>(complex)</sub> value due to the following reasons: (1) the  $\delta$

changes are so small that they may contain uncertainty from the experimental errors; (2) the  $\delta$  vs pD plots in **Figure 4.4.2** are limited by the fact that taking pD beyond 13 leads to instability of the ferrocene guests in strong basic media.

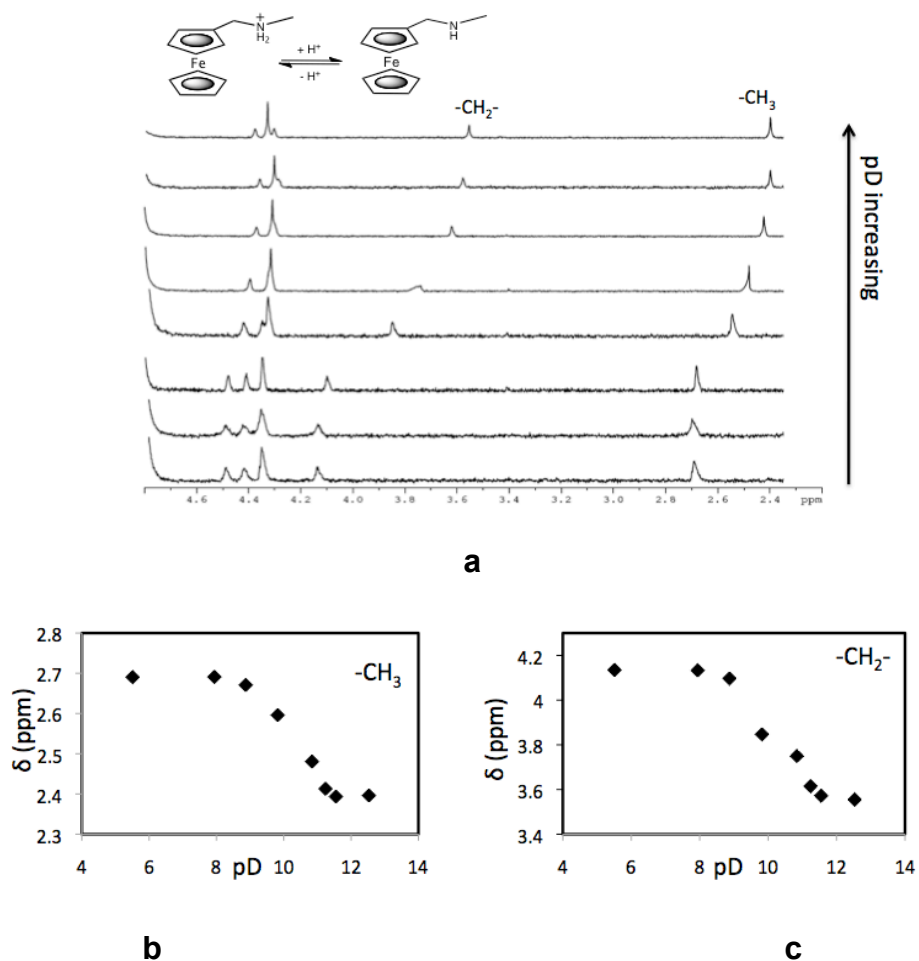


**Figure 4.4.1** (a)  $^1\text{H}$  NMR spectra of 1 mM free MFC in 0.1 M NaCl/D<sub>2</sub>O solutions of increasing pD range of 4-12. Plots of chemical shifts of protons on (b)  $-\text{CH}_3$  and (c)  $-\text{CH}_2-$  versus the pD values of solutions

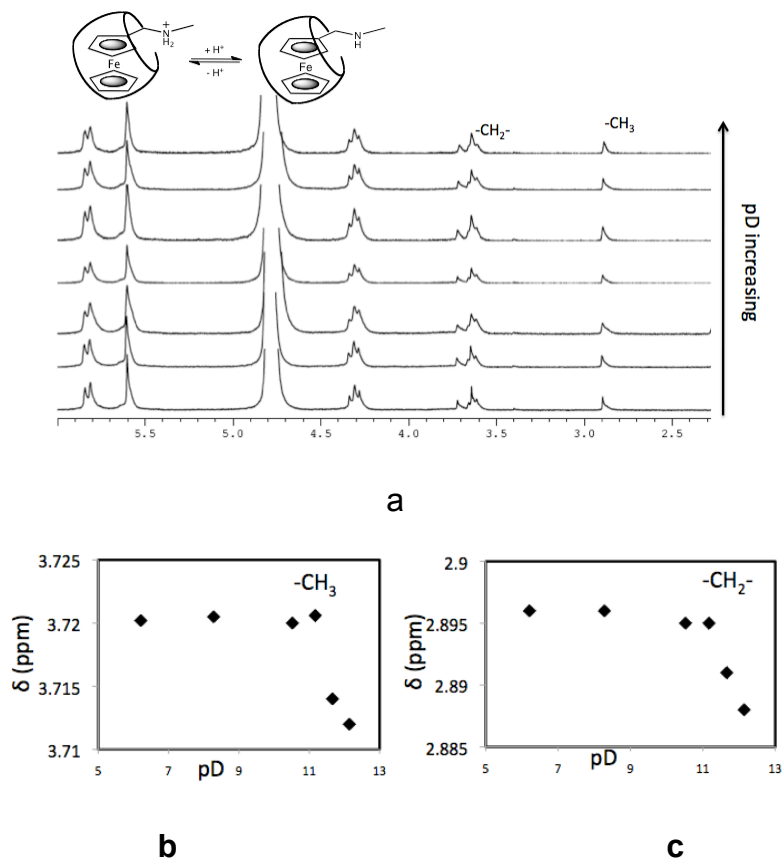


**Figure 4.5.2** (a)  $^1\text{H}$  NMR spectra of 1 mM free MFC in 0.1 M NaCl/ $\text{D}_2\text{O}$  solutions of increasing pD range of 4-12. Plots of chemical shifts of protons on (b)  $-\text{CH}_3$  and (c)  $-\text{CH}_2^-$  versus the pD values of solution

## 4.6 Thermodynamics

### 4.6.1 Prediction of CB7-Complexation-Induced pKa Shift of $\text{MFcH}^+$ by the Thermodynamic “ Four-State Model”

So far we have described a quantitative analysis of the changes in the binding affinities between our model ferrocene guest MFC and the CB7 host through a simple chemical process: protonation/deprotonation, by direct determination of the values of the association equilibrium constants  $K$  and  $K^+$

using  $^1\text{H}$  NMR competition experiments. Clearly, deprotonation of the complex  $\text{MFcH}^+\cdot\text{CB7}$  leads to a substantial decrease in its overall stability. It is shown that the association equilibrium constant comes down from  $1.3\times 10^{12}\text{ M}^{-1}$  for  $\text{MFcH}^+\cdot\text{CB7}$  to  $3.4\times 10^9\text{ M}^{-1}$  for  $\text{MFc}\cdot\text{CB7}$ .

Also, according to the thermodynamic cycle in **Scheme 4.2**, we expected to estimate the changes in the binding affinities upon deprotonation indirectly from the value of the complexation-induced pKa shift ( $\Delta pKa$ ). However, the  $\Delta pKa$  value is not very clear in either electrochemical or  $^1\text{H}$  NMR spectroscopic experiments due to the chemical properties of the model guest and its CB7-complex, which leaves the value of  $pKa_{(\text{complex})}$  very uncertain. By knowing the  $K^+$  and  $K$ , we can still calculate the pKa shift ( $\Delta pKa = pKa_{(\text{complex})} - pKa_{(\text{free})}$ ) induced by the complexation. Consequently, the  $\Delta pKa$  and  $pKa_{(\text{complex})}$  of our model guest can be calculated as follows:

$$\Delta pKa = pKa_{(\text{complex})} - pKa_{(\text{free})} = \log \frac{K^+}{K} = \log \frac{1.3 \times 10^{12}\text{ M}^{-1}}{3.4 \times 10^9\text{ M}^{-1}} = 2.6 \quad \text{Eq. 4.6.1.1}$$

$$pKa_{(\text{complex})} = pKa_{(\text{free})} + 2.6 = 9.3 + 2.6 = 11.9 \quad \text{Eq.4.6.1.2}$$

This large complexation-induced pKa shift of 2.6 units indicates a positioning of the positive charge on  $-\text{NH}_2^+$  in proximity of the carbonyl groups on the opening of CB7, such that stabilizing electrostatic interactions (here specifically ion-dipole interactions) now favor the protonated form  $\text{MFcH}^+$  over the deprotonated form  $\text{MFc}$ . In other words, binding of  $\text{MFcH}^+$  by CB7 weakens the ability of  $\text{MFcH}^+$  to release one proton.

According to the thermodynamic “four-state model”, the protonation of the guest MFc accounts for the variation in the binding affinities to CB7. From the comparison of the values of  $K$  for the deprotonated form MFc and  $K^+$  for the protonated form MFcH<sup>+</sup>, the hydrophobic interactions contribute largely to the strong binding affinities of both the deprotonated and protonated forms. Electrostatic interactions play an important role to strengthen the binding of the protonated MFcH<sup>+</sup>, increasing the  $K^+$  value up to 380 times higher than that for deprotonated MFc.

Furthermore, the thermodynamic cycle rationalizes that the electrostatic stabilization of the complex is responsible for the stronger binding of the protonated MFcH<sup>+</sup> with CB7 as well as the pKa shifts. We therefore generalize tentatively as follows: (1) The protonation of the neutral guest increases the binding affinity with CB7, leading to a net gain of 14.7kJ/mol in the stability of the inclusion complex upon protonation. Specifically, for some neutral ferrocene guests, it could increase the equilibrium association constant values from the range of  $10^9$ -  $10^{11}$  M<sup>-1</sup> to the range of  $10^{12}$ -  $10^{13}$  M<sup>-1</sup>; (2) The associated electrostatic stabilization adds to an existing hydrophobic stabilization, The neutral guest forms a weaker complex than the protonated form due to the absence of the electrostatic interactions.

#### **4.6.2 Thermodynamic Cube**

The one-electron oxidation of the ferrocene residue in the guest also leads to changes in its binding affinities with CB7. For example, the  $E_{1/2}$  values

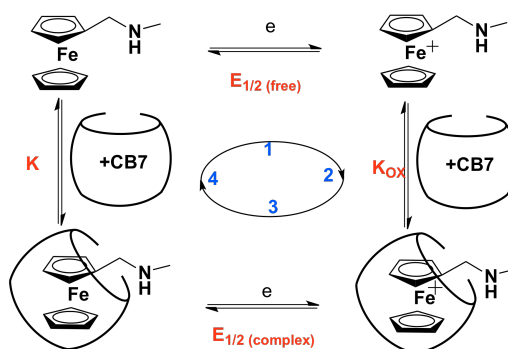
measured in the cyclic voltammetric experiments shifts to more positive value with diminished currents upon CB7-complexation with both MFcH<sup>+</sup> and MFc. Based on the value of  $E_{1/2}$  shift ( $\Delta E_{1/2}$ ), the association equilibrium constant can be estimated for the complex between CB7 and the oxidized forms of either MFcH<sup>+</sup> or MFc. For instance, a second “thermodynamic four-state model” can be established as shown in **Scheme 4.6.2.1** for the redox process of the free MFc and its CB7-complex. According to **Equation 4.6.2.1** and **Equation 4.6.2.2**, applying the electrochemical data:  $E_{1/2(\text{free})} = 0.264$  V and  $E_{1/2(\text{complex})} = 0.391$  V as well as the K value of  $3.4 \times 10^9$  M<sup>-1</sup> will give a  $K_{\text{ox}}$  value of  $2.4 \times 10^7$  M<sup>-1</sup> for the complex between the oxidized form of MFc and CB7.

$$\Delta G = -RT \ln K = -nFE \quad \text{Equation 4.6.2.1}$$

$$K_{\text{ox}} = K \exp \frac{F(E_{1/2(\text{free})} - E_{1/2(\text{complex})})}{RT} \quad \text{Equation 4.6.2.2}$$

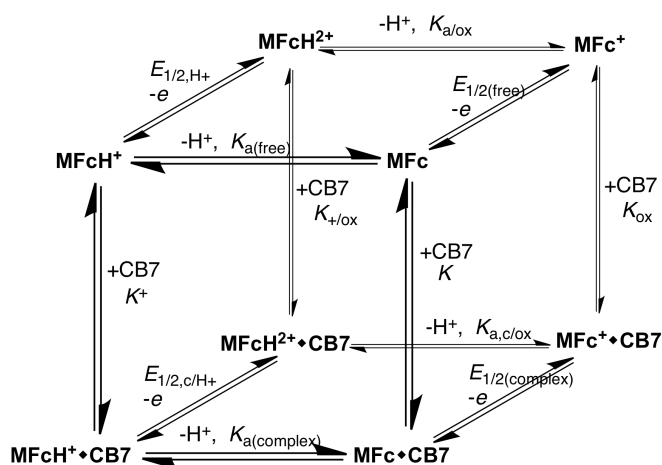
This reflects a net loss of 12.3 kJ/mol in the stability of the inclusion complex and the oxidation of MFc will decrease the binding affinity to CB7 by 2 orders of magnitude, that is, the reduced form of the complex (MFc•CB7) is favored. Overall, deprotonation and oxidation combine to bring down the binding affinity from  $1.3 \times 10^{12}$  M<sup>-1</sup> to  $2.4 \times 10^7$  M<sup>-1</sup>, which corresponds to a net loss of 27 kJ/mol in the stability of the inclusion complex from the protonated form MFcH<sup>+</sup>•CB7 to oxidized form MFc<sup>+</sup>•CB7.





**Scheme 4.6.2.1** Thermodynamic “four-state model” of redox of MFC and complexation with CB7

The binding interactions between CB7 and various forms of MFC resulting from protonation/deprotonation and redox will allow us to establish a very complicated thermodynamic cube, which is displayed in **Scheme 4.6.2.2**. All the thermodynamic data have been estimated accordingly and collected in **Table 4.6.2.1** as well as the electrochemical data obtained in cyclic voltammetric experiments in **Table 4.6.2.2**.



**Scheme 4.6.2.2** Schematic thermodynamic cube of CB7 and various forms of guest MFC

Acid Dissociation Constants		Equilibrium Association Constant	
$K_{a(\text{free})}$	$1.0 \times 10^{-9}$	$K^+$	$1.3 \times 10^{12} \text{ M}^{-1}$
$K_{a(\text{complex})}$	$2.6 \times 10^{-12}$	$K$	$3.4 \times 10^9 \text{ M}^{-1}$
$K_{a/\text{ox}}$	$2.8 \times 10^{-7}$	$K_{+/\text{ox}}$	$1.7 \times 10^{10} \text{ M}^{-1}$
$K_{a,\text{c}/\text{ox}}$	$4.1 \times 10^{-10}$	$K_{\text{ox}}$	$2.4 \times 10^7 \text{ M}^{-1}$

**Table 4.6.2.1** The equilibrium constants values as labeled in **Scheme 4.6.2.2**, the values in red are determined directly from  $^1\text{H}$  NMR and electrochemical experiments and the values in black are obtained through the thermodynamic circles cube in **Scheme 4.6.2.2**

Half-Wave Potential	$E_{1/2, \text{H}^+}$	$E_{1/2(\text{free})}$	$E_{1/2, \text{c}/\text{H}^+}$	$E_{1/2(\text{complex})}$
V	0.409	0.264	0.521	0.391

**Table 4.6.2.2** The half-wave potentials obtained from cyclic voltammetric experiments

## 4.7 Experimental

Cobaltocinium hexafluorophosphate, 1-(1-adamantyl)-pyridinium bromide, deuterium chloride, d-sodium acetate, ferrocenecarboxaldehyde, N-methylamine and  $\text{NaBH}_4$  are commercial available. N-methylaminomethyl ferrocene was synthesized as reported.<sup>67</sup>

Cyclic voltammetric experiments were performed on a BAS-100 electrochemical station at room temperature. Glassy carbon working electrodes, Pt counter electrode and Ag/AgCl reference electrodes were used. The glassy carbon electrodes were polished by  $5\mu\text{m}$   $\text{Al}_2\text{O}_3$  powder (0.05 MICRON, BUEHLER<sup>®</sup> MICROPOLISH<sup>®</sup>II) before every measurement.  $^1\text{H}$  NMR spectra were obtained on a Bruker 500MHz spectrometer.

The pH measurements in H<sub>2</sub>O and D<sub>2</sub>O were done using a PHR-146 Micro Combination pH Electrode on Accumant<sup>®</sup> model 50 pH/ion/conductivity meter from Fisher Scientific, calibrated using standard buffers, pH 4, 7 and 10.

#### 4.7.1 Synthesis of MFc

Ferrocenecarboxaldehyde (200 mg, 0.93 mmol) was dissolved in 20 mL EtOH solution of MeNH<sub>2</sub> (1.25 g, 4.02 mmol) under a nitrogen atmosphere. The red solution was refluxed for 1 h. After cooling down to 0°C, NaBH<sub>4</sub> (40 mg, 1.06 mmol) was added to the solution. The mixture was stirred at 0°C for 30 mins and heated up to room temperature for another 4 h. The EtOH was evaporated and the residue was extracted with water (10 mL) and ethyl ether (10 mL). The aqueous phase was extracted three times with ethyl ether (3×5 mL) and the combined ether phase was washed once with brine and dried over Na<sub>2</sub>SO<sub>4</sub>. Evaporation yielded a red oil, which was purified on a neutral Al<sub>2</sub>O<sub>3</sub> column with ethyl ether/ MeOH (30%) as the eluent. 80 mg of yellow solid was collected with a yield of 40%. The product was confirmed by <sup>1</sup>H NMR spectroscopy. ESI-MS: found m/z=229.0568 [M], C<sub>12</sub>H<sub>15</sub>FeN, Calcd. 229.0548.

#### 4.7.2 pH Adjustment and Measurement

The pH values of the electrochemical experiments and the pD values of the <sup>1</sup>H NMR experiments are of importance for obtaining accurate pK<sub>a</sub>s in our project. Sufficient amount of data points should be collected for plotting pK<sub>a</sub> determination curves (see **Figure 4.3.2** and **4.4.1** for example).

In electrochemical experiments, the pH was adjusted by addition of either HCl/H<sub>2</sub>O solution or NaOH solution. Extra care should be taken in this procedure in order to ensure a small pH change within every adjustment.

The <sup>1</sup>H NMR experiments require deuterated solutions DCI/D<sub>2</sub>O and NaOD/ D<sub>2</sub>O. The pD values were recorded on a pH meter and correlated to the pH meter reading value (pH<sub>reading</sub>) as shown in **Eq.4.7**.<sup>68</sup>

$$pD = pH_{reading} + 0.4 \quad \text{Eq. 4.7}$$

Small amount of DCI/D<sub>2</sub>O or NaOD/ D<sub>2</sub>O was carefully added into samples.

#### 4.7.3 Confirmation of CB7-inclusion Complex by ESI-MS

The complex MFcH<sup>+</sup>•CB7 is confirmed by the high-resolution ESI-TOF mass spectroscopy. The m/z value of [M+H+Na]<sup>2+</sup> is found to be 707.6986 at 100% isotopic distribution for the complex chemical formula of C<sub>54</sub>H<sub>59</sub>FeNaN<sub>29</sub>O<sub>14</sub><sup>2+</sup>, while the calculated result is 707.6978 (**Figure 4.7.3**).

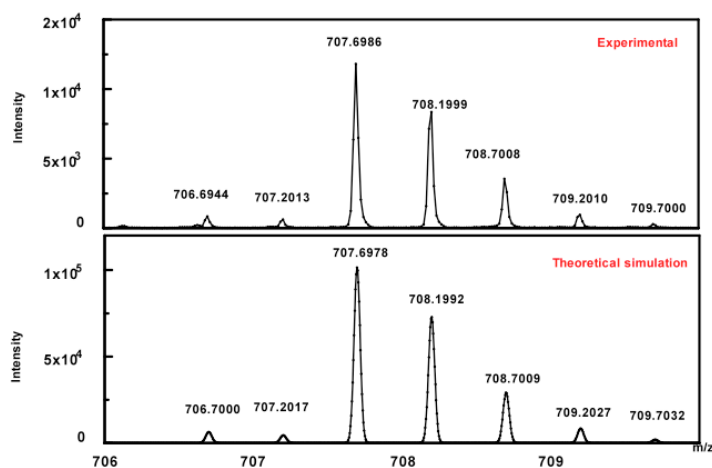


**Figure 4.7.3** Experimental and theoretical simulation of high-resolution ESI-TOF mass spectra of the complex MFcH<sup>+</sup>•CB7+Na<sup>+</sup> in water solution (pH ~4)

## 4.8 Conclusion

In this chapter, we introduced a model guest-host system: MFc and CB7.  $^1\text{H}$  NMR spectroscopic and electrochemical data clearly show that this synthetic system can reach a binding affinity as high as  $10^{12} \text{ M}^{-1}$  upon protonation of the amine group in MFc. Deprotonation of  $\text{MFcH}^+$  to MFc leads to a decrease in the stability of the inclusion complex from  $10^{12} \text{ M}^{-1}$  to  $10^9 \text{ M}^{-1}$  in terms of the association equilibrium constants. Also, the one-electron oxidation of the ferrocene residue in MFc further brings down the binding affinity to  $10^7 \text{ M}^{-1}$ . Overall, the complex  $\text{MFcH}^+\cdot\text{CB7}$  losses ca  $27.1 \text{ kJ mol}^{-1}$  in thermodynamic stability as a result of deprotonation and one-electron oxidation.

This work shows unambiguously that simple chemical transformations can be combined to achieve substantial decrease in high binding affinities between CB7 and the protonated form of our model guest, while providing accessible mechanisms to facilitate dissociation of highly stable complexes on demand under mild conditions.

## References

1. Green., N. M., *Adv. Protein Chem.* **1975**, *29*, 85-133.
2. Swamy, M. J., *Biochem. Mol. Biol. Int.* **1995**, *36*, 219-225.
3. (a) Hofmann, K.; Kiso, Y., *Proc. Natl. Acad. Sci. USA.* **1976**, *73*, 3516-3518; (b) Korpela, J. *Med. Bio.* **1984**, *62*, 5-26; (c) Kohanski, R.; Lane, M. *Methods in Enzymology* **1990**, *184*, 194-200.
4. (a) Reznik, G. O.; Vajda, S.; Cantor, C. R.; Sano, T., *Bioconjugate Chem.* **2001**, *12*, 1000-1004; (b) Ladd, J.; Boozer, C.; Yu Q.; Chen S.; Homola J.; Jiang, S., *Langmuir* **2004**, *20*, 8090-8095; (c) Kim, K.; huang, H.; Jon, S.; Kim, E.; Kwark, J., *J. A. Chem. Soc.* **2004**, *126*, 15368-15369; (d) Tao, S.-C.; Zhu, H., *Nat. Biotechnol.* **2006**, *24*, 1253-1254; (e) Christman, K. L.; Requa, M. V.; Enriquez-Rios, V. D.; Ward, S. C.; Bradley, K. A.; Turner, K. L.; Maynard, H. D., *Langmuir* **2006**, *22*, 7444-7450.
5. Takechi, R.; Taniguchi, A.; Ebara, S.; Fukui, T.; Watanabe, T., *J. Nutr.* **2008**, *138*, 680-684.
6. (a) Zhang, W.; Zhou, G.; Zhao, Y.; White, M. A.; Zhao, Y., *Electrophoresis* **2003**, *24*, 2855-2863; (b) Jaffrey, S. R.; Erdjument-Bromage, H.; Ferris, C. D.; Tempst, P.; Snyder, S. H., *Nat. Cell Biol.* **2001**, *3*, 193-197; (c) Cui, L.; Gadde, S.; Li, W.; Kaifer, A. E. *Langmuir* **2009**, *25*, 13763-13769.
7. Behrend, R.; Meyer, E.; Rushe, F., *Justus Liebigs Ann. Chem.* **1905**, *339*, 1-37.
8. Freeman, W. A.; Mock, W. L.; Shih, N.-Y., *J. Am. Chem. Soc.* **1981**, *103*, 7367-7368.
9. Lagona, J.; Mukhopadhyay, P.; Chakrabarti, S.; Issacs, L., *Angew. Chem. Int. Ed.* **2005**, *44*, 4844-4870.
10. Rekharsky, M. V.; Ko, Y. H.; Selvapalam, N.; Kim, K.; Inoue, Y., *J. Supramol. Chem.* **2007**, *19*, 39-46.
11. Rekharsky, M. V.; Yamamura, H.; Mori, T.; Sato, A.; Shiro, M.; Lindeman, S. V.; Rathore, R.; Shiba, K.; Ko, Y. H.; Selvapalam, N.; Kim, K.; Inoue, Y., *Chem.-Eur. J.* **2009**, *15*, 1957-1965.
12. Florea, M.; Nau, W. M., *Angew. Chem. Int. Ed.* **2011**, *50*, 9338-9342.

13. (a) Day, A.; Arnonld, A. P.; Blanch, R. J.; Snushall, B., *J. Org. Chem.* **2001**, *66*, 8094-8100; (b) Kim, J.; Jung I.-S.; Kim S.-Y.; Lee, E.; Kang, J.-K.; Sakamoto, S.; Yamaguchi, K.; Kim, K., *J. A. Chem. Soc.* **2000**, *122*, 540-541; (c) Huang W.-H.; Liu, S.; Issacs, L., *Cucurbit[ulurils* in: *Supramolecular Chemsitry: Strategies for Macrocycle Synthesis*. Wiley-VCH Verlag GmVH & Co.: Weinheim, **2008**, 113. (d) Issacs, L., *Chem. Commun.* **2009**, 619-629; (e) Liu, S.; Zavalij, P. Y.; Isaacs, L., *J. A. Chem. Soc.* **2005**, *127*, 16798-16799.

14. Lee, J. W.; Samal, S.; Selvapalam, N.; Kim H.-J.; Kim, K., *Acc. Chem. Res.* **2003**, *36*, 621-630.

15. (a) Lu, X.; Masson, E., *Langmuir* **2011**, *27*, 3051-3058; (b) Corma, A.; H.Garcia; Montes-Navajas, P.; Primo, A.; Calvino, J. J.; Trasobares, S., *Chem.-Eur. J.* **2007**, *13*, 6359-6364; (c) Montes-Navajas, P.; Damonte, L. C.; Garcia, H., *ChemPhysChem.* **2009**, 812-816; (d) Montes-Navajas, P.; Garcia, H., *J. Phys. Chem. C* **2010**, *114*, 18847-18852; (e) Lee, T.-C.; Scherman, O. A., *Chem. Commun.* **2010**, *46*, 2438-2440.

16. (a) Hwang, I.; Jeon, W. S.; Kim H.-J.; Kim, D.; Kim, H.; Selvapalam, N.; Fujita, N.; Shinkai, S.; Kim, K., *Angew. Chem. Int. Ed.* **2007**, *46*, 210-213; (b) Constabel, F.; Geckeler, K. E., *Tetrahedron. Lett.* **2004**, (45), 2071-2073; (c) Jiang, G.; Li, G., *J. Photochem. Photobiol. B.* **2006**, *85*, 223-227.

17. (a) Jeon, Y. J.; Kim, S.-Y.; Ko, Y. H.; Sakamoto, S.; Yamaguchi, K.; Kim, K., *Org. Biomol. Chem.* **2005**, *3*, 2122-2125; (b) Montes-Navajas, P.; Gonzales-bejar, M.; Scaiano, J. C.; Garcia, H., *Photochem. Photobiol. Sci.* **2009**, *8* (12), 1743-1747; (c) Wheate, N. J.; Day, A. I.; Blanch, R. J.; Arnold, A. P.; Cullinane, C.; Collins, J. G., *Chem. Commun.* **2004**, *12*, 1424-1425; (d) Wheate, N. J.; Buck, D. P.; Day, A. I.; Collins, J. G., *Dalton Trans.* **2006**, (3), 451-458; (e) Wheate, N. J., *J. Inorg. Biochem.* **2008**, *102* (12), 2060-2066. (f) Masson, E.; Ling, X.; Joseph, R.; Kyeremeh-Mensah, L.; Lu, X., *RSC Adv.* **2012**, *2*, 1213-1247. (g) Ma, D.; Hettiarachchi, G.; Nguyen, D.; Zhang, B.; Wittenberg, J. B.; Zavalij, P. Y.; Briken, V.; Isaacs, L., *Nature Chemistry* **2012**, *4*, 503-510.

18. (a) Liu, S.; Ruspic, C.; Mukhopadhyay, P.; Chakrabarti, S.; Zavalij, P. Y.; Isaacs, L., *J. A. Chem. Soc.* **2005**, *127*, 15959-15967; (b) Jeon, W. S.; Moon, K.; Park, S. H.; Chun, H.; Ko, Y. H.; Lee, J. Y.; Lee, E. S.; Samal, S.; Selvapalam, N.; Rekharsky, M. V.; Sindelar, V.; Sobransingh, D.; Lnoue, Y.; Kaifer, A. E.; Kim, K., *J. A. Chem. Soc.* **2005**, *127*, 12984-12989; (c) Cui, L.; Gadde, S.; Li, W.; Kaifer, A. E., *Langmuir* **2009**, *25* (24), 13763-13769.

19. Rekharsky, M. V.; Mori, T.; Yang, C.; Ko, Y. H.; Selvapalam, N.; Kim, H.; Sobransingh, D.; Kaifer, A. E.; Liu, S.; Isaacs, L.; Chen, W.; Moghaddam, S.; Gilson, M. K.; Kim, K.; Inoue, Y., *Proc. Natl. Acad. Sci. USA.* **2007**, *104* (52), 20737-20742.

20. Moghaddam, S.; Yang, C.; Rekharsky, M.; Kim Y.-H.; Kim, K.; Inoue, Y.; Gilson, M. K., *J. A. Chem. Soc.* **2011**, *133*, 3570-3581.
21. (a) Moghaddam, S.; Inoue, Y.; Gilson, M., *J. A. Chem. Soc.* **2009**, *131*, 4012-4021; (b) Montes-Najavas, P.; Corma, A.; Garcia, H., *ChemPhysChem.* **2008**, *9* (5), 713-720; (c) Halterman, R. L.; Moore, J. L.; Yakshe, K. A.; Halterman, J. A. I.; Woodson, K. A., *J. Inclusion Phenom. Macrocyclic. Chem.* **2010**, *66*, 231-241; (d) Shaikh, M.; Mohanty, J.; Singh, P. K.; Nau, W. M.; Pal, H., *Photochem. Photobiol. Sci.* **2008**, *7*, 408-414; (e) Koner, A. L.; Nau, W. M., *Supramolecular Chemistry* **2007**, *19*, 55-66.
22. Bhasikuttan, A. C.; Mohanty, J.; Nau, W. M.; Pal, H., *Angew. Chem. Int. Ed.* **2007**, *46*, 4120-4122.
23. Wang, R.; Macartney, D. H., *Tetrahedron. Lett.* **2008**, *49*, 311-314.
24. (a) Montes-Navajas, P.; Teruel, L.; Corma, A.; Garcia, H., *Chem.-Eur. J.* **2008**, *14* (6), 1762-1768; (b) Montes-Navajas, P.; H.Garcia, *J. Phys. Chem. C* **2010**, *114* (5), 2034-2038.
25. (a) Liu, Y.; Shi, J.; .Chen, Y.; Kim C.-F, *Angew. Chem. Int. Ed.* **2008**, *47* (38), 7293-7296; (b) Mezzina, E.; Cruiciani, F.; Pedulli, G. F.; Lucarini, M., *Chem.-Eur. J.* **2007**, *13*, 7223-7233; (c) Mileo, E.; Casati, C.; Franchi, P.; Mezzina, E.; Lucarini, M., *Org. Biomol. Chem.* **2011**, *9*, 2920-2924.
26. Song, Y.; Captain, B.; Kaifer, A. E., *Chem. Commun.* **2011**, *47*, 5500-5502.
27. (a) Gadde, S.; Batchelor, E. K.; Weiss, J. P.; Ling, Y.; Kaifer, A. E., *J. A. Chem. Soc.* **2008**, *130*, 17114-17119; (b) Gadde, S.; Bathchlor, E. K.; Kaifer, A. E., *Chem.-Eur. J.* **2009**, *15*, 6025-6031.
28. (a) Ko, Y. H.; Kim, H.; Kim, Y.; Kim, K., *Angew. Chem. Int. Ed.* **2008**, *47* (22), 4016-4109; (b) Ko, K. H.; Kim, Y.; Kim, H.; Kim, K., *Chem.-Asian J.* **2011**, *6*, 652-657.
29. Baek, K.; Kim, Y.; Kim, H.; Yoon, M.; Hwang, I.; Ko, Y. H.; Kim, K., *Chem. Commun.* **2010**, *46*, 4091-4093.
30. Xiao, X.; Wang, Q.; Yu, Y.-H.; Xiao Z. -Y.; Tao, Z.; Xue, S.-F.; Zhu, Q.-J.; Liu, J.-X.; Liu, X.-H., *Eur. J. Org. Chem.* **2011**, 2366-2371.



31. (a) Wang, R.; Bardelang, D.; Waite, M.; Udachin, K. A.; Leek, D. M.; Yu, K.; Ratcliffe, C. I.; Ripmeester, J. A., *Org. Biomol. Chem.* **2009**, *7* (11), 2435-2439; (b) Wu, X.; Meng, X.; Cheng, G., *J. Inclusion Phenom. Macrocyclic. Chem.* **2009**, *64*, 325-329; (c) Wang, R.; Yuan, L.; Ihmels, H.; Macartney, D. H., *Chem.-Eur. J.* **2007**, *13* (22), 6468-6473; (d) Shaikh, M.; Choudhury, S. D.; Mohanty, J.; Bhasikuttan, A. C.; Pal, H., *Phys. Chem. Phys. Chem.* **2010**, *12*, 7050-7055.
32. Jeon, W. S.; Kim H, -J.; Lee, C.; kim, K., *Chem. Commun.* **2002**, 1828-1829.
33. Ziganshina, A. Y.; Ko, Y. H.; Jeon, W. S.; Kim, K., *Chem. Commun.* **2004**, 806-807.
34. Ling, Y.; Wang, W.; Kaifer, A. E., *Chem. Commun.* **2007**, 610-612.
35. Sindelar, V.; Cejas, M. A.; Raymo, F. M.; Chen, W.; Parker, S. E.; Kaifer, A. E., *Chem.-Eur. J.* **2005**, *11*, 7054-7059.
36. Kim, H.-J.; Heo, J.; Jeon, W. S.; Lee, E.; Kim, J.; Sakamoto, S.; Yamaguchi, K.; Kim, K., *Angew. Chem. Int. Ed.* **2001**, *40*, 1526-1529.
37. Uhlenheuer, D. A.; Young, J. F.; Nguyen, H. D.; Scheepstra, M.; Brunsveld, L., *Chem. Commun.* **2011**, *47*, 6798-6800.
38. (a) Wang, W.; Kaifer, A. E., *Angew. Chem. Int. Ed.* **2006**, *118*, 7200-7204; (b) Wang, W.; Kaifer, A. E., *Angew. Chem. Int. Ed.* **2006**, 7042-7046.
39. Bush, M. E.; Bouley, N. D.; Urbach, A. R., *J. A. Chem. Soc.* **2005**, *127*, 14511-14517.
40. Liu, S.; Shukla, A. D.; Gadde, S.; Wagner, B. D.; Kaifer, A. E.; Isaacs, L., *Angew. Chem. Int. Ed.* **2008**, *47*, 2657-2660.
41. Liu, S.; Zavalij, P. Y.; Lam, Y.-F.; Isaacs, L., *J. A. Chem. Soc.* **2007**, *129*, 11232-11241.
42. Jiao, D.; Zhao, N.; Scherman, O. A., *Chem. Commun.* **2010**, *46*, 2007-2009.
43. Pisani, M. J.; Zhao, Y.; Wallace, L.; Woodward, C. E.; Keene, F. R.; Day, A. I.; Collins, J. G., *Dalton Trans.* **2010**, *39*, 2078-2086.
44. Yi, S.; Kaifer, A. E., *J. Org. Chem.* **2011**, *76* (24), 10275-10278.
45. Hwang, I.; Baek, K.; Jung, M.; Kim, Y.; Park, K. M.; Lee, D.-W.; Selvapalam, N.; Kim, K., *J. A. Chem. Soc.* **2007**, *129*, 4170-4171.

46. Jon, S. Y.; Selvapalam, N.; Oh, D. H.; Kang J.-K.; Kim S. -Y.; Jeon, Y. J.; Lee, J. W.; Kim, K., *J. A. Chem. Soc.* **2003**, *125*, 10186-10187.
47. Zhao, N.; Lloyd, G. O.; Scherman, O. A., *Chem. Commun.* **2012**, *48*, 3070-3072.
48. Rekharsky, M. V.; Mori, T.; Yang, C.; Ko, Y. H.; Selvapalam, N.; Kim, H.; Sobransingh, D.; Kaifer, A. E.; Liu, S.; Isaacs, L.; Chen, W.; Moghaddam, S.; Gilson, M. K.; Kim, K.; Inoue, Y., *Proc. Natl. Acad. Sci. USA.* **2007**, *104* (52), 20737-20742.
49. Kaifer, A. E., Molecular Encapsulation of Redox-active Guests. In *Electrochemistry of Functional Supramolecular Systems*, Ceroni, P.; Credi, A.; Venturi, M., Eds. A John Wiley & Sons, Inc. : Hoboken, New Jersey, 2010; Vol. 2, pp 59-85.
50. Schalley, C. A.; Springer, A., *Mass Spectrometry and Gas-Phase Chemistry of Non-Covalent Complexes*. John Wiley & Sons, Inc.: New Jersey, 2009.
51. (a) He, X.; Li, G.; Chen, H., *Inorganiiic Chemistry Communications* **2002**, *5*, 633-636; (b) Montes-Navajas, P.; Corma, A.; Garcia, H., **2008**, *Journal of Molecular Catalysis: chemical*, 165-169; (c) Rauwald, U.; Birdermann, F.; Deroo, S.; Robinson, C. V.; Scherman, O. A., *J. Phys. Chem. B.* **2010**, *114*, 8606-8615.
52. Sobransingh, D.; Kaifer, A. E., *Langmuir* **2006**, *22*, 10540-10544.
53. (a) Plenio, H.; El-Desoky, H.; Heinze, J., *Chem. Ber.* **1993**, *126*, 2403-2408; (b) Medina, J. C.; Goodnow, T. T.; Rojas, M. T.; Atwood, J. L.; Lynn, B. C.; Kaifer, A. E.; Gokel, G. W., *J. A. Chem. Soc.* **1992**, *114* (26), 10583-10595; (c) Hammond, P. J.; Bell, A. P.; Hall, C. D., *J. Chem. Soc., Perkin Trans. 1* **1983**, 707-715.
54. Tendero, M. J. L.; Benito, A.; Lloris, J. M.; Martínez-Máñez, R.; Soto, J.; Payá, J.; Edwards, A. J.; Rathby, P. R., *Inorganica Chemica Acta* **1996**, *247*, 139-142.
55. Lloris, J. M.; Martínez-Máñez, R.; Padilla-Tosta, M. E.; Pardo, T.; Soto, J.; Beer, P. D.; Cadman, J.; Smith, D. K., *J. Chem. Soc. Dalton Trans.* **1999**, 2359-2369.
56. Georgopoulou, A. S.; Mingos, D. M. P.; White, A. J. P.; Williams, D. J.; Horrocks, B. R.; Houlton, A., *J. Chem. Soc. Dalton Trans.* **2000**, 2969-2974.
57. Sobransingh, D.; Kaifer, A. E., *Chem. Commun.* **2005**, 5071-5073.

58. Kaifer, A. E.; Gómez-Kaifer, M., *Supramolecular Electrochemistry* Wiley-VCH: Weinheim, New York, 1999.
59. Soransingh, D.; Kaifer, A. E., *Langmuir* **2006**, 22 (25), 10540-10544.
60. (a) Honig, B.; Nicholls, A., *Science* **1995**, 265, 1144-1149; (b) Matulis, D.; Bloomfield, V. A., **2001**, *Biophys. Chem.* (93), 37-51.
61. Carvalho, C. P.; Uzunova, V. D.; Silva, J. P. D.; Nau, W. M.; Pischel, U., *Chem. Commun.* **2011**, 47, 8793-8795.
62. Zhang, X.; Gramlich, G.; Wang, X.; Nau W. M., *J. A. Chem. Soc.* **2002**, 124 (2), 254-293.
63. Marquez, C.; Nau, W. M., *Angew. Chem. Int. Ed.* **2001**, 40 (17), 3155-3160.
64. Mohanty, J.; Bhasikuttan, A. C.; Nau, W. M.; Pal, H., *J. Phys. Chem. B.* **2006**, 110 (10), 5132-5138.
65. Saleh, N.; Koner, A. L.; Nau, W. M., *angew. Chem.* **2008**, 120, 5478-5481.
66. Barooah, N.; Mohanty, J.; Pal, H.; Bhasikuttan, A. C., *J. Phys. Chem. B.* **2012**, 116 (12), 3683-3689.
67. Norrild, J. C.; Sotofte, I., *J. Chem. Soc., Perkin Trans. 2* **2002**, 303-311.
68. Krężel, A.; Bal, W., *Journal of Inorganic Biochemistry* **2004**, 98, 161-166.